INFORMATION TO USERS

This manuscript has been reproduced from the microfilm master. UMI films the text directly from the original or copy submitted. Thus, some thesis and dissertation copies are in typewriter face, while others may be from any type of computer printer.

The quality of this reproduction is dependent upon the quality of the copy submitted. Broken or indistinct print, colored or poor quality illustrations and photographs, print bleedthrough, substandard margins, and improper alignment can adversely affect reproduction.

In the unlikely event that the author did not send UMI a complete manuscript and there are missing pages, these will be noted. Also, if unauthorized copyright material had to be removed, a note will indicate the deletion.

Oversize materials (e.g., maps, drawings, charts) are reproduced by sectioning the original, beginning at the upper left-hand corner and continuing from left to right in equal sections with small overlaps. Each original is also photographed in one exposure and is included in reduced form at the back of the book.

Photographs included in the original manuscript have been reproduced xerographically in this copy. Higher quality 6" x 9" black and white photographic prints are available for any photographs or illustrations appearing in this copy for an additional charge. Contact UMI directly to order.

U·M·I

University Microfilms International
A Bell & Howell Information Company
300 North Zeeb Road, Ann Arbor, MI 48106-1346 USA
313/761-4700 800/521-0600

Order Number 9405533

Free-space optical interconnects for multiprocessing computers

Ha, Berlin, Ph.D.

City University of New York, 1993

U·M·I
300 N. Zeeb Rd.
Ann Arbor, MI 48106

A

FREE-SPACE OPTICAL INTERCONNECTS

FOR MULTIPROCESSING COMPUTERS

by

Berlin Ha

A dissertation submitted to the Graduate Faculty in Engineering in partial fulfillment of the requirement of the degree of Doctor of Philosophy, The City University of New York.

1993

This manuscript has been read and accepted for the Graduate Faculty in Engineering in satisfaction of the dissertation requirement for the degree of Doctor of Philosophy.

July 13, 1993
Date

Chairman of Examining Committee Prof. Y. Li

July 13, 1993
Date

Executive Officer Prof. G. Lowen

Prof. S. Ahmed

Prof. P. P. Ho

Prof. J. Barba

Dr. M. Wu

Supervisory Committee

The City University of New York

ABSTRACT

FREE-SPACE OPTICAL INTERCONNECTS FOR MULTIPROCESSING COMPUTERS

by

Berlin Ha

Mentor: Dr. Yao Li, Research Scientist at NEC Research Institute
and Associate Professor at City College of New York,
and Dr. George Eichmann, Herbert G. Kayser Professor
of Electrical Engineering

Various new free-space optical interconnects are studied in this thesis. The focus of the research is to design and to develop fast, reliable and efficient free-space optical interconnects for linking multiprocessing digital computers.

New approaches to realize optical crossover and perfect shuffle interconnects are presented in the first two chapters. To implement the optical crossover interconnects, two methods, one based on reflective components, such as mirrors and beam-splitters, and the other based on diffractive components, such as Fresnel zone plate, are used to provide controllable data permutations among digital processing elements. A new optical perfect shuffle, which can form a cascade network of shuffles,

is also proposed. This new cascadable optical shuffle makes it possible to realize optical interconnects for multiple-instruction-and-multiple-data processing applications.

Optical implementation of binary symmetric logic functions is also studied in this thesis. The proposed optical binary symmetric logic networks provide a new means of using a set of spatially interconnected contact switches as computation tools to execute various binary arithmetic operations, such as arithmetic addition and multiplication.

In this thesis, processing element distribution methods for different interconnect topologies are also studied. A new concept to distribute processing elements in a ring array rather than in a rectangular array is proposed. Employing a pair of Dove prisms, the designed optical ring array imaging system can provide both bi-directional and unidirectional links for digital processing nodes. A reflective prism is also specially designed to perform a pair of conjugated image rotation operations for the proposed reflective ring array interconnect. Both the transmissive and reflective ring array networks offer a high speed clock-skew-free data communications among single-instruction-and-multiple-data processors.

Finally, a detailed in depth investigation of interconnect capacity limitations due to the system aberration, diffraction, and power consumption efficiency is carried out. The analytical results are used to guide the corresponding optical system design. A particular design exercise with its aim to correct all the system aberrations is presented. To optimizing the design, a computer aided lens design software is also used.

This research was supported by the NEC Research Institute and by the Air Force Office of Scientific Research under grants AFOSR 84-0144 and 88-0260.

To my parents Yu Ha and Yunfang Zheng

ACKNOWLEDGEMENT

I would like to take this opportunity to express my sincere thanks to Late Doctor George Eichmann, Herbert G. Kayser Professor of Electrical Engineering at The City College of New York, who offered me the scholarship seven years ago, and made it possible for me to study at The City College of New York towards my Ph.D degree.

It is a great pleasure to acknowledge my deep appreciation to my thesis advisers Professor Yao Li and Professor George Eichmann, for their patient guidance, continuous encouragement, rigorous training and invaluable suggestion during the course of this research.

To carry out the research, the financial support provided by the NEC Research Institute and by the Air Force Office of Scientific Research under the grants ASOFR-84-0144 and 88-0260 is deeply appreciated.

Finally, special thanks go to my husband, Chih-Yuan Yao, for his love, understanding and encouragement.

Table of Contents

Table of Figures

Table of Tables

I. INTRODUCTION

1.1 Thesis Statement and Organization

Various free-space optical interconnects are studied in this thesis. A new optical implementation of cascadable crossover and perfect shuffle networks is presented. An array of interconnected optical contact switches is also proposed to perform binary symmetric logic functions. A novel architecture of distributing all interconnected nodes in a circular rather than in a rectangular array is introduced in this thesis, and the corresponding optical ring array interconnects provide a fast and synchronized data communications among various single-instruction-and-multiple-data (SIMD) processors. The goal of this research is to design and develop new free-space optical interconnects with high speed, low cross talk and efficient energy consumption for multiprocessing computers.

The thesis is divided into eight chapters. This introduction provides a general background of what optics can offer to interconnect networks for multiprocessing computers. In the second and the third chapters, new optical implementations of crossover networks and perfect shuffles are presented. In chapter four, an idea to employing an array of optical contact switches to implement binary symmetric logic functions is introduced. In the two following chapters, a new concept to distribute interconnected processing elements along a ring array rather than a linear or a rectangular array for the SIMD processing environment is proposed. A pair of Dove prisms is employed to perform unidirectional or bidirectional optical ring interconnects in chapter five, while in chapter six, a reflective prism is specially designed to implement a couple of reflective interconnects among the nodes in a ring. Finally, the performance quality of the free-space optical interconnects is evaluated based on the system aberration, diffraction and power consumption efficiency analysis.

1.2 What Can Optics Do for Interconnects?

Data communications among digital processors and between processors and their supporting memory are handled by interconnect networks. One of the main

approaches to increase computing speed and efficiency is parallel processing. In an advanced computer a huge number of processors is often used. For example, the number of processors in the Connection Machine 2 is 65,536 [1]. In the near future, the number of processors will increase very rapidly. The Hughes 3-D Machine 2 which is designed to have 262,144 processors will be operational in the late 1990s. To manufacture so many processors and to integrate them monolithically is not a problem in the view of today's technology. The technological advance of very large scale integrated (VLSI) circuits makes it possible to establish parallel processing computers with huge number of processors. However, to link so many processors with sufficient flexibility and reliability remains to be a difficult task. The bandwidth required for a 40 MHz 64-bit processing element (PE) (such as i860) is 2.56 GHz. With current technology, this bandwidth can only be provided by using the state-of-the-art GaAs logic circuits. The interconnect bandwidth problem becomes worse when more sophisticated PEs are used. For example, for a GaAs reduced instruction set computer (RISCs) operating at 100MHz, no present electronic circuit can provide the space-bandwidth product required for parallel data transfer from one PE to another.

Can optics give a better approach to solve this problem? The answer reveals to be positive. The main features of optics are its ultrafast beam propagating speed, wide processing bandwidth, and massive parallelism. In addition, optical switches with very high speed, and low power requirements are or will be available in the near future. With all these advantages, optical interconnects may partly replace the electrical conducting wires to handle data communications for the future computers.

Optical interconnects can provide benefit to either an electronic computer or a future optical computer. The level of useful optical interconnects could range from gate-to-gate, chip-to-chip, board-to-board, to even computer-to-computer, depending on specific applications.

In recent years, research has been performed for the optical interconnect implementations, such as switching architecture, communication topology, device fabrication and system integration. The optical interconnects can be used not only for SIMD computers but also for multiple-instruction-and-multiple-data (MIMD) computers. Both free-space devices, such as mirror-, prism-, lens-, and hologram-array, acousto-optic devices, and guided wave optical elements, such as fibers, waveguides and their couples, are used as interconnect elements. These new and novel topology may help deliver a competent challenge to practical exploitation of highly parallel optical interconnects in advanced computer design.

1.3 Background

Advanced computer architectures are centered around the concept of parallel processing. For any kind of parallel processing (pipeline processors, array processors, and multiprocessors) interconnect network is one of the main components of its architecture. The multiprocessing computer can be classified into SIMD or MIMD machines. SIMD computers are usually used for vector evaluations, matrix calculations and fast Fourier transformations. Since the structure is simple, the number of processors in a SIMD is much more than in a MIMD computer. For example, the number of processors in NCUBE-10, which is a MIMD computer, is 1,024; while the number of processors in a SIMD Connection Machine 2 is 65,536[1]. This is why more attention is paid to the interconnect networks for SIMD computers. However, the main purpose for either machine is identical: to achieve an efficient interconnect between any two arbitrary processors using as few steps as possible, with a certain reliability and flexibility.

Interconnect networks can be classified into a single-stage or a multiple-stage network. A single-stage network is a switching system with N input selectors (IS) and N output selectors (OS). Each IS and OS is essentially a N-to-D demultiplexer and a M-to-N multiplexer, respectively, where $1<D<N$, and $1<M<N$. The most common crossbar network is a typical single-stage network with $M = D = N$. A single-stage network should realize any arbitrary interconnects, and it should be

reconfigurable. The main draw back of a single-stage network is the power inefficiency and hardware complexity. To overcome this problem, multiple stage networks are presented. A multiple-stage network is described by three characteristic features: the switching function, the network topology, and the control structure. Examples of multiple-stage networks are a nearest neighbor (NN), a hypercube network (HN), a plus-minus 2^i(PM2I), a perfect shuffle (PS) and a Delta network. Usually, the NN, HN, PM2I and PS are used for SIMD computers, while the Delta networks are designed for MIMD computers.

An optical interconnect could be built with free-space or guided-wave interconnect schemes. A guided wave interconnect is based on optical waveguide couplers and fibers. A free-space parallel scheme is classified to space-variant and space-invariant approaches. Computer generated holograms, spatial filters and photorefractive crystals could be used to achieve the space-variant interconnects; while lenses, mirrors and prisms are examples of space-invariant interconnect.

Optical free-space interconnects can employ either a set of individual light emitters and receivers, or a collimated light beam and modulate it spatially. The individual emitter array is easier to control, specially for a relatively small PE array. Recently, inexpensive bit high quality laser emitting diodes (LEDs) (narrow spectrum and small emitting angle) are available.

The are two approaches to complement an optical free-space interconnect: holography or non-holography. Although the holographic approach can perform both space-invariant and space-variant interconnect tasks, its power efficiency and aperture are somehow limited. The non-holographic interconnect approach, such as a imaging system, can proved higher efficiency and a larger aperture. As this dissertation emphasizes, the non-holographic structure is more competitive.

Efficient power utilization, high repetition rate, and low cross talk are the main factors to evaluate an optical interconnect. In a free-space optical interconnect, the processing capacity, measured by the number of PEs being handled, is limited by the power distribution loss, the cross talk, caused by the system

diffraction and aberrations. The interconnect features, such as performance reliability, the processing relativity, in terms of element bit rate (EBR), and power consumption efficiency are studied in details in this thesis.

1.4 References

[1] S. Hunter *et Al*, "Potentials of two-photon based 3-D optical memories for high performance computing," Appl. Opt., 29, 2058-2066 (1990).

[2] A. Guha, J. Bristow, C. Sullivan, and A.Husain, "Optical interconnections for massively parallel architectures," Appl. Opt., 29, 1077-1093 (1990).

[3] A. W. Lohmann, "What classical optics can do for the digital optical computer," Appl. Opt., 25, 1543-1549 (1986).

[4] J. W. Goodman, F. J. Leonberger, S. Y. Kung, and R. A. Athale, "Optical interconnections for VLSI systems," Proc. IEEE 72, 850-866 (1984).

[5] K. Hwang and F. A. Briggs, *Computer Architecture and Parallel Processing* (McGraw-Hill, New York, 1984) ch.5-7.

II NEW OPTICAL IMPLEMENTATION OF CROSSOVER NETWORKS

2.1 Preliminary

One of the major advantages of the crossover network is that interconnects between any two nodes have exactly the same length so that the system's synchronization problems are relieved [1].

A crossover interconnect has N input and N output ports where $N = 2^i$, and i is an integer. Each of the outputs receives signals from two different input ports. In particular, the j^{th} output port where j = 0,1,..., N-1 receives input from m^{th} and n^{th} input ports, where

$$m = \left\{ \left| \frac{N-2j-1}{2} \right| \right\}, \qquad n = \left\{ N - \left| \frac{N-2j-1}{2} \right| \right\} \tag{2.1}$$

where $|p|$ and {p} denote the absolute value of p and the integer equal to or immediately smaller than p, respectively. It has been shown that by keeping the same input-output permutation relation while rearranging the output ports, a simplified input-output relation, i.e.

$$m' = j, \qquad n' = N - j - 1 \tag{2.2}$$

is obtained. A crossover and a rearranged crossover are shown in Fig.2.1, respectively. It can be seen that the rearranged connection consists of two parts: straight connects and cross connects.

Optical implementation of a crossover network was first proposed by J. Jahns and M. J. Murdocca [1]. A Michelson interferometer with a prism grating array as one of reflectors was used to realize the rearranged crossover network. One arm with a mirror performs the straight connections, while the other arm performs the crossing connections using a prism grating reflector. On different stages, prism gratings with various periods were employed to achieve different period crossing permutations. However, this setup can only perform the rearranged optical crossover, whose output set order is changed. The main draw back of this setup

is that the numerical aperture, which is proportional to the space-bandwidth-product (SBP), is limited by the prism array structure. Besides, these prism gratings are difficult to manufacture, especially when the period of the grating is very small.

In this chapter, two new approaches to perform both optical crossover (OCO) and rearranged optical crossover (ROCO) are proposed [2]. One scheme simply uses mirrors and beam splitters, while the other employes a Fresnel zone plate. A potential advantage of these new schemes is that a cascade of several controllable OCO with large numerical aperture is available.

2.2 Free-space Collinear Optical Cross-Over Interconnect

The optical setup, using mirrors and beam-splitters to carry out the operation of Eq.2.1, is illustrated in Fig.2.2. Each processing element (PE) is illuminated by two optical beams whose directions are separated by an angle of 2θ. The two beams are combined at the N identically spaced (with spacing Δl) PEs at the first stage (input ports), which consists of switching devices. Then part of these beams is reflected by two plane mirrors placed on the two sides of input plane. The N identically spaced (Δl) PEs at the second stage are placed parallel to the input plane. Thus, each PE receives signal from the two input ports with a permutation relation as specified by Eq.2.1, by both a direct and a reflected beams. At the advanced stages, $2^i - 1$ additional bi-surface mirrors are needed.

In general, to permute N inputs, I stages of OCOs need to be cascaded, where $I = \log_2 N$. For the i^{th} stage, where $0<i<I$, to realize OCO_i, $2^i = 1$ mirrors are needed. The spacing L_i between the OCO_i input and output planes is

$$L_i = \frac{N \Delta l \, ctg\theta}{2^{i+1}} \tag{2.3}$$

The interconnect quality mainly depends on the geometric spatial dispersion-related signal cross talk and system diffraction. The diffraction is basically a Fresnel diffraction, which is proportional to the propagating distance

[3]. To reduce the diffraction-based channel cross talk, the total distance z between the input and the output planes should be limited. This restriction also limits the numerical aperture of the optical system, and its effect will be discussed in details later in the chapter seven.

2.3 Optical Rearranged Cross-Over Interconnect Using Fresnel Zone Plate

In addition to the permutation rule of Eq.2.1, by rearranging the interconnect output ports, a rearranged optical cross over (ROCO), can also be constructed based on Eq.2.2. It has been indicated that for a ROCO, both collimated and focused optical beams are needed, which can be generated simultaneously by a Fresnel zone plate (FZP).

Illuminated by a collimated plane wave, a normalized 1D FZP can be characterized by the transmission function [4]:

$$T(x) = \frac{1}{2} + \frac{1}{2}\cos\left[2\pi\left(\frac{x}{R}\right)^2\right] \tag{2.4}$$

where R is a FZP distance constant. With collimated illumination light wavelength λ, a FZP can generate a collimated, a diverging and a converging wave simultaneously. The focal length of both the converging and diverging beams is $f_{FZP} = \pm R^2\lambda/2$. To block the converging beam, an optical stop is placed at focal distance $f_{FZP} = R^2\lambda/2$. After the optical stop, a cylindrical lens with focal length of $f \geq 2f_{FZP}$ is used to convert the collimated and the diverging beams to a converging and a collimated beams, respectively. When N ROCO input ports are activated past the lens, N ROCO output are generated at a distance 2f. From Eq.2.4, it is clear that the collimated beam's intensity is four times larger than the corresponding diverging beam. In addition, only a portion of the FZP aperture contributes to the diverging beam. To equalize the two beam intensities, the collimated beam must be attenuated by α, where

$$\alpha = 2\left[\frac{f}{f_{FZP}}\right]^2 \tag{2.5}$$

This attenuation may be performed by inserting a neutral density filter at the beam's crossing point.

An additional advantage of this scheme is its capability of performing 2D permutation of 1D data. A 16-pixel 2D ROCO permutation geometry is shown in Fig.2.3. A 1D data string is arranged in a raster-scan fashion. At the output plane, a 2D detector array is placed in an identical raster-scan fashion. When a 2D FZP together with a spherical lens replaces their corresponding 1D elements, a 2D ROCO of 1D data can be performed in the setup shown in Fig.2.4. In this case, while the collimated beams transmit the data between the identically numbered input and output ports, the converging beams, after crossing on the optical axis, link the correspondingly numbered input and output ports, as specified by Eq.2.2. As a result, the use of a 2D ROCO leads to a larger input data density and a higher interconnect efficiency than 1D counterpart.

2.4 Control of Interconnect Direction

The most important advantage of these new schemes to implement a crossover is its possibility to control the connect direction, because switching devices are employed at each connect node. For the OCO's cascading, the switching boxes must only change the beam's direction but not their collimation. For this task, an acousto-optic (AO) or electro-optic (EO) deflecting device could be a qualified candidate. To direct the two angular inputs to the two output directions, two back-to-back deflector cell should be used. In Fig.2.5(a), a schematic EO exchange box is sketched. The device contains a switchable layer of ferroelectric liquid-crystal (FELC) [5] material that changes the refractive index upon the applied voltage. This switching layer is sandwiched between two index matching glass prisms. The initial FELC's refractive index is smaller than that of the matching glass. Each input beam is incident at an angle that is larger than the total internal reflection critical angle. For a bypass operation (see Fig.2.5(b)), both inputs are internal reflected. When a appropriate voltage is applied to the FELC layer, the increase of the material's refractive index matches the index of the glass prisms,

and therefore the input beam passes through the FELC layer, indicating an exchange operation (see Fig.2.5(c)). Recently, the FELC material research shows the potential of its applications for high speed cascade ROCO applications [6]. For the FZP approach, an opto-electronic switching is preferred, since the cross-over beam is divergent at the output. To process the ROCO at the next stage, it is easier first to detect the optical signals and switch them electrically, than to regenerate and collimate them optically.

2.5 Proof-of-principle Experimental Results

In our proof-of-priciple experiments a two-stage OCO setup was implemented. A collimated He-Ne laser beam was split and recombined at an angle $\theta = 45^{\circ}$ by an equal ratio beam-splitter. An input plane containing an 8 x 8 array of equally spaced circular holes was illuminated by this beam. The two side-mirrors were front-surface-coated 25.4 X 25.4 mm^2 reflectors. A diffuser screen was placed at the output plane, which is 12 mm past the input plane. Out of the 64 available inputs, only sixteen diagonal inputs were activated while all the other inputs were blocked (see Fig.2.6(a)). Correspondingly, the OCO_0 output pattern was recorded (see Fig.2.6(b)) at the output screen. For a OCO_1 stage implementation, the screen was placed 18 mm past the input plane. An additional 6 X 25.4 mm^2 polished aluminum reflector film (about 250 μm) was used as the second stage's middle reflector. The corresponding output of the OCO_1 is shown in Fig.2.6(c).

A 2D ROCO of 1D signal string was also carried out in our demonstration experiments. A hologram was recorded as a FZP, with a 9 cm focal length and a 20% diffraction efficiency. This Fresnel lens was placed immediately behind the input array and was illuminated by the He-Ne plane wave (see Fig.2.4). The output screen was placed 18 cm behind the FZP. With the input as shown in the Fig2.7(a), the recorded 2D ROCO of the 1D data string is shown in Fig.2.7(b). It was noted that the intensity of the collimated beams were stronger than that of the cross-over beams because of the unbalanced intensities due to holographic diffraction.

2.6 Summary

Two new approaches to implement optical crossover were studied in this chapter. Compared with Jahns's approach, these two new schemes have some potential advantages. First, the numerical aperture can be much larger, since it is only limited by the diffraction due to the propagation length, which is proportional to the aperture. Secondly, a cascade of several OCOs or ROCOs becomes feasible because of the collinear interconnect geometry. Above all, the control of the interconnect direction is possible because switching devices are employed on the location of each node. The features of different switching devices were discussed. Some proof-of-principle experimental results were also presented.

2.7 References

[1] J. Jahns and M. J. Murdocca, "Crossover networks and their optical implementation," Appl. Opt., 27, 3155-3160 (1988).

[2] Y. Li, B. Ha and G. Eichmann, "Free-space collinear optical cross-over interconnects," Appl. Opt. 30, 3288-3293 (1991).

[3] J. W. Goodman, *Introduction to Fourier Optics* (McGraw-Hill, New York, 1968) ch.4.

[4] A. W. Lohmann,"An interferometer with a zone plate as beamsplitter," Optica Acta, 32, 1465-1470 (1985).

[5] N. A. Clark and S. T. Lagerwall, "Submicrosecond bistable electrooptic switching in liquid crystals." Appl. Phys. Lett., 36, 899-901 (1980).

[6] K. M. Johson, M. R. Surette and J. Shamir, "Optical interconnection network using polarzation-based ferroelectic liquid crystal gates," Appl. Opt., 1727-1733 (1988).

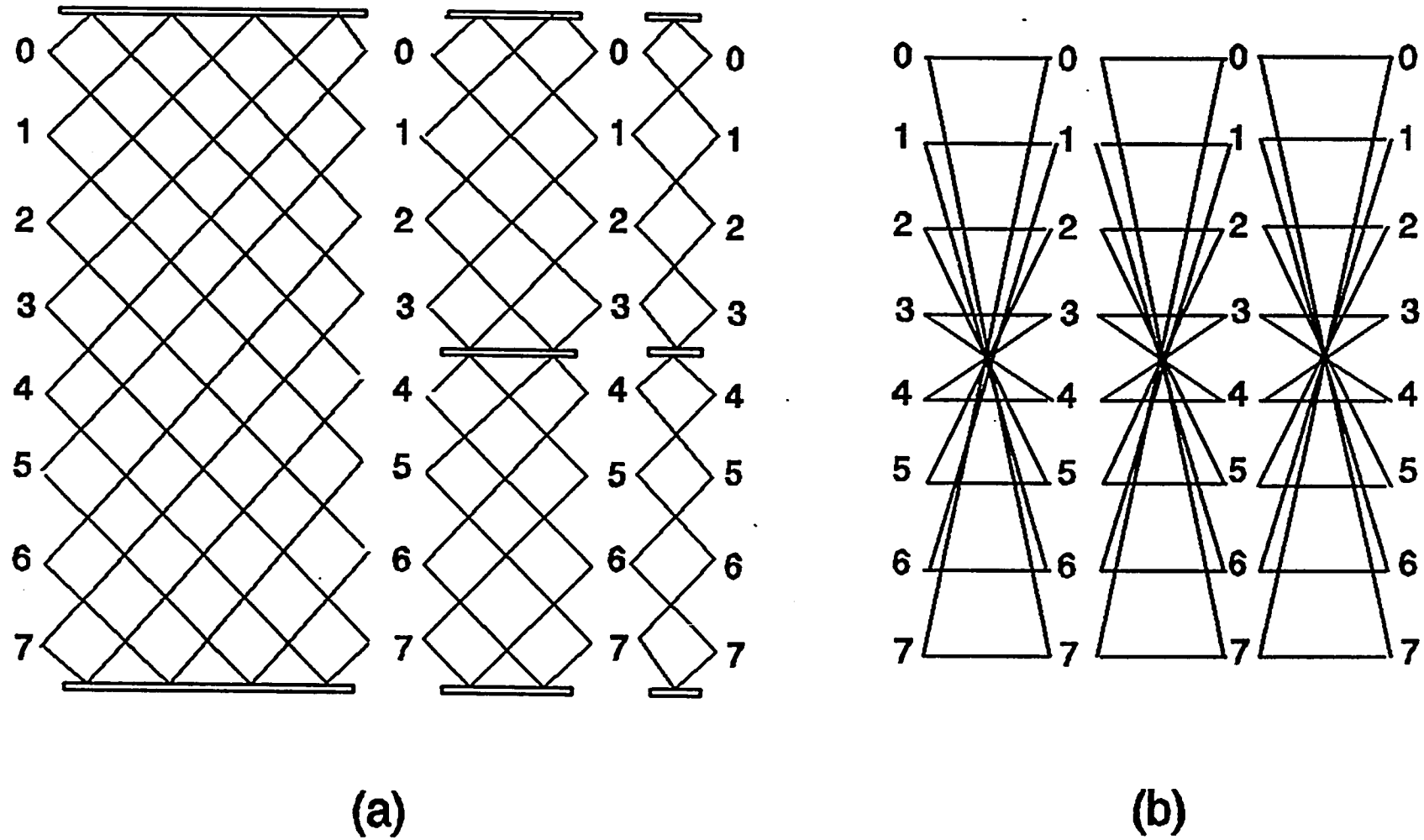

Fig.2.1 (a) A schematic of a crossover network of order 8
(b) A rearranged cross-over network of order 8

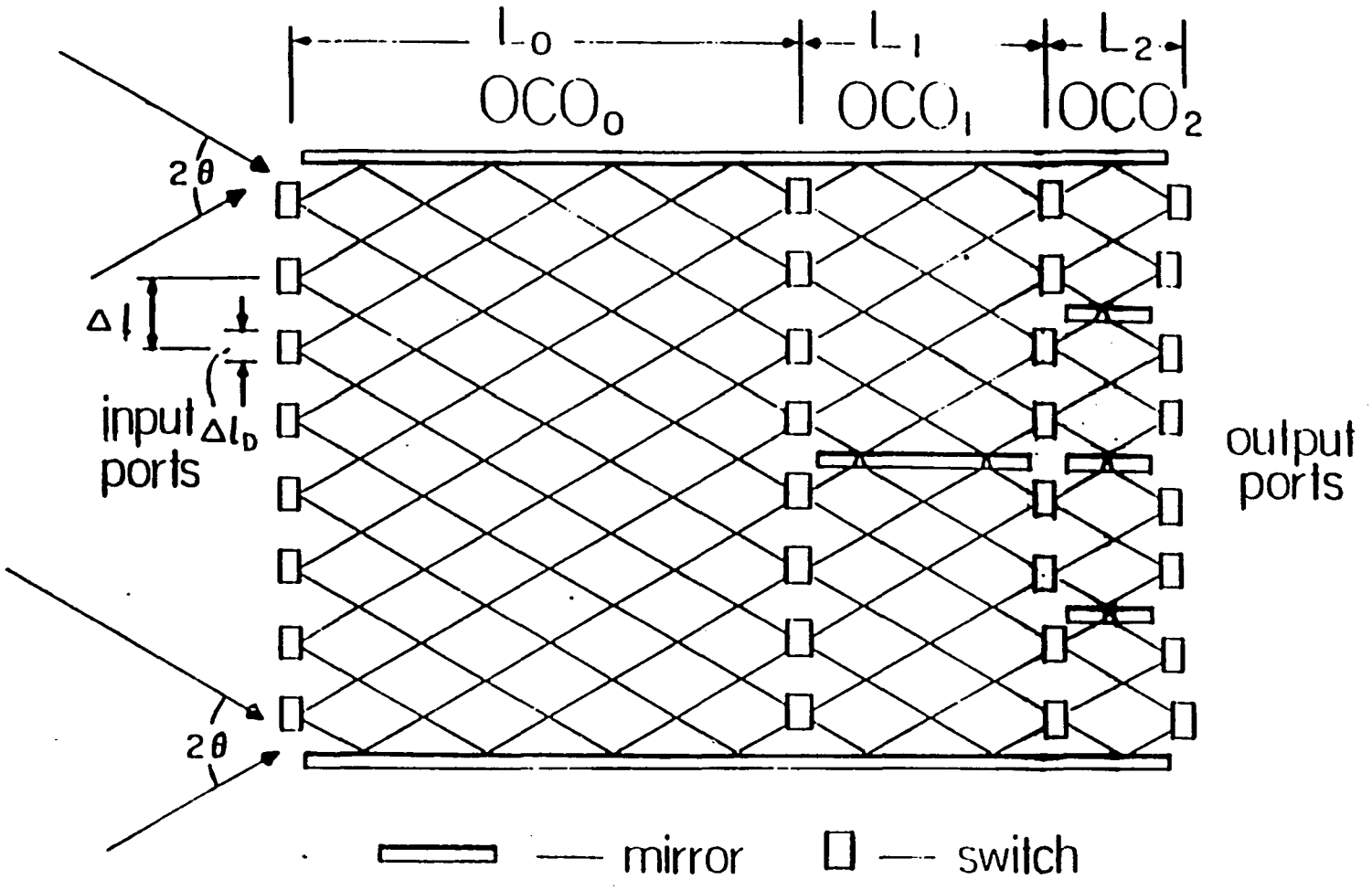

Fig.2.2 A schematic of collinear optical cross-over

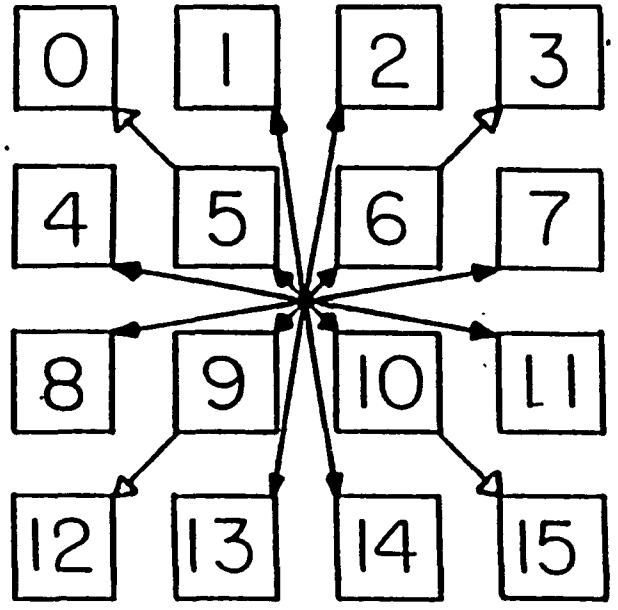

Fig.2.3 A 2D rearranged optical cross-over topology

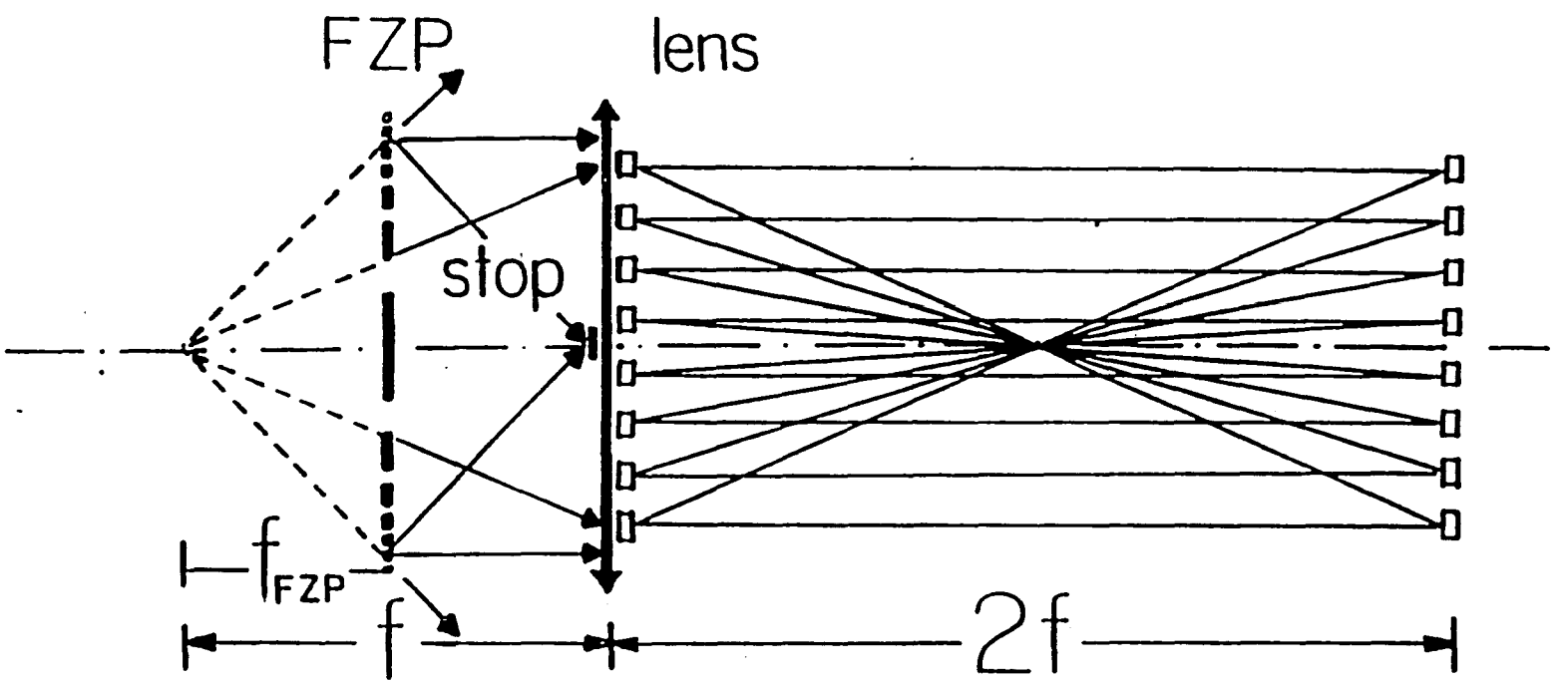

Fig.2.4 A schematic of collinear rearranged cross-over

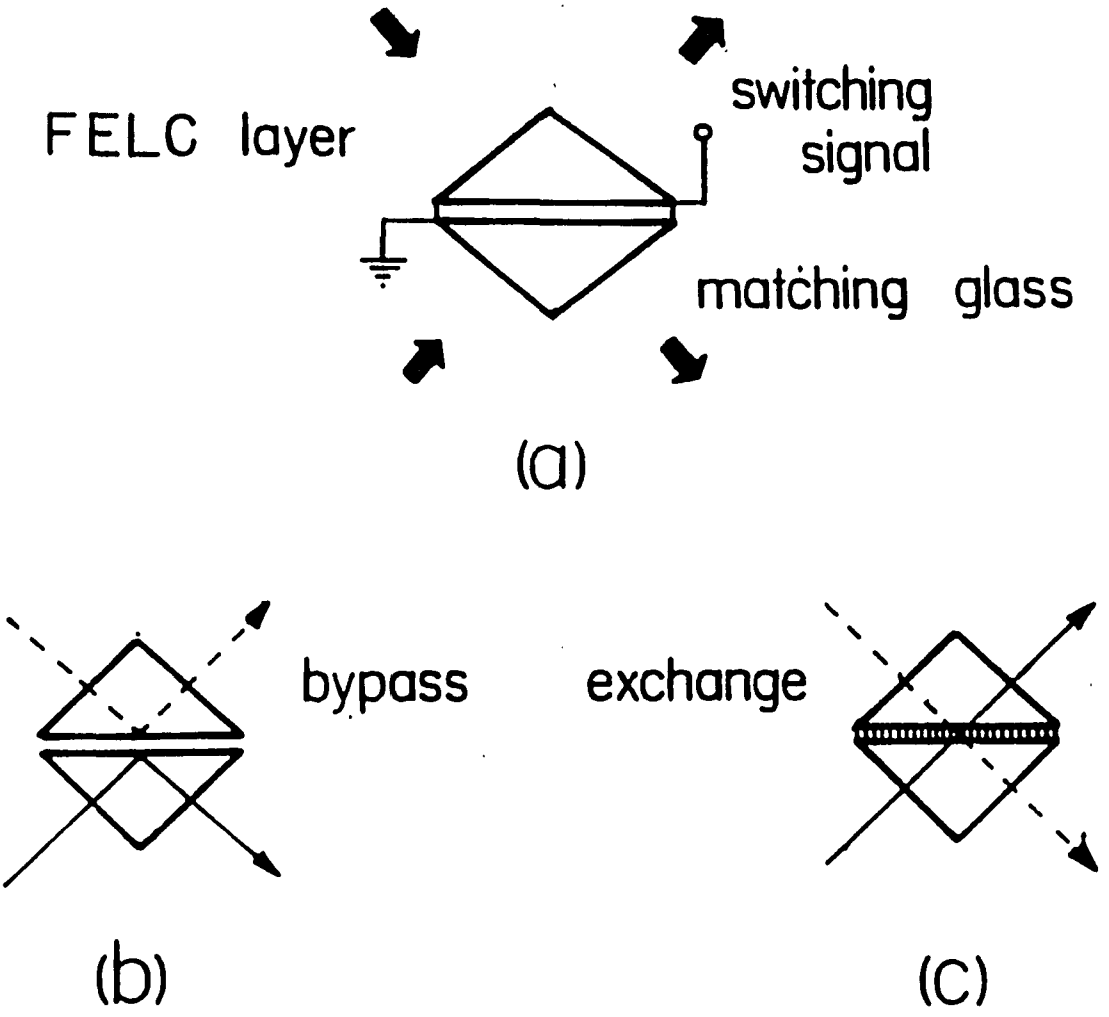

Fig.2.5 (a) A schematic of an electro-optical switching box
(b) The bypass operation performed by switch (a)
(c) The exchange operation performed by switch (a)

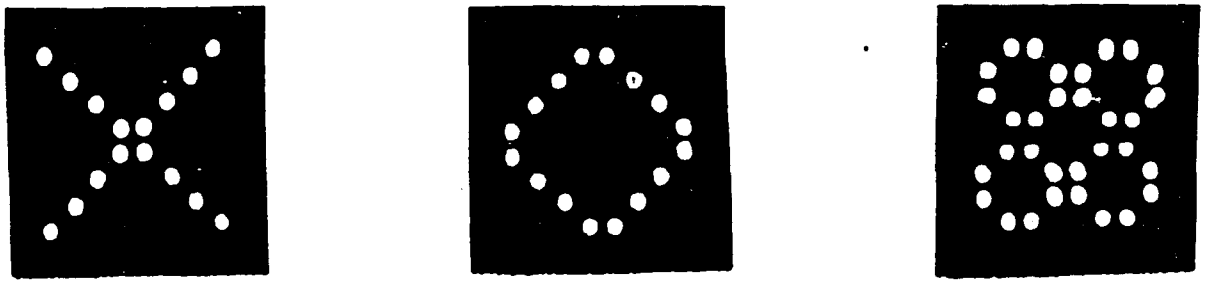

Fig.2.6 Experimental results of a two stage OCO
(a) An 8x8 input pattern for the experiments
(b) The first stage OCO result of the input (a)
(c) The second stage OCO result of input (a)

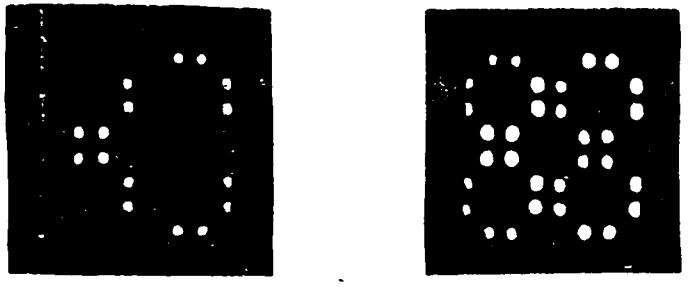

FIg.2.7 Experimental results of a 2D ROCO
(a) The input 1D 8x8 data for a one stage 2D ROCO
(b) The 2D output of the input (a)

III OPTICAL CASCADABLE PERFECT SHUFFLES AND AN OPTICAL DELTA NETWORK FOR MIMD PROCESSORS

3.1 Preliminary

A shuffle is a data permuter widely used to perform data communications in many multiple-stage interconnect networks, such as the Omega network and the Delta networks [1].

Let a binary sequence $A = a_{n-1}...a_1a_2$ represents the vertex (PE) address for $0 \le A \le N-1$, where $n = \log_2 N$. The definition of a perfect shuffle is a cyclic shifting of the bits to the left with one bit position as the S function:

$$S(a_{n-1}...a_1a_0) = a_{n-2}...a_1a_0a_{n-1} \tag{3.1}$$

where $0 \le A \le N-1$ and $n = \log_2 N$. This action corresponds to splitting a linear array of $N = 2^n$ items into two halves and interleaving them afterwards, as depicted in Fig. 3.1(a).

To establish the link patterns between stages of the Delta network, a q-shuffle of qc objects, denoted by S_{q*c}, is defined as

$$S_{q*c}(i) = \left(qi + \left[\frac{i}{c}\right]\right) \bmod qc \tag{3.2}$$

where q and c are positive integers, and $0 \le i \le qc-1$. A q-shuffle can be viewed as to splitting a linear array of N=qc objects into q parts and interleaving them afterwards.

The perfect shuffle and q-shuffle interconnect networks have wide applications in sorting, polynomial evaluation, matrix transposition, and discrete Fourier transformation. Because of its wide usage, various optical PS networks have been presented up to now. One optical PE approach was proposed by Lohmann [2]. Four wedges and two positive spherical lenses are used to bend the light beam in order to perform the PS shift (Fig.3.1(b)). The system is 4f long and is not easy to align. To simplify the setup, a negative cylindrical lens array to perform the PS was

suggested by Li and Eichmann [3]. Although the setup is more compact, the cylindrical lens array is not easy to manufacture and the relative positions of these lenses are difficult to adjust. Another folded PS using masking and magnification techniques was presented by Stirk, *et.al.*[4]. Four lenslets perform the magnification and shifting operations by overlapping the quadrants at the output plane. Yu and his co-workers also presented an optical PS using an optical spatial filter [5]. The spatial filter at the Fourier transform plane shifts the position of the input set. However, the spaces between the elements at the output plane are not uniform.

3.2 Conditions for a Cascadable Perfect Shuffle

Basically, the shuffles are used to perform the data permutation among stages in a multiple stage network, and therefore a cascadable PS performance is necessary. For example, to build a Delta or a Omega network, a number of PE stages is needed. However, the above mentioned approaches can not provide a cascadable operation. Besides, the entire system is difficult to align, because the perfect shuffle permutation is only obtained at one specific output plane.

In order to realize an optical cascadable PS, two conditions must be satisfied. (1) The collimated light illumination for every stage, implying that the output beam from every stage must be kept as a plane wave; (2) The spacing between the output nodes should be equal to the input node's space. Up to now, however, all the existing proposed optical PS can not satisfy these two conditions. For example, using Lohmann's scheme (see Fig.3.2), although the PS permutation can be obtained at a specific plane, after passing through the two lenses and four wedges, the light rays bend with different angles, and the illumination beam is not a plane wave any more at the output plane. Besides, the spacing among the PEs at the output plane is not uniform. The same problems happen to the other presented approaches. To solve these problems, a new optical implementation of PS and q-shuffle is proposed to generate more useful multiple-stage optical PS and q-shuffle networks.

3.3 New Cascadable Optical Shuffles

The novel optical PS is based on the shifting and folding technique. A schematic of an eight node PS is shown in Fig.3.2. The eight nodes are split to two subsequences. One subsequence, containing nodes 1-4, propagates straight forward the output plane, while the other subsequence (nodes 5-8) is flipped over in the order of 8-5. A mask is used to block a half of the apertures in lower part for the 1-4 nodes and in higher part for the 5-8 nodes. The overlapped two subsequences form a perfect shuffle permutation on the output plane. The important feature of this setup is the light beam keeps as a collimated beam, and it is possible to connect a second stage past the output plane. Basically, we can have as many stages as we want. The setup is simple and easy to align because the position of the output plane can be any where along the propagation direction, not limited to a particular position.

To satisfy the second condition, the size and the spacing of the output sequence should be exactly the same as that at its input plane. Since the input apertures are halfway blocked, the beam profile size of the output set is a half of the input set. In order to keep the beam size on one dimension while shrink the beam size along the other dimension, a Brewster telescope is used. The Brewster telescope can convert a square-shaped beam into a rectangular one with an aspect ratio of 2:1. It magnifies the input data to twice the size on one dimension and keeps its size on the other dimension. Then a mask is used to block the useless half part. Finally the output sequence has identical size to the input sequence in both dimensions.

The optical elements (OEs) used in this system include prisms and beam-splitters, which are simple and inexpensive. Except the wedge prisms, these OEs only perform reflections, and therefore can generate perfect images. This design, together with the perfect imaging ability of the optical elements, creates an opportunity to reduce the cross talk. An additional advantage of this new OPS allows for an array of data to be processed in parallel.

The disadvantage of this scheme is the inefficient utilization of the light power due to the masking. However, the most common case to use the perfect shuffle is to communicate among the MIMD processors with less than four stages, and therefore power loss is not a main problem.

3.4 Optical Delta Networks for MIMD Computers

In order to achieve the communication between processors within a MIMD computer, multiple stage networks are required. A typical MIMD network is a delta network, which is a rearrangeable and nonblocking network. The delta network is defined as an $a^n X b^n$ switching network with n stages consisting of a X b crossbar modules. The link patterns between stages are q-shuffles, and q is equal to a here (Fig.3.3). The requirement for an optical delta network is that all the crossbars and the q-shuffles should be used in a serial fashion. Up to now, optical Delta network implementation has not yet been presented. The new optical q-shuffle approach proposed here offers a chance to implement an optical Delta network. Employing the same technique explained in the last section, separating the light beam to q- parts rather than two parts, an optical q-shuffle can be easily established. Using cylindrical lenses and a SLM as a mask, an optical crossbar network is also available. Therefore a Delta network is possible to be built optically for the MIMD computers.

3.5 Summary

In this chapter, a new approach to implement optical shuffle network was studied. Compared with the presented optical perfect shuffles, this new scheme can offer a cascadable, inexpensive, low-crosstalk perfect shuffles and q-shuffles. These cascadable optical shuffles make it possible to employ optical devices to perform interconnects among various useful networks for both SIMD and MIMD computers.

3.6 References

[1] K. Hwang and F. A. Briggs, *Computer Architecture and Parallel Processing* (McGraw-Hill, New York, 1984), ch.5.

[2] A. W. Lohmann, "What classical optics can do for the digital optical computer," Appl. Opt., 25, 1543-1549 (1986).

[3] G. Eichmann and Y. Li, "Compact optical generalized perfect shuffle," Appl. Opt., 26, 1167-1169 (1987).

[4] C. W. Stirk, R. A. Athale and M. W. Haney, "Folded perfect shuffle optical processor," Appl. Opt., 27, 202-203 (1988).

[5] Q. W. Song, and F. T. S. Yu, "Generalized perfect shuffle using optical spatial filtering," Appl. Opt., 27, 1222-1223 (1988).

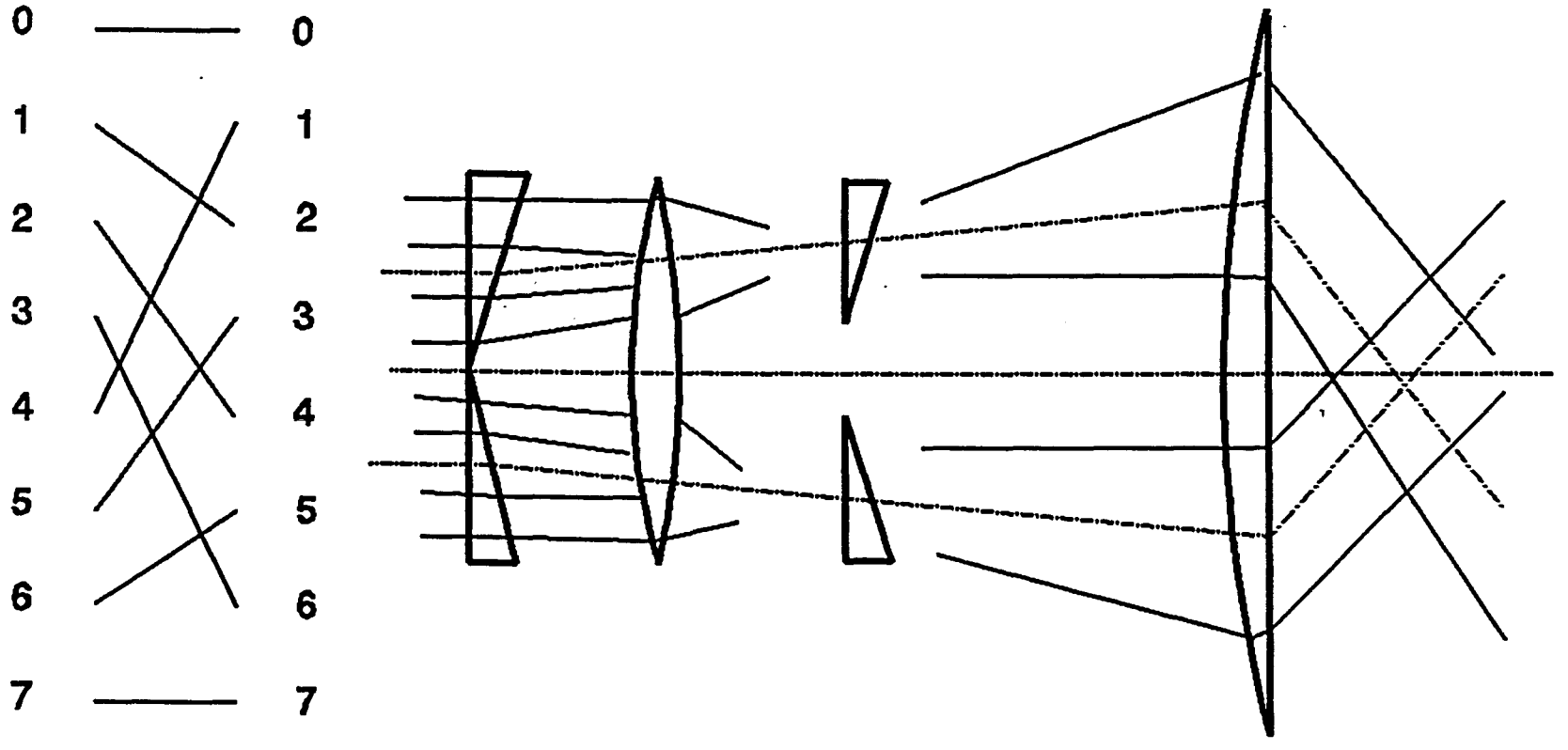

Fig.3.1 (a) A schematic of perfect shuffle in the order of 8
(b) Lohnmann's approach of optical perfect shuffle

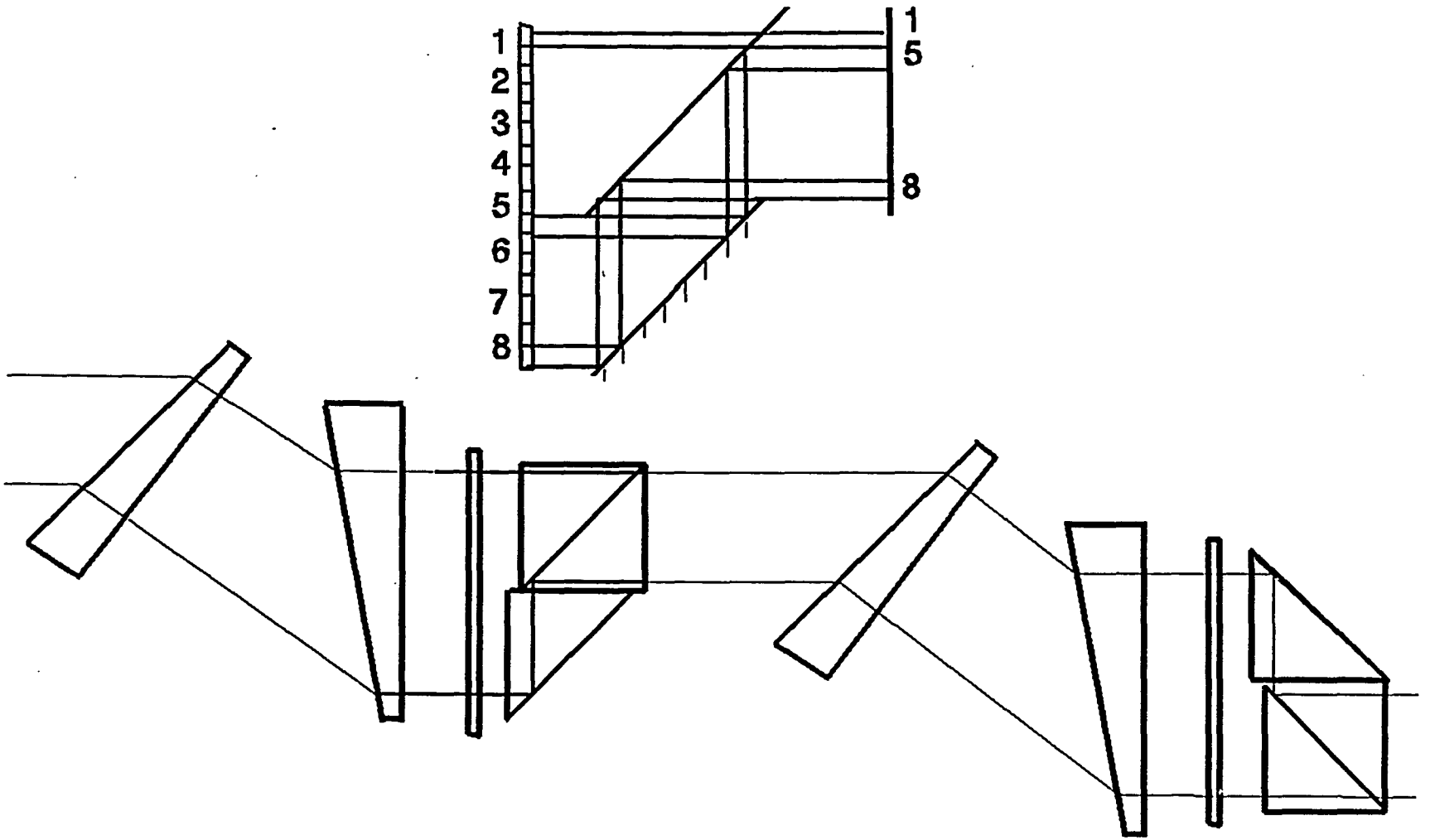

Fig.3.2 A cascadable optical perfect shuffle in order of 8

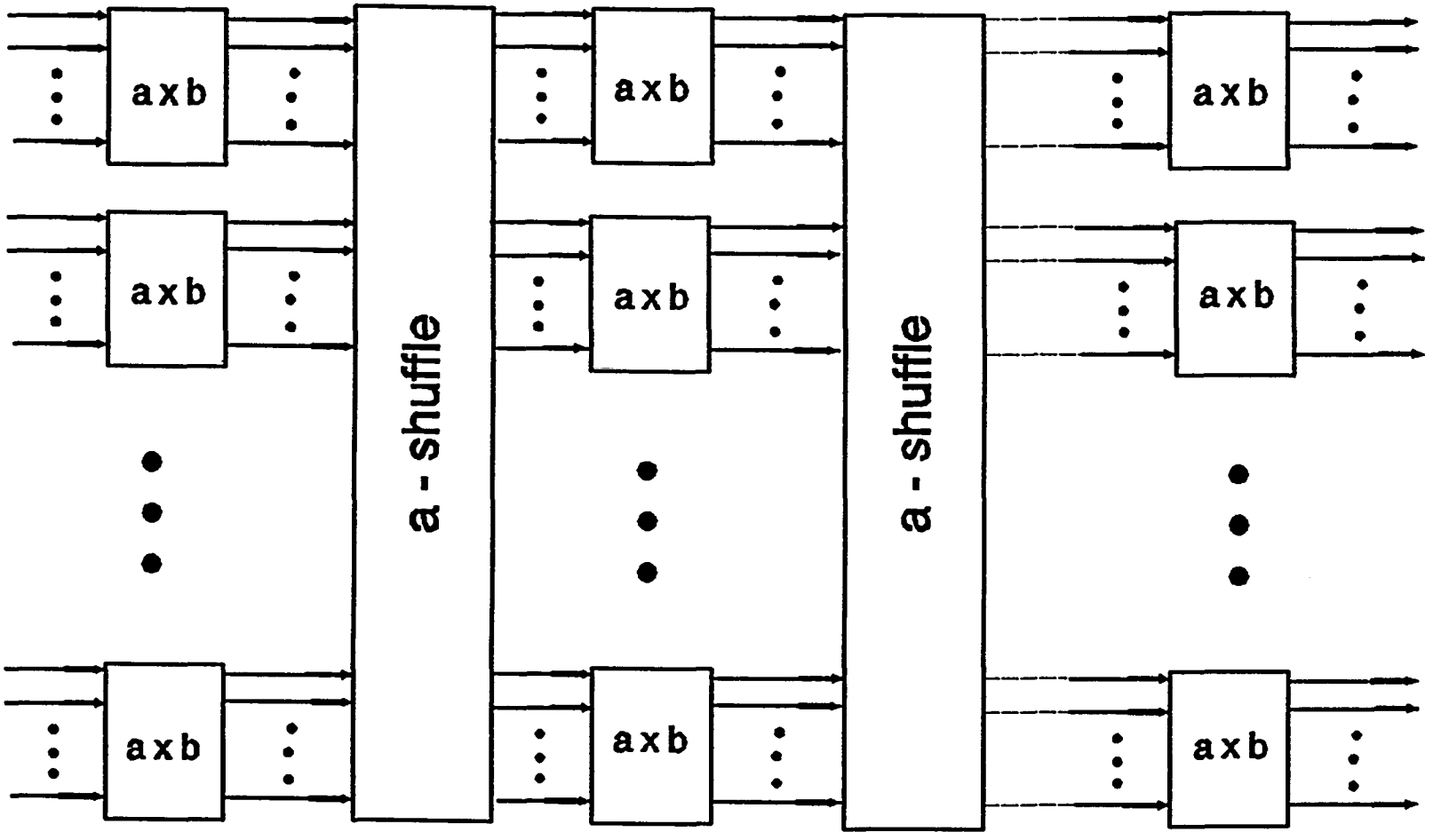

Fig.3.3 A schematic of a delta network using a-shuffles

IV OPTICAL BINARY SYMMETRIC LOGIC NETWORKS

4.1 Preliminary

An important class of Boolean logic functions is the so-called binary symmetric logical function (BSLF) [1]-[5], which is invariant under the permutation of its variables. An array of optical contact switches and a regular interconnect scheme are introduced to implement an optical binary symmetric logic network (OBSLN). An OBSLN could be considered as a gate-level interconnect network used to perform certain binary logic computing tasks. Instead of logic gate operation, this new interconnect-based technique provides a fast and efficient way of executing various binary symmetric logic computations. In this chapter, various OBSLN architectures are studied, together with their applications to optical digital, symbolic and neural computing, data communication, signal and image processing. Some proof-of-principle experiments are demonstrated, and some optical implementation issues are also discussed.

4.2 Binary Symmetric Logic Function (BSLF)

A function f of n variables $(x_1, x_2, \ldots, x_n)$ is called a binary symmetric (or completely symmetric) logic function (BSLF) , if and only if it is invariant under any permutations of its variables ; it is called partially symmetric in the variables x_i and x_j if and only if the interchange of the variables x_i and x_j does not change the functions [1]. For example, the function

$$f_1(x,y,z) = \bar{x}\bar{y}\bar{z} \tag{4.1(1)}$$

$$f_2(x,y,z) = \bar{x}\bar{y}z + x\bar{y}\bar{z} + \bar{x}y\bar{z} \tag{4.1(2)}$$

$$f_3(x,y,z) = \bar{x}yz + x\bar{y}z + xy\bar{z} \tag{4.1(3)}$$

$$f_4 = xyz \tag{4.1(4)}$$

are symmetric with respect to the variables x, y, and z, where the overbar denotes the logic complement; while the function

$$g(x,y,z)=\bar{x}\bar{y}z+x\bar{y}\bar{z} \tag{4.2}$$

is partially symmetric in x and $\bar{z}$.

The maximum number of completely symmetric functions of n variables is n+1. For a partially symmetric logic function, the variables in which a function is symmetric are called the variables of symmetry. It has been shown that a necessary and sufficient condition for a function f $(x_1, x_2, \ldots, x_n)$ to be symmetric is that it can be specified by a set of numbers $[\alpha_1, \alpha_2, \ldots, \alpha_k]$, where $0 \le \alpha_i \le n$, such that the function assumes the value 1 only when α_i of the variables are equal to 1. The numbers $[\alpha_1, \alpha_2, \ldots, \alpha_k]$ are called the a-numbers. Thus a symmetric function can be denoted as $S_{\alpha_1,\alpha_2,\ldots,\alpha_k}(x_1, x_2, \ldots x_n)$, where S designates the symmetry property, the subscripts $\alpha_1, \alpha_2, \ldots, \alpha_k$ designate the a-numbres, and $(x_1, x_2, \ldots, x_n)$ designate the variables of symmetry. Using this definition, $f_1(x,y,z), f_2(x,y,z), f_3(x,y,z), f_4(x,y,z)$ and $g(x,y,z)$ can be rewritten as $S_0(x,y,z), S_1(x,y,z), S_2(x,y,z), S_3(x,y,z)$ and $S_2(x,y,\bar{z})$, respectively.

Both a completely and a partially symmetric function can be synthesized by an interconnected array of contact switches in a regular geometry. Since logic AND operation can be achieved by a cascade of contact switches, a triangular lattice pattern can perform such an interconnect task. All of the make- (break-) contact switches are inserted into the network's horizontal (vertical) sections. Each of the n+1 output ports is linked with a common input source by k different paths, where n is the number of the variables and k is the number of minterms. For example, the symmetric function Eq.4.1 can be realized by a triangular array of contact switches shown in Fig.4.1. The Four possible symmetric functions Eq.4.1(1) to Eq.4.1(4) are available at its four ports.

4.3 Optical Contact Switches

The key elements for an optical implementation of BSLFs are the optical contact switches. To construct a contact network, two basic elements must be established: a switch and an interconnect used for both splitting and combining

the transfer signals. An optical interconnect can be either a beamsplitter or a wave-guide. Optics can be used to build a contact switch with a fast switching speed and high power efficiency.

A simple optical contact switch is an optical bistable etalon [6][7] which is controlled by a switching beam (see Fig.4.2(a)). Its cavity length is designed so that at the initial state, the light is either totally transmitted or totally blocked. Upon activation of the switching beam, the total power in cavity reaches an activation threshold, resulting in either blocking of the transmitted signal (for a break-contact) or passing of the blocked signal (for a make-contact). Depending on the materials used, the nonlinear etalon switching speed has been reported to a range from microseconds to picoseconds [3]. Another new optical bistable switch is a self-electro-optic-effect device (SEED) [8], which requires much less switching power than a conventional bistable switch and could be a better candidate for an optical contact switch application.

A polarization switching element can also form an optical contact switch, for which a possible candidate is the so-called surface-stabilized ferroelectric liquid crystal (SSFLC) devices [9][10] together with a polarization beamsplitter. A SSFLC consists of a thin layer of ferroelectric liquid-crystal and it acts as an EO-switchable half-wave plate. When an SSFLC is placed in front of a polarizing beamsplitter, an EO polarization transfer-contact switch is formed (Fig.4.2 (B)). A recent study showed that for a 1000x1000 SSFLC switch array with a 10 W/cm^2 power dissipation, a megahertz frame rate can be pursued.

The acousto-optic device, such as a Bragg cell (Fig.4.2(c)), can also perform as a good contact switch. Application of a RF signal to a transducer generates an acoustic pressure which modulates an AO material in a direction perpendicular to the input optical beam. When the Bragg condition is satisfied, the beam is deflected to a new output direction. Depending on its direction assignment, an AO deflector may act as a make-, a beak- or a transfer-contact switch. Controlled by a RF

signal, two deflection angles of the output beam indicate the two output directions. With this device, a deflection efficiency of almost 100% of 500mW with 600MHz repetition rate for 3 dB bandwidth has been observed [11].

Additional choice of the contact switches is the wave guide directional coupler (WDC)(Fig.4.2(d))[12]. The WDCs are so designed that without an external signal they guide the input light to either I_1-O_1 or I_2-O_2 . While an external electric field is applied, the signal will be coupled to either I_1-O_2 or I_2-O_1 channels as a result of the nonlinear interaction of the optical wave and electric field inside the material. Using a single input and double output channels, a directional-coupler-based EO transfer-contact can be obtained. Recent research has demonstrated that with a GaAs traveling-wave geometry, an EO modulation bandwidth in excess 20 GHz is possible [13].

4.4 Optical Binary Symmetric Logic Network (OBSLN)

Based on the various optical contact switches described, together with different interconnect elements, an optical implementation of the binary symmetric logic functions can be realized. Both free-space and guided-wave optical contact switches are used to implement the OBSLN. To synthesize an OBSLN, two conditions have to be satisfied. First, the optical network must have a source, n control input ports, and n+1 output ports, each of which generates a particular a-number BSLF. Secondly, each a-number output channel should create a logic OR function for its corresponding k minterms.

4.4.1 Free-space Schemes and Guided Wave Schemes

To satisfy the first condition, either free-space or guided wave interconnect schemes can be employed. The first approach consists of beam-splitters to form a triangular lattice array, with optical make- (break-) switches and 50/50 splitting ratio beamsplitter forming its branches (Fig.4.3(a)). Since the optically switched signal must reach one of the possible output ports, none of the optical energy from the input ports is wasted. The total number of beamsplitters and switches needed for an n variables OBSLN are p and q, respectively, where

$$p = \frac{(n+1)(n+2)}{2}, \quad q = (n+1)n \tag{4.3}$$

Fig.4.3(b) shows a guided-wave interconnect scheme using an array of optical transfer-contact switches. To merge the outputs of the two previous stages into the next transfer-contact's input port, a Y junction combiner or an integrated optical directional coupler [12][13][14] could be employed. For an OBSLN with n variables, a number p' of transfer-contact switches and q' of Y combiners are used, where

$$p' = \frac{(n+1)n}{2}, \quad q' = \frac{(n-1)n}{2} \tag{4.4}$$

It is obvious that this scheme uses reduced number of optical elements than the free-space scheme. An additional advantage of this scheme is that only logic variables but their complements are needed to control the array.

4.4.2 Optical Logic OR Operation

For both approaches, the logic OR operations are achieved automatically because the result of an a-number BSLF emerges to one port. If the function is symmetric with more than one a-number, a cylindrical lens should be used to realize the OR function. To generate a combination of various a-number outputs, an optical spatial light modulator (SLM) should be used, together with a cylindrical lens that selects the outputs of the corresponding a-number channels.

For some BSLF applications, not all n+1 a-number outputs are required. In this case, as a reduced BSLF circuit, various BSLF network reduction methods can be used. The first type of reduction excludes those branches that are connected to unused output ports. A second type of reduction merges more branches pertaining to an identical logic variable. When the a-numbers form an arithmetic progression contains all possible integer numbers between a start

integer and n, the reduction can be achieved by folding method [2]. All these reduction methods are not difficult to be carried out by optical components such as mirrors, beamsplitters, lenses or prisms.

4.4.3 Optical Implementation Considerations

To satisfy a real-time OBSLN-based computation requirement, the network power consumption needs to be considered. Using optical nonlinear-etalon-based switches, it is possible to reduce the switching energy to the picojoules level. An analysis of an SSFLC has shown that for a minimum switching area of $4\mu m^2$ with a 2 μs switching speed, 1 pJ switch is achievable [10]. Since an OBSLN processes data in a synchronized wave propagation fashion, no extra cycle time-integration is needed, and data can be fetched into the network in a systolic fashion.

For the free-space OBSLN, diffraction through a gapped array of switches and beamsplitters may result in signal spatial channel broadening and crosstalk. For a large-array application, an integrated micro relay lens array should be used to reduce diffraction by changing the object projecting to imaging. Another issue needed to be taken into account is the OBSLNs asymmetric power requirement. Compared with the first logic variable, the control of the last logic variable requires a larger amount of power.

4.5 Applications of the OBSLN

There are various applications of the OBSLN, including optical digital and symbolic computation, data communication, text processing, imaging processing and neural networks. As some examples, a full adder, a parity checker, a weighted threshold element, and a counter based parallel multiplier, with a high speed and efficient power consumption, are suggested [2].

4.5.1 An Optical Full Adder

Basically, any arithmetic computation can be decomposed into binary additions together with some logic operations, the implementation of a fast

adder has attracted increasing interest. Because an electronic digital full adder is limited by the switching speed of the electronic logic gate employed, extensive research has been conducted to seek a higher-speed optical full adder device. In this sub-section, an OBSLN-based approach for a fast optical full adder is investigated.

The bitwise full adder sum S'_i and carry C_{i-1} as a function of the input A_i, B_i, and C_i can be expressed as

$$S'_i = A_i \oplus B_i \oplus C_{i-1}$$
$$C_i = (A_i \cdot B_i) \oplus (B_i \cdot C_{i-1}) \oplus (C_{i-1} \cdot A_i) \qquad (4.5)$$

where $\oplus$ and $\cdot$ denote Boolean XOR and AND operations, respectively. It also can be rewritten as two BSLFs, $S_{1,3}(A_i, B_i, C_{i-1})$ and $S_{2,3}(A_i, B_i, C_{i-1})$, respectively. Using an array of three variable free-space or guided-wave OBSLNs, together with two SLMs and two cylindrical lenses, both the sum and the carry can be generated optically. Here, the SLMs are programmed to only select the outputs α_1, α_2 for the sum and α_2, α_3 for the carry, and to block all other outputs. Because the optical switching is potentially faster than electronic ones, the OBSLN-based full adders can work with higher speed than the electronic gate-based adders. In addition, instead of using three AND and four XOR as the gate-based full adder, the guided-wave OBSLN only implies six active elements. Thus, this new approach offers not only a potential speed advantage but also a computation efficiency.

4.5.2 Parity Checker and Weighted Threshold Element

The mathematical expressions for an even (odd) parity checker is a binary multiple-variable XOR (XNOR) logic function. One approach to perform this function is to decompose a large dynamic range XOR device into a set of small dynamic range optical switches which can be realized by an OBSLN. The OBSLN-based parity checker selects all α_{odd} or α_{even} channels for the even or odd parity, respectively.

Using an OBSLN, a programmable optical binary-weighted threshold element can also be implemented. For an OBSLN that generates an n-input BSLF $S_{0,1,\ldots,n}(x_1, x_2, \ldots, x_n)$, an optical summer at a threshold level of j is realized by grouping its output ports correspondingly to the a-number from j to n. This grouping can be performed optically by adjusting the spatial blocking positions of a SLM placed in front of the summing cylindrical lens.

4.5.3 Fast Digital Optical Multiplication

Fast digital optical multiplication using an array of binary symmetrical logic counters is another good application of the OBSLN [15]. As an example, Fig.4.5 shows a multiplication of two four-bit numbers. A novel optical (3,2) and (7,3) counters are used to process the partial products $m_1, m_2, \ldots, m_7$. For this example, four (7,3) and two (3,2) counters are needed, and the (3,2) counter acutely is a full adder (see Fig.4.5). These counters can be formed by OBSLNs, using the same technique described in previous sections (see Fig.4.6). The inputs to each counter may include inputs from the partial product (denoted as $U_0 - U_6$) and the outputs from the previous stage counters. Instead of processing in serial, the counter based multiplication can operate in a serial-parallel fashion, which offers a much higher speed.

As a possible opto-electronic implementation, an OBSLN counter-based 8-bit binary digital multiplier architecture is sketched (see Fig.4.7). This multiplier contains three main parts: a parallel partial product generator, an optical counter array and an electronic feedback network. The two 8-bit input A and B are introduced into an optical cross-bar generator, creating a parallel array of 64 light dots, each representing a partial product. The possible hardware devices of the partial product generator could be various electro-optic, acousto-optic, and nonlinear optical SLMs. A total of fourteen OBSLN counters are employed to carry out the fifteen minterms $m_1, m_2, \ldots, m_{15}$ by diagonally grouping the partial product outputs. Part of the counter results are fedback with a passive feedback network to the neighboring counters. When all the

counters complete their count, the final multiplication result is obtained. In this sense, this is a quasi-serial multiplication method, but its potential processing speed is much faster than other serial multiplication schemes.

4.6 Preliminary Experimental Results

To experimentally demonstrate the OBSLN's operational principle, a three variable 8-bit free-space OBSLN was set up (see Fig.4.4). An Ar^+ ion Laser was spatially filtered and then masked to provide eight biased input channels. For a passive triangular shape interconnect array, seven 50/50 ration beamsplitters were mounted on a special breadboard. To provide exact beam position matching at the output, a 3-D beamsplitter adjustment was used. Also, an identical spacing of 0.5 cm between every two beamsplitters was made. In our proof-of-principle experiments, the switching array consisted of an assembly of binary masks. At each of the two output directions, the three masked biased beam array passes a 2-D SLM and a vertically placed cylindrical lens before reaching an optical detector.

The first experiment was a full addition operation of A=11001011, B=01101101, and the carry-in C_{in} =01001101. The insertion of an array of binary switching masks represents the three digital numbers and their logic complements (see Fig.4.8(a)). Using two additional masks that select the $S_{1,3}(A, B, C_{in})$ and $S_{2,3}(A, B, C_{in})$ for the two outputs (Fig.4.8(b)), the selected patterns are displayed. Finally, at the focal planes of the two cylindrical lenses, an 8-bit optical full addition sum S=1101011 and carry C_{out} =01001101 were obtained (Fig.4.8(c)).

Using the same input strings and a combination of BSLF selection masks that select the output's even and odd columns, an optical parity checking operation was also implemented. Fig.4.9 shows the results $S_{0,2}$ and $S_{1,3}$ for odd and even parity check, obtained before and after the final cylindrical-lens-based logic OR operation, respectively.

As a programmable OBSLN-based four-level threshold summer for the previous input string, different level of thresholding were performed. The threshold level 1, 2, 3 are equivalent to the BSLFs $S_{1,2,3}, S_{2,3}$, and S_3 , respectively. By

programming the output SLM to block the corresponding a-number channels, the above-mentioned BSLFs were obtained. The thresholding experimental BSLF results are presented in Fig.4.10.

4.7 Summary

In this chapter, an optical contact-network-based computation method was introduced. Instead of gate-based logic computation, a novel concept of interconnecting an regular array of contact-switches to realize the binary logic computation was presented. The main advantages of the OBSLN devices are the efficient utilization of the optical power, the high processing speed and the propagation synchronization. Secondly, it can replace a large dynamic range device by a network of smaller dynamic range switches. Besides, it also allows for a programmable BSLF network implementation so that by choice of different a-number channels, a single BSLF device can implement various computation applications simultaneously.

4.8 References

[1] Z. Kohavi, *Switching and Finite Automata theory*, Ch.6, McGraw-Hill, New York (1978).

[2] Y. Li, B. Ha and G. Eichmann, "Optical Binary Symmetric Logic Functions and Their Applications", Opt. Eng. Vol.28, 380-389 (1989).

[3] G. J. Klir, *Introduction to the Methodology of Switching Circuits*, Chaps. 5 and 6, D. Van Nostrand Co., New York (1972).

[4] M. P. Marcus, "The detection and identification of symmetric switching functions," IRE Trans. Electron. Comput. EC-5, 237 (1956).

[5] R. F. Arnold and M. A. Harrison, "Algebraic properties of symmetric and partial symmetric functions," IEEE Trans. comput. EC-12, 244 (1963).

[6] H. M. Gibbs, S. L. McCall and T. N. C. Venkatesan, "Differential gain and bistability using sodium-filled Fabry-Perot interferometer," Phys. Rev. Lett. 36, 1135 (1976).

[7] J. L. Jewell, Y. H. Lee, H. M. Gibbs, N. Peyghambarian, A. C. Cossard, and W. Wiegmann, "3 pJ 82 MHz optical logic gates in a room temperature GaAs-AlGaAs multiple quantum well etalon," Appl. Phys. Lett., 46, 918 (1985).

[8] D. A. B. Miller, D. S. Chemla, T. C. Damen, T. H. Wood, C. A. Burrurs, A. C. Gossard, and W. Wiegmann, "The quantum well self-electrooptic effect device: optoelectronic bistability and oscillation and self-linearized modulation," IEEE, Quantum Electron, QE-21, 1462 (1985).

[9] N. A. Clark, and S. T. Lagewall, "Submicrosecond bistable electrooptic switching in liquid crystal," App. Phys. Lett., 36, 899 (1980).

[10] K. M. Johson, M. R. Surette, and L. A. Pagano-Stauffer, "Optical computing and image processing with ferroelectric liquid crystals, " Opt. Eng., 26(5), 385-391 (1987).

[11] P. Li, D. Y. Zang and C. S. Tsai, "Integrated electrooptic Bragg modulator modules for matrix-vector and matrix-matrix multiplications," Appl. Opt. 27(9), 1780-1785 (1988).

[12] Y. Surmatsu and S. Arai, "Integrated optics approach for advanced semiconductor laser, "Proc. IEEE 75, 1472 (1987).

[13] S. Y. Wang, S. H. Lin, and Y. M. Houng, "GaAs traveling-wave polarization electrooptic wave guide modulator with bandwidth in excess of 20 GHz at 1.3 μm," Appl. Phys. Lett. 51, 83 (1987).

[14] S. R. Friberg, A. M. Weiner, Y. Siberberg, B. G. Sfez, and P. S. Smith, "Femtosecond switching in a dual-fiber nonlinear coupler," Opt. Lett., 13, 904 (1988).

[15] Y. Li, B. Ha, and G. Eichmann, "Fast Digital Optical Multiplication Using An Array of Binary Symmetric Counters," Appl. Opt. 30, 531-539 (1991).

$f_1(x,y,z)=\bar{x}\bar{y}\bar{z}$

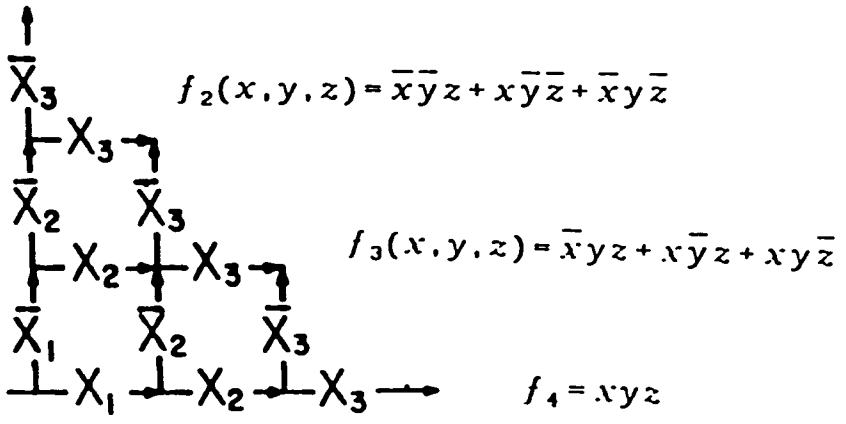

$f_2(x,y,z)=\bar{x}\bar{y}z+x\bar{y}\bar{z}+\bar{x}y\bar{z}$

$f_3(x,y,z)=\bar{x}yz+x\bar{y}z+xy\bar{z}$

$f_4=xyz$

Fig.4.1 An contact switch array to perform a 4-variable BSLF

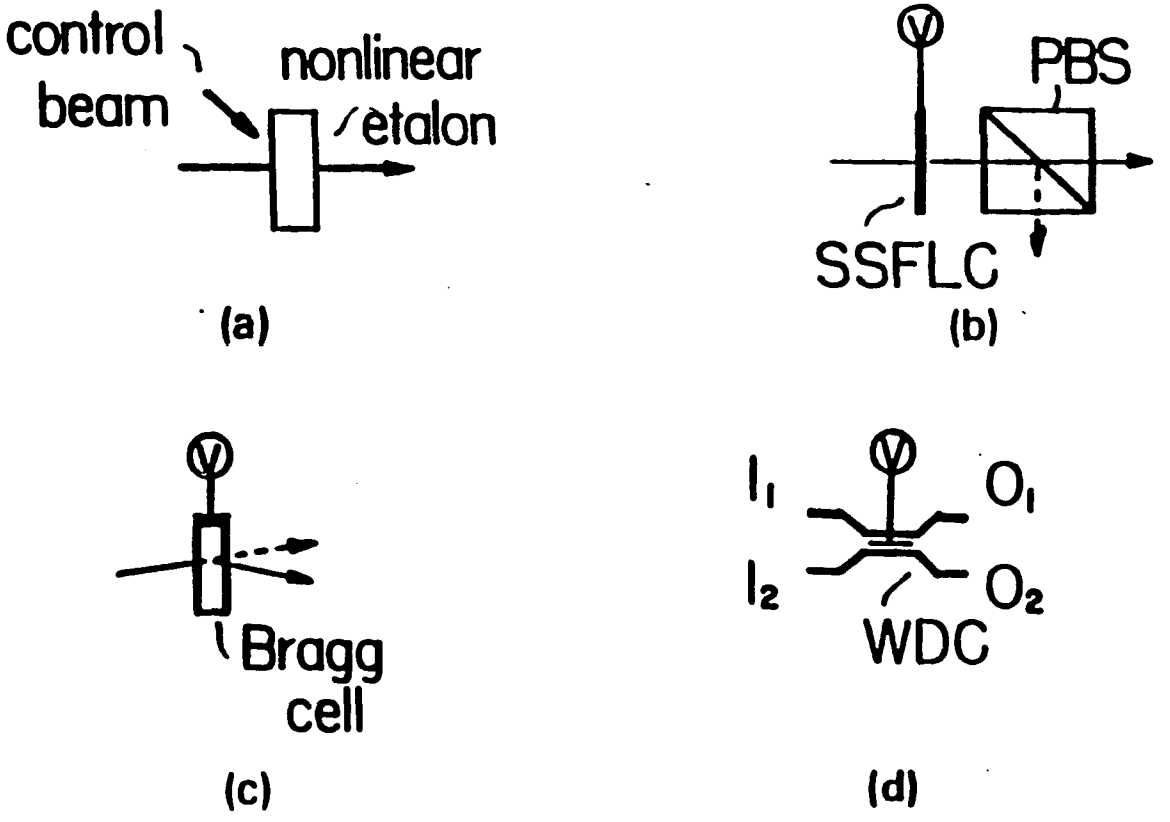

Fig.4.2 Schematics of potential optcal contact switches

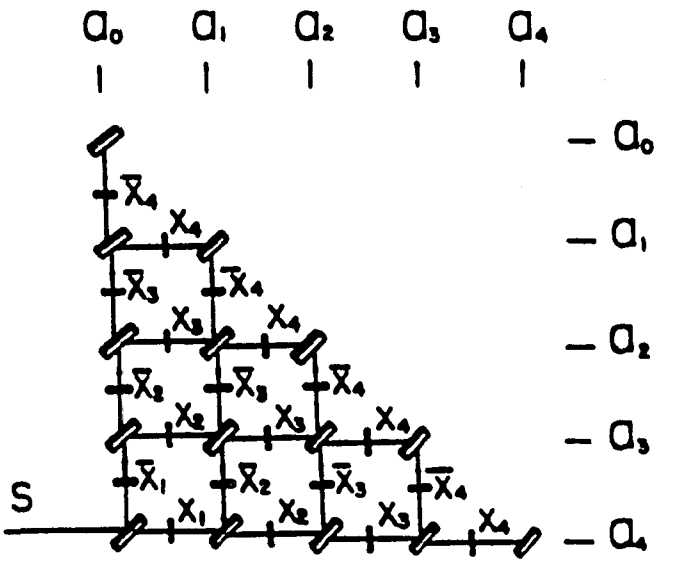

Free-space schematic of a four-variable OBSLM

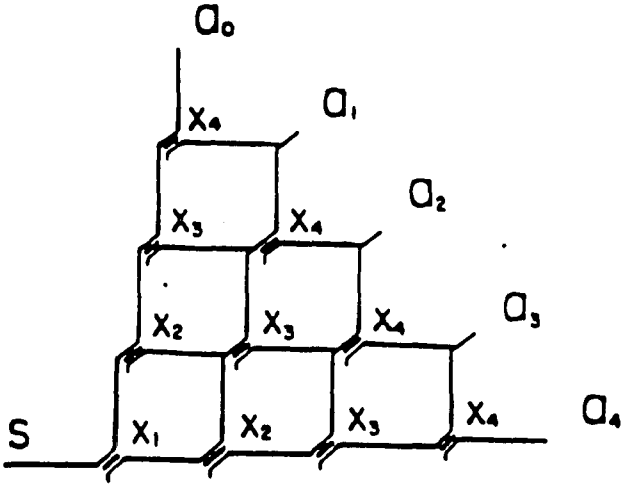

Guided-wave schematic of a four-variable OBSLM

Fig.4.3 An optical binary symmetric logic network

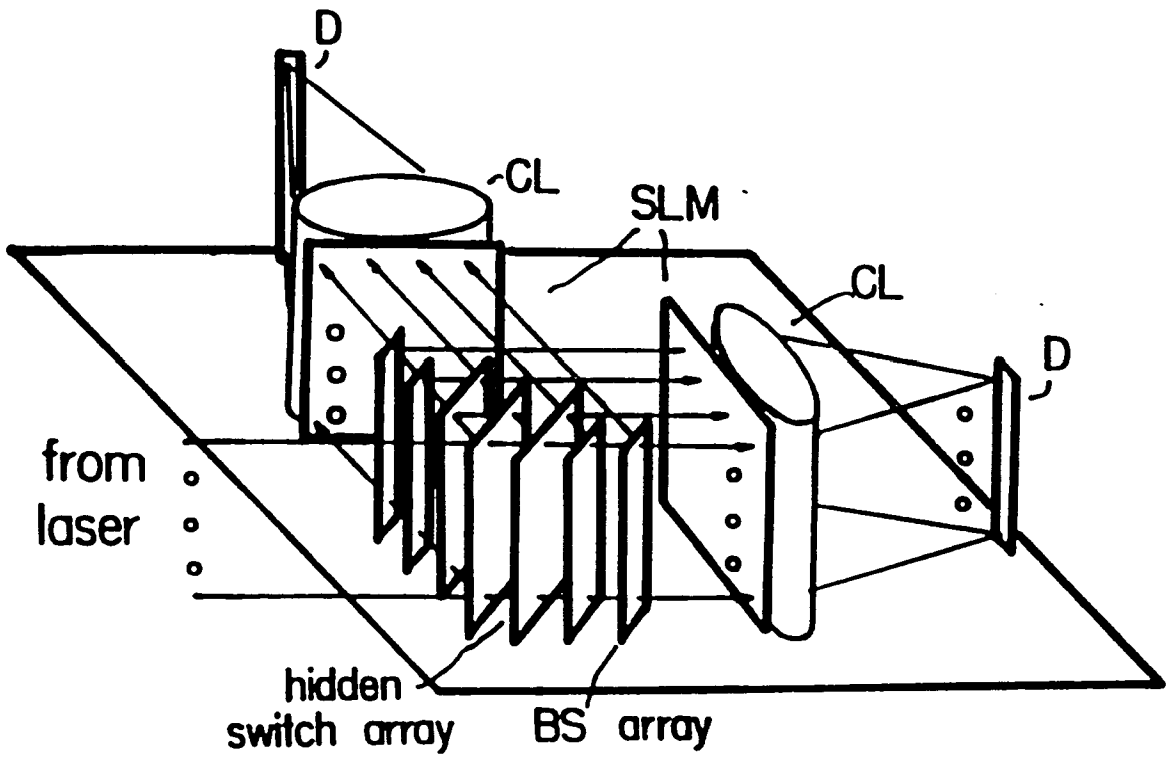

Fig.4.4 A schematic of experimental setup for 8-bit OBSLN

U_6	U_5	U_4	U_3	U_2	U_1	U_0
			a_3	a_2	a_1	a_0
		x	b_3	b_2	b_1	b_0
-	-	-	-	p_{03}	p_{02}	p_{01}	p_{00}
-	-	-	p_{13}	p_{12}	p_{11}	p_{10}	
-	-	p_{23}	p_{22}	p_{21}	p_{20}		
-	p_{33}	p_{32}	p_{31}	p_{30}	c_{11}		
-	-	-	c_{22}	c_{21}			
-	-	c_{32}	c_{31}				
-	c_{42}	c_{41}					
c_{52}	c_{51}						
c_{61}							
m_7	m_6	m_5	m_4	m_3	m_2	m_1	m_0

Fig.4.5 A 4-bit binary multiplication through counting

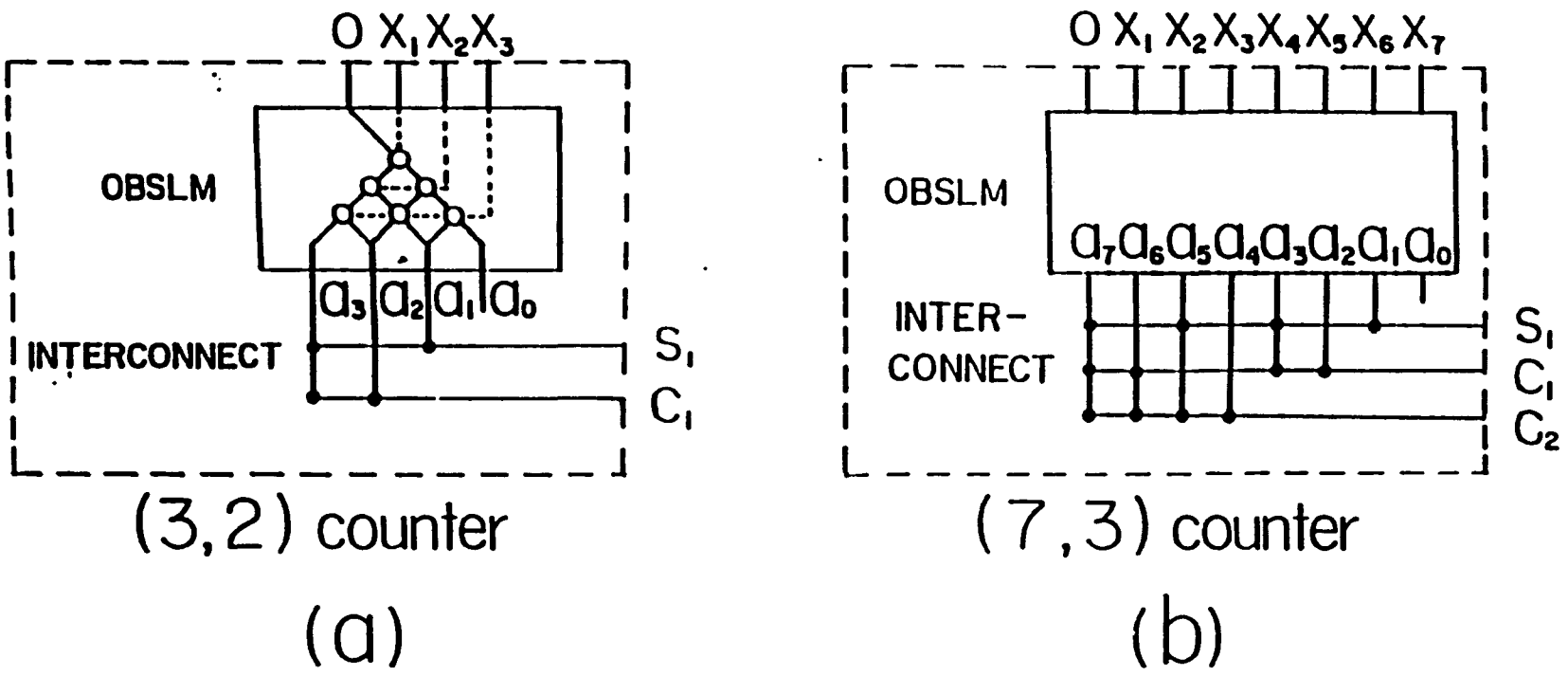

Fig.4.6 A schematic of OBSLN-based parallel digital counters

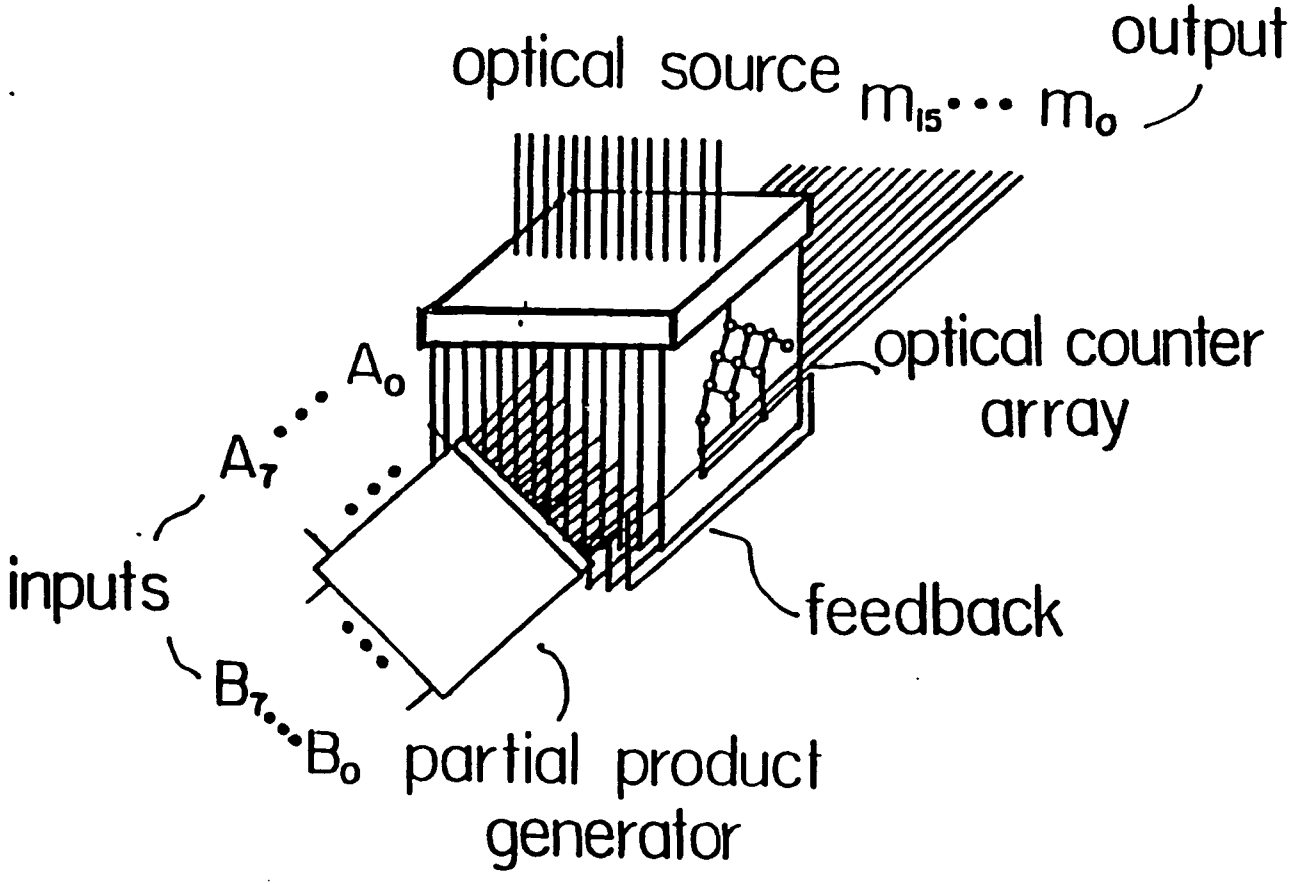

Fig.4.7 An OBSLN-based 8-bit binary multiplier architecture

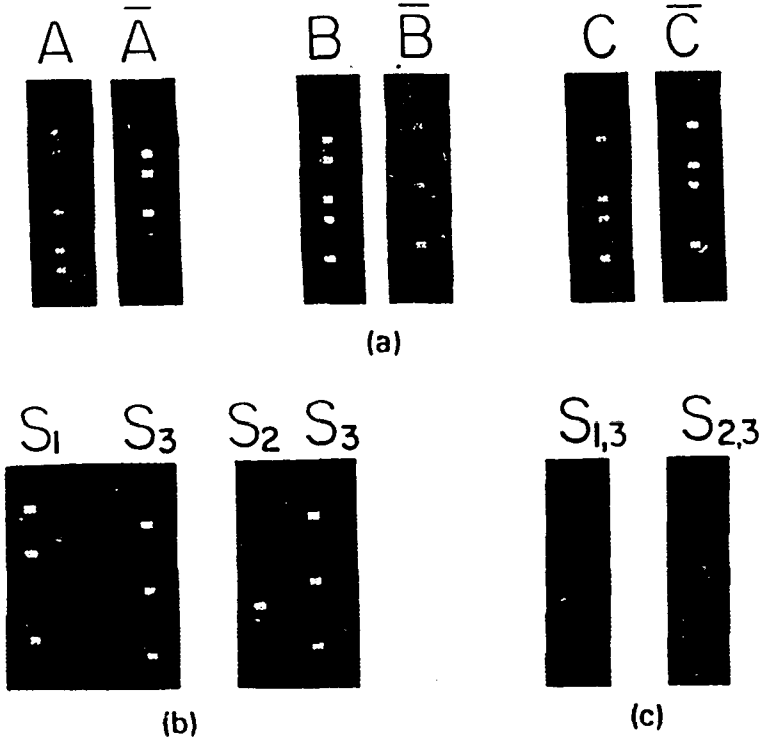

Fig.4.8 Experimental result of an 8-bit binary full adder
(a) input masks of A, B and C_{in} and their complements
(b) BSLF results $S_{1,3}$ $S_{2,3}$ on the selection plane
(c) Final results of summation and carry

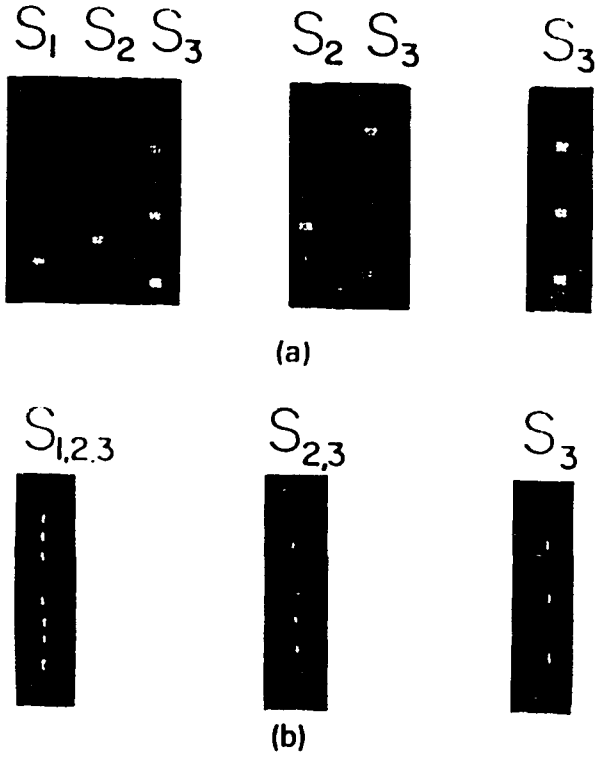

Fig.4.9 Experimental results of three parity checking of the input string of Fig.4.8

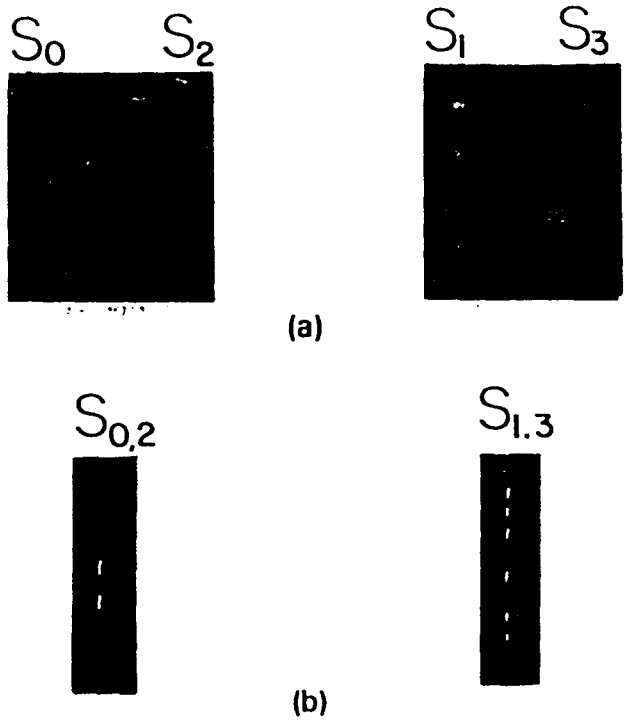

Fig.4.10 Experimental results of a binary weighted threshold summer

V OPTICAL INTERCONNECT OF A RING ARRAY OF SIMD PROCESSORS

5.1 Preliminary

In this chapter, the topology to distribute processing elements (PEs) for optical interconnect is discussed. Most interconnect networks suggested to use rectangular topology to distribute the processors: all the PE nodes are located along a linear or on a rectangular array. Rectangular array distribution has successfully provided optical implementation of some interconnects, such as perfect shuffles and crossover networks. However, for a number of very useful networks, it is very difficult to find implementation by arranging the PEs on a rectangular array. In this chapter, a new ring array based optical interconnect for various SIMD machines is proposed [2][3]. Using Dove prisms, both unidirectional and bi-directional implementations are presented to offer a clock-skew-free, low crosstalk and high speed data communications for SIMD machines.

5.2 Optical Interconnects for SIMD Machines

A SIMD machine is of particular interest to arithmetic computations, such as matrix-vector processing, discrete Fourier transformation, data sorting, as well as to various image processing applications. The SIMD machine is a computer system that consists of a control unit, N processing elements (PEs) and an interconnect network [1]. Each of the N PEs with its own local memory and registers simultaneously executes an identical instruction, while an interconnect network provides the communication link. All the control and communication commands are broadcast from a central control unit, and all the processors execute the identical commands simultaneously. Therefore, the interconnect synchronization is specially important for SIMD machines. Since the number of processors is very large (up to 65,536) for SIMD machines, the interconnect latency becomes a processing

bottleneck [4]. In this chapter, various useful interconnect networks for SIMD processors are investigated. Among them are three useful networks: a nearest neighbor (NN), a plus-minus 2^2 (PM2I), and a n-cube network (NC).

5.2.1 Nearest Neighbor Networks

A major problem for the widely used rectangular array distribution and processing topology is that its optical realizations require the use of both space-invariant (SI) and space-variant (SV) optical elements. For example, let's consider the implementation of a NN. The NN provides, for each of its N PEs ,four routing interconnect functions $R_{\pm 1,\pm r}(i)$:

$$R_{\pm 1}(i) = (i \pm 1) \mod N \qquad (5.1(a))$$

$$R_{\pm r}(i) = (i \pm r) \mod N \qquad (5.1(b))$$

where $r = \sqrt{N}$ and $0 \le i \le N-1$. If N PEs are distributed as a rxr square array, each PE is connected to its north, south, east and west neighbors (see Fig.5.1(a) for N=16 case). However, the PEs located at the edges (or corners) should be connected to the PEs on the opposite edges (or corners). If electrical wires were used to perform the connection, the latency of different connections would be different. If an optical implementation is adopted, nine different interconnect modules (one for the interior, four each for the corners and the edges) are needed. To achieve these interconnects optically, SI neighboring communications for the interior PEs, and SV global communications for the edge and corner PEs, must be established, respectively. However, if we arrange the interconnected PEs along a ring, the interconnect patterns for all PEs are exactly the identical (see Fig.5.1(b)): each PE is connected with its four neighbors. It is thus evident that, only SI operations are sufficient to achieve such a interconnect task with a ring distribution.

5.2.2 Plus Minus 2^i

The same constraint happens to the PM2I networks (Fig.5.2(a)). The PM2I is a very useful network, whose interconnect pattern is based on the following routing functions:

$$B_{+i}(j) = (j + 2^i) \mod N \qquad (5.2(a))$$

$$B_{-i}(j) = (J - 2^i) \mod N \qquad (5.2(b))$$

where $0 \le j \le n-1, 0 \le i \le n-1$, and $n = \log_2 N$. This implies that on the i^{th} stage, the j^{th} node interconnects to the nodes $(j \pm 1)^{th}$, $(j \pm 2)^{th}$,...., $(j \pm 2^i)^{th}$ on the $(i+1)^{th}$ stage. In each stage, connections may be required from one edge to the other, and in the i^{th} stage, the total number of nodes interconnecting to the other edges is 2i. To implement all these interconnects optically, both SI and SV operations should be employed. It leads to a very complicated interconnect pattern for an augmented PM2I network, and this is why an optical PM2I experimental implementation has not yet been reported so far. Although Cloonan and Herrer proposed [5] an optical PM2I network, it can only be applied to a so-called trimmed PM2I network (TDM). The TDM is such a modified PM2I network where all the connects from one edge to its opposite edge are canceled out, so that all the connects can be generated by using SI elements only. In their approach, SI element was a computer generated binary phase grating which performs a one to nine imaging operation to create a one to nine fan out. However, it is impossible to control which one of these nine routing it goes, because no additional switching devices were employed.

To solve this problem, a ring array topology is investigated in this chapter [2]. Instead of being distributed on a line or in a square array, all the PEs are placed along a ring. As shown Fig.5.2(b), the interconnect pattern for all PEs are identical: the same amount of angular shifts along the ring. To perform these shifts, the key optical element is a Dove prism.

5.3 An Optical Dove Prism Based Image Rotator

When a light beam passes through a Dove prism, it is reflected by its base with a flipped image. If the Dove prism is tilted with an angle of α, the flipped output image is rotated by an angle of 2α. In order to erect the flipped image, a cascade of two Dove prisms are used (see Fig.5.3). The first Dove prism is used to guarantee the erect of the upside-down ring array image. To shift the light ray from one position to another along the ring by an angle of 2α at the output plane, another Dove prism is tilted by an angle of α. If N PEs are distributed along a ring uniformly, the separation angle between any two nearest nodes is $\frac{2\pi}{N}$. In order to shift the light by m elements ($m \leq N$), the Dove prism should be tilted by an angle of

$$\theta = \frac{\pi m}{N}. \tag{5.3}$$

With a Dove prism rotator, all the input image points along the ring rotate the same angle, so that the interconnect patterns of all PEs are the same, and this condition is satisfied by all SIMD processors.

5.4 Different Approaches

Given an interconnect topology, a system architecture design will be in order. Such a design is highly technological and application dependent. In the context of optical interconnects, various architectures have been proposed and can be briefly categorized into the following four types (See Fig.5.4). In Fig.5.4(a) a multistaged system is shown. Optical transmitters and receivers are separated to different planes, between which the optical channels are situated. As can be seen, both optical channels and electronic PEs are duplicated into many copies in order to achieve a fast routing with a fixed optical network. This architecture is suitable for applications where both electronic PEs and optical interconnects have simple structures. Examples of using this architecture can be found in the AT&T optical processor and in other references [6-13]. For a more computationally complicated PE array, an interconnect architecture proposed for the POEM processor [14] is

depicted in Fig.5.4(b). Optical transmitters and receivers are placed at the same processor plane. To establish bilateral communication, two identical opto-electronic arrays are placed face to face. As compared to the Fig.5.4(a), the hardware has been reduced from multiple arrays to only two. In the Fig.5.4(c), a slightly different approach is shown. The interlaced transmitter/receiver arrays are placed on the two opposite sides of the same PE array. An optical ring cavity is used to link the two transmitter/receiver arrays [15-16]. One improvement of this system is that the Stoke's reversibility principle is used so that the optical bilateral communication is achieved at the cost of using a single set of optical hardware instead of two used in Fig.5.4(b). However, as far as the array control is concerned, this structure is identical to that of Fig.5.4(b). To further simplify the control overhead to a level where an optical network is ready for plug-in without a structural change of the electronic PE array, an architecture model sketched in Fig.5.4(d) was also recently proposed [17-20]. The transmitter/receiver array is directly connected to the electronic PE array, while the interconnect is achieved via optical reflections.

Basically, there are two kinds of interconnect requirements. One is to yield a data permutation among of PEs on the different planes (see Fig.5.4(a) and (b)), and the other is to perform the data communication among the PEs located on the same plane (see Fig.5.4(c) and (d)). For the first case, a unidirectional interconnect is established, while for the interconnects within the same plane, a bi-directional interconnect setup should be arranged.

5.4.1 Unidirectional Ring Array Optical Interconnects

A scheme of a unidirectional interconnect is shown in Fig.5.5. The light source could be either a set of point sources or a collimated beam. The Dove prism shared by all light channels is employed to erect the flipped images. Different permuting operations are performed in different channels by the correspondingly tilted Dove prisms. To choose a particular routing function, controlled polarization retardation switch masks are placed in front of the polarizing beam-splitters (PBS) to control the light beam's propagation direction.

The input sources are polarized in such a way that to switch the signal to a particular path, a polarization switch placed in front of the corresponding PBS must be activated.

5.4.2 Bi-directional Ring Array Optical Interconnects

To satisfy the bi-directional communication requirement, a configuration as a resonant ring cavity, which contains K channels is shown in Fig.5.6. The data ring consists of sources and detectors placed on either side of a bi-surface plane. To illuminate the system, optical point sources like light emitting diodes (LEDs) rather than a collimated beam is preferred. The first Dove prism is shared by all K channels. Controlled by the polarizing beam-splitters, the light beam travels through one of the K channels. For each channel, a rotation-invariant routing operation is yielded by a correspondingly tilted Dove prism. It is also possible to connect one PE to several PEs, activating these channels at the same time. Using the ring cavity, an identical bilateral communication latency between any two PEs can be established, due to Stokes' reversibility [21]. Because all light path lengths in all different channels are identical, a connection synchronization through different channels can be achieved.

An alternative bidirection ring interconnect adopts a reflective scheme, where both the transmitters and receivers are located on the same side of the PE array. The interconnect is implemented by a specially designed reflective prism [22]. It is interesting to note that when an optical reflective geometry is adopted, a single routing element may perform two symmetric routings simultaneously. The details about the reflective ring array interconnect will be discussed in chapter 6.

5.5 Techniques to Improve the Interconnect Quality

5.5.1 Crosstalk Reduction Using Imaging Rather than Beam Projection

To analyze the crosstalk, influence of diffraction must be taken into account. The crosstalk due to the diffraction is proportional to the projecting

length. For a mulple-stage uni-direction approach, the diffraction on the rare stages may be out of the tolerate. However, employing a lens, a projecting system can be changed to an imaging system, which provides a much better output. The details about the processing capability limited by the crosstalk due to the system diffraction will be analyzed in chapter 7.

5.5.2 The Advantage of Incoherent Light Illumination

Two types of input illuminations, i.e. spatially coherent and incoherent are often encountered. A collimated Laser beam provides a coherent light wave, while array of individual sources, such as LEDs, is an example of incoherent source array. According to the principle of an imaging system, the frequency response of a diffraction-limited coherent imaging system yields an *image amplitude* function, while the frequency response of an incoherent imaging system acts as an *image intensity* function [23]. In general, incoherent illumination offers a better image because its cutoff frequency is twice as that of a coherent illumination. Besides, in a coherent illumination, the resolution also depends on the phase distribution associated with the object. If more than one PEs are connected to a PE, what a detector receives is the summation of signals from several sources. For the coherent illumination, the data received might be miss-interpreted because of the wave interference among those light waves. In addition, for medium size array, incoherent individual light source (LED) array is much easier to control electrically than the use of expensive spatial light modulator.

5.5.3 Optical Component Design Based on Aberration Compensation

One of the main image quality degradation as a result of using a ring array interconnect is the aberrations caused by the optical components, such as Dove prisms and lenses. If a projecting approach is used, the light beam enters into the Dove prism with an 45°angle, and a diverging beam illumination courses serious oblique aberrations, such as coma, astigmatism, field curvature,

and distortion. Employing a lens, an imaging system provides the Dove prism a plane wave illumination, and therefore the prism does not generate any aberrations. However, the lens also brings in some aberrations, depending on the lens structure and the pupil stop positions. Details about the optimum design based on the aberration correction will be discused in Chapter 6 and 7.

5.5.4 Reconfiguration Ability

Another advantage of this novel ring array interconnect architecture is its network reconfigurability. A ring array reconfigurable interconnect system can be used to realize different interconnect tasks by tilting the Dove prisms with different angles. When the interconnect application is changed, the only change to be incorporated is to rearrange the Dove prism's tilt angle.

5.6 Experimental Results

A number of principle-proof experiments have been performed for the proposed Dove prism based ring array interconnects.

The first experimental setup was a system similar to that shown in Fig.5.5. Instead of using microlasers that are not available to us, we used the masks containing a ring of pixels illuminated by an Ar^{+}ion Laser as the input. The diameter of the input source ring was 10 mm, while the imaging lens diameter and focal length were D = 20 mm and f = 75 mm, respectively. All the lenses and beamsplitters are anti-reflectively coated. The Dove prisms with an aperture 15 mm x 15 mm and a 64 mm longitudinal base length were made by Edmund Scientific Co.. The output was detected by a CCD camera.

In the first experiment, a 64 node NN with the interconnect patterns of ± 1 and $\pm\sqrt{64} = \pm 8$ was performed. Two split optical paths to perform the 1 node and 8 nodes shifts. For observing this interconnect operation, a marked coaxial ring containing five pixels along the ring was placed inside the 64 pixel ring, shown in Fig.5.7(a). Fig.5.7(b) shows the overlapped output of the 8 and 1 shifts. The second experiment was a 16-node optical PM2I. The prisms in the four optical

channels were used to rotate the 16 pixel ring by 1, 2 and 4 nodes. Fig.5.8(b) was recorded at the output plane for an input ring shown in Fig.5.8(a). A 16-node optical HC was also realized. Since the HC requires an additional mask operation, an 8f imaging system containing a middle image plane was used instead of the 4f imaging system. A marked inner ring was used as a reference (see Fig.5.9(a)). The input was split into four copies that were imaging onto a middle image plane 4f distance away, where a set of absorbing masks was placed. The masked images (see Fig.5.9(b)) were again imaged and rotated to generate the channelized output shown in Fig.5.9(c). Finally, the four signals were combined to form the final HC interconnect pattern shown in Fig.5.9(c).

The second experiment set is shown in Fig.5.10. A 36-node ring-array of light emitting diodes (LEDs) (Panasonic P371-ND) was used as the light source. The LEDs were connected to an address decoder chip (74LS138) and an array of data latch/driver chips (E591) so that the switching of these LEDs could be controlled by a IBM PC. As receivers, 36 lens-capped Si photodiodes (Hamamatsu S2386-181C) were mounted on receiver ring board consisting of five switch chips (CD4051). Through a Dove prism and lens combination, the transmitter ring was imaged onto the detector ring. The detection result was displayed on the computer terminal.

5.7 Summary

The ring array based OIN for SIMD processors provides an opportunity to carry out interconnect only using space-invariant optical element. To generate the interconnect along a ring, Dove prisms are employed. Since only reflections are performed in the prisms, light efficiency is expected to be high. The use of both in-coherent illumination and an imaging scheme offer a low-crosstalk performance. Above all, the most important issue for a SIMD machine, the synchronism, is well dealt with as the result of using the ring cavity structure. Thus, this new compact optical interconnect scheme shows a bright future that optics can offer to digital computing.

5.8 References

[1] K. Hwang and F. A. Briggs, *Computer Architecture and Parallel processing*, (McGraw-Hill, New York, 1984), ch.5.

[2] Y. Li, T. Wang, and B. Ha, "Optical interconnect for a ring array of SIMD processors," Opt. Lett. 279-281 (1991).

[3] Y. Li, B. Ha, T. Wang, S. Wang, A. Katz, X.J. Lu, and E. Kanterakis, "Ring-array processor distribution topology for optical interconnects," Appl. Opt. 31, 5548-5558 (1992).

[4] S. Hunter *et. Al*, "Potentials of two-photon based 3-D optical memories for high performance computing," Appl. Opt., 29, 2058-2066 (1990).

[5] T. J. Cloonan and M. J. Herron, "Optical implementation and performance of one-dimensional and two-dimensional trimmed inverse augmented data manipulator networks for multiprocessor computer systems," Opt. Eng., 28, 305-314 (1989).

[6] J. Jahns and M. J. Murdocca, "Cross-over networks and their optical implementations," Appl. Opt. 27, 3155-3160 (1988).

[7] A. W. Lohmann, W. Storck and G. Stucke, "Optical perfect shuffle," Appl. Opt. 25, 1530-1531 (1986).

[8] G. Eichmann and Y. Li, "Compact optical generalized perfect shuffles," Appl. Opt. 26, 1167-1169 (1987).

[9] S-H Lin, T. F. Krile and J. F. Walkup, "2D optical multistage interconnect networks," Proc. SPIE, 752, 209-216 (1987).

[10] C. Stirk, R. Athale and M. Haney, "Folded perfect shuffle optical processor," Appl. Opt. 27, 202-203 (1988).

[11] Q. W. Song and F. T. S. Yu, "Generalized perfect shuffle using optical spatial filtering," App. Opt. 27, 1222-1223 (1988).

[12] Y. Sheng, "Light effective 2D optical perfect shuffle," Appl. Opt. 28, 3290-3292 (1989).

[13] R. A. Spanke and V. E. Benes, "N-stage planar optical permutation network," Appl. Opt. 26, 1226-1229 (1987).

[14] F. Kiamilev, S. Esener, V. H. Ozguz, and S. H. Lee, "Programmable opto-electronic multiprocessor systems," Proc. SPIE CR-35, 197-220 (1990).

[15] A. Huang, "Architecture considerations involved in the design of an optical digital computer," Proc. IEEE, 72, 780-786 (1984).

[16] B. S. Wherrett, "All-optical computation: a design for tackling a pecific physical problem," Appl. Opt. 24, 2876-2883 (1985).

[17] J. W. Goodman, F. J. Leonberger, S. Y. Kung, and R. A. Athale, "Optical interconnects for VLSI systems," Proc. IEEE, 72, 850-860 (1984).

[18] O. Wada and S. Yamakoshi, "Optoelectronic integrated components for digital optical computing systems," Proc. SPIE, 1215, 28-37 (1990).

[19] M. J. Goodwin, A. J. Moseley, D. J. Robbins, J. Thompson, and R. C. Goodfellow, "Opto-electronic array for optical interconnection of circuits," Proc. SPIE, 1215, 55-62 (1990).

[20] R. Linke, "Power distribution in a planar-waveguide-based broadcast STAR network, " IEEE Photon. Tech. Lett. 3, 1991.

[21] S. L. Esener, Proc. OE/LASE 90 Conference on Digital Optical Computing (Critical Reviews), Los Angelas, CA. Jan., 15-19, 1990.

[22] B. Ha and Y. Li, "Reflective ring array onterconnects: an optical system design study," accepted by Appl. Opt.

[23] J. W. Goodman, *Introduction to Fourier Optics* (Mc.Graw-Hill, New York, 1986) ch.5.

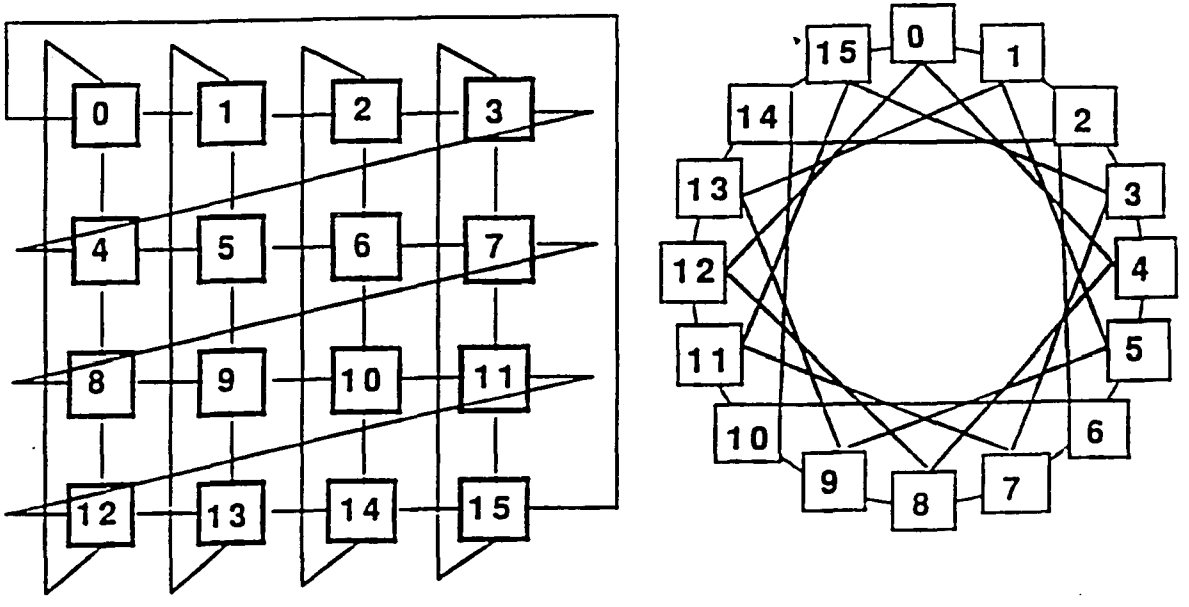

Fig.5.1 (a) A retangular array nearest neighbor with 16 PEs
(b) A ring array based nearest neighbor with 16 PEs

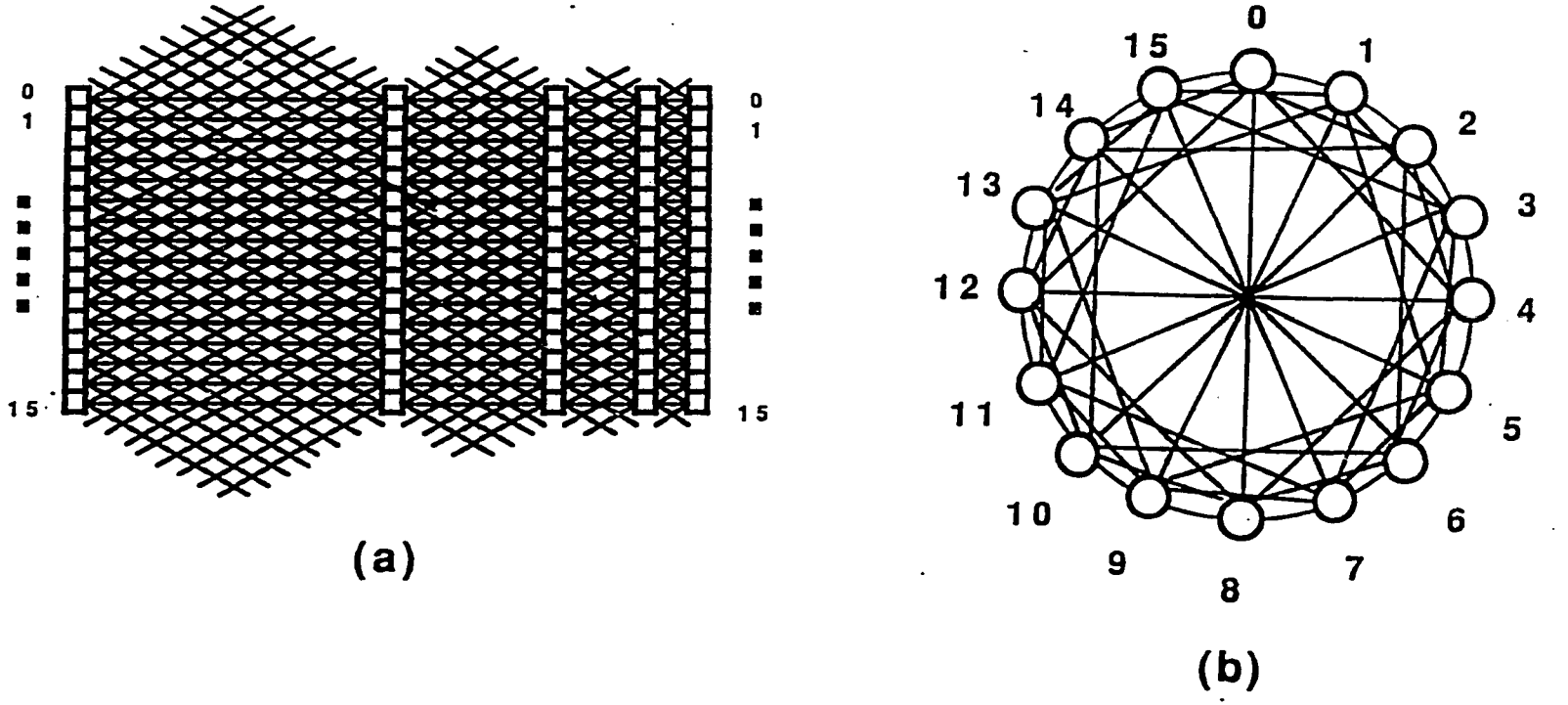

Fig.5.2 (a) A rectangular array based PM2I with 16 PEs
(b) A ring array based PM2I with 16 PEs

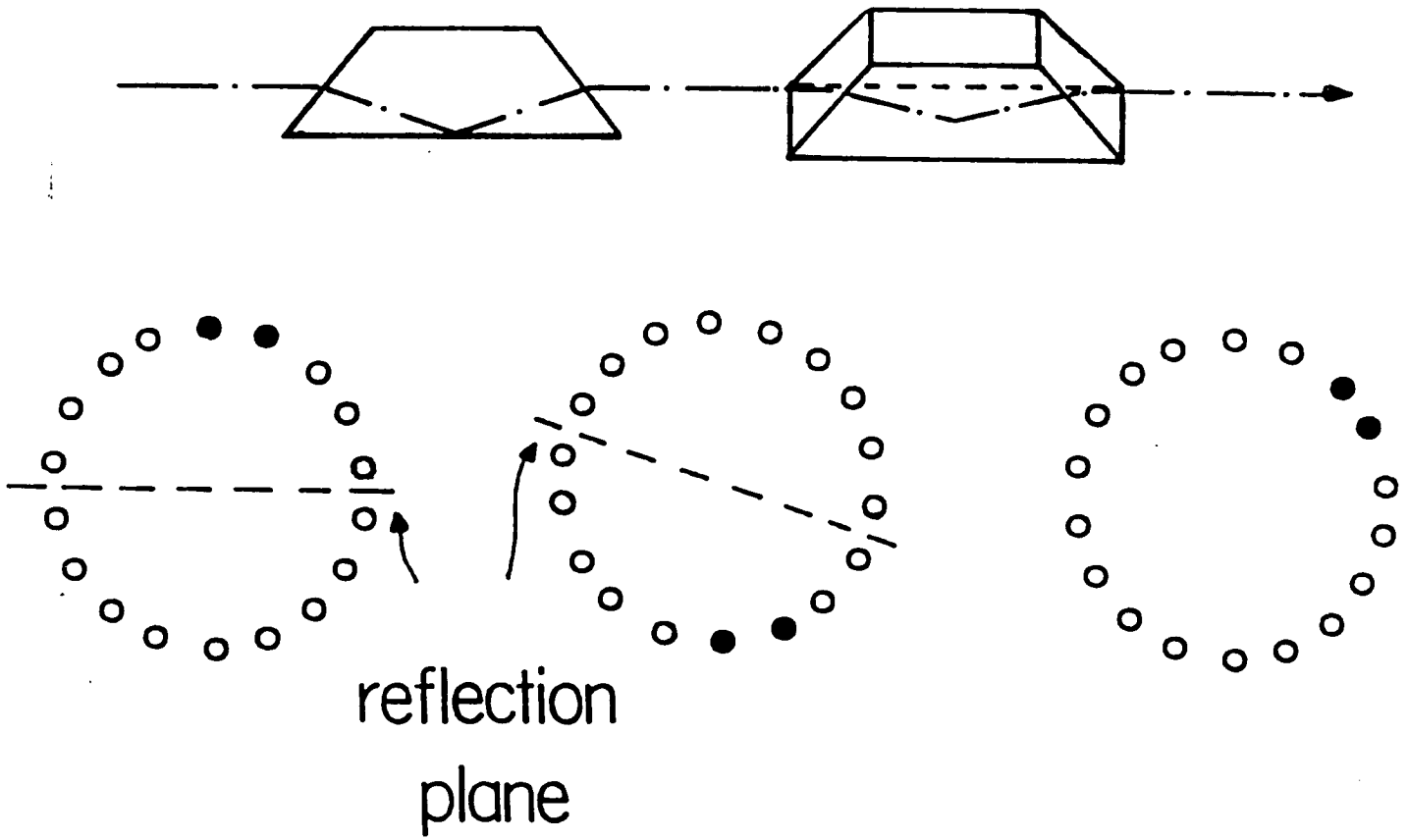

Fig.5.3 A Dove prism based image rotator

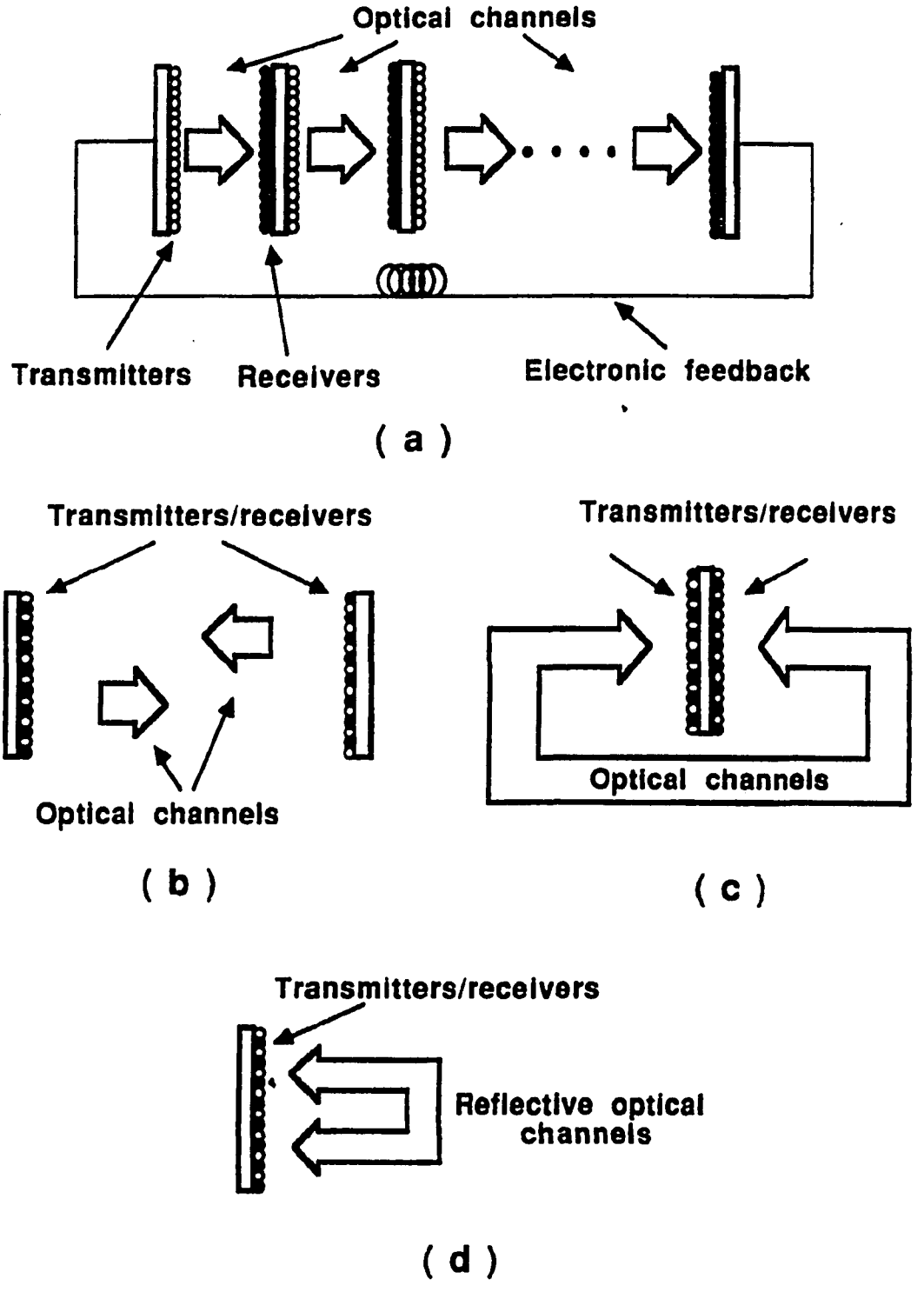

Fig.5.4 Four different optical interconnect architectures
(a) A multiple stage approach
(b) Two duplicated processors facing each other
(c) One processor with two transmitter/receivers
(d) A reflective interconnect

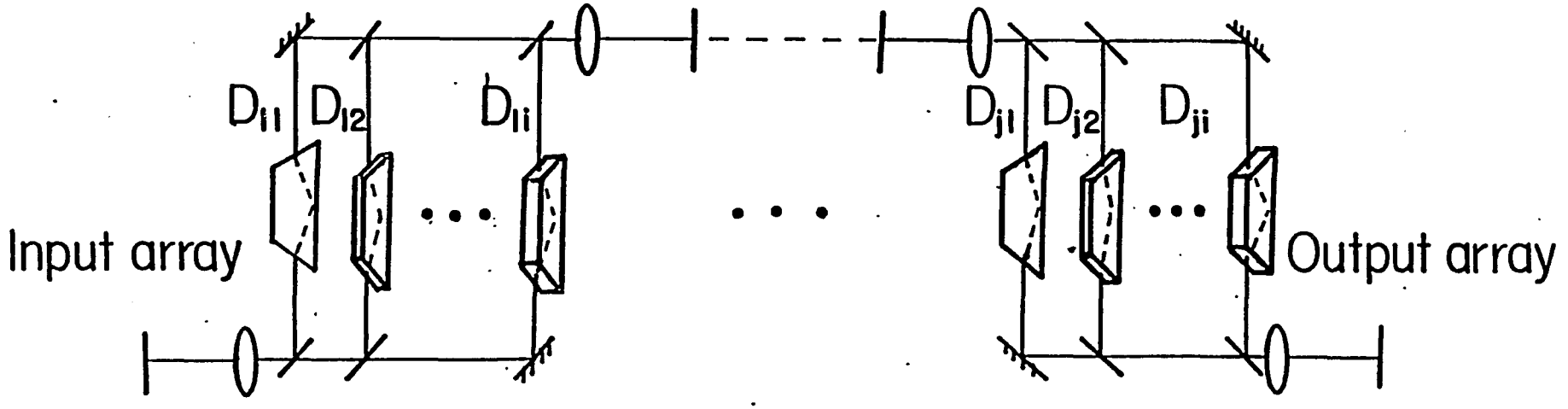

Fig.5.5 A uinidirectional ring array interconnect

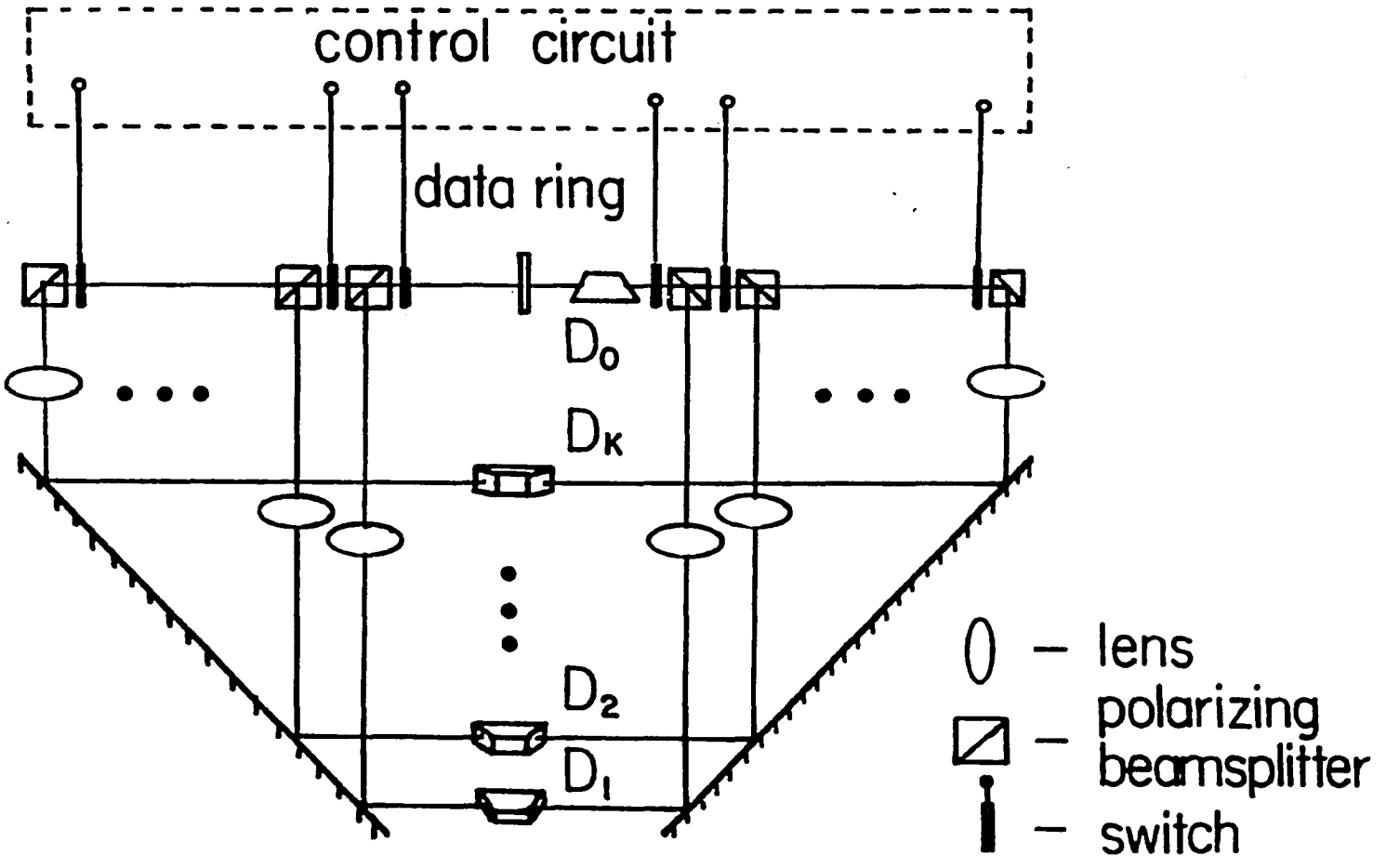

Fig.5.6 A bi-directional ring array interconnect

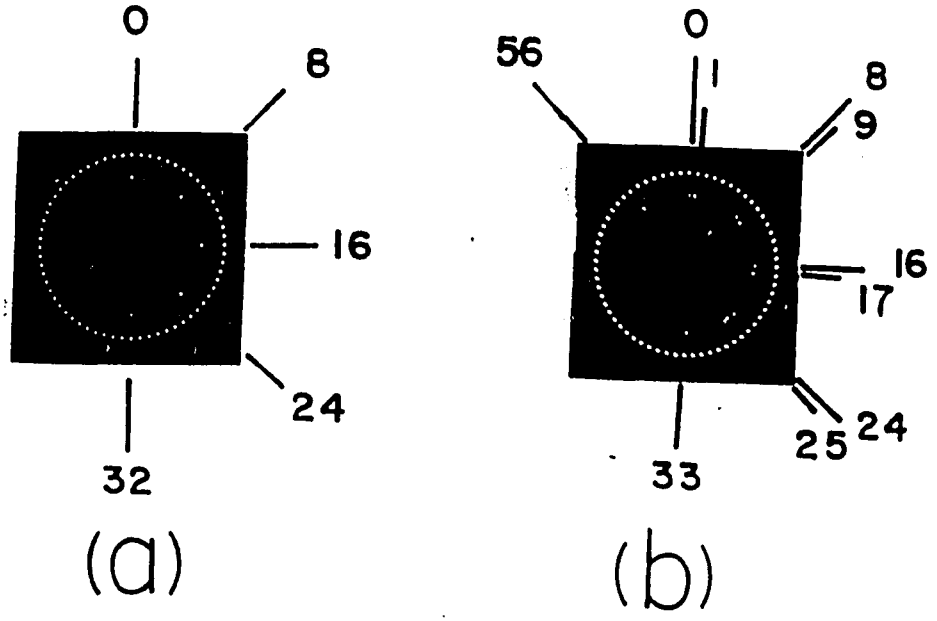

FIg.5.7 Experimental results of 64-PE optical NN
(a) The input ring with 5 reference points
(b) The NN results of input (a)

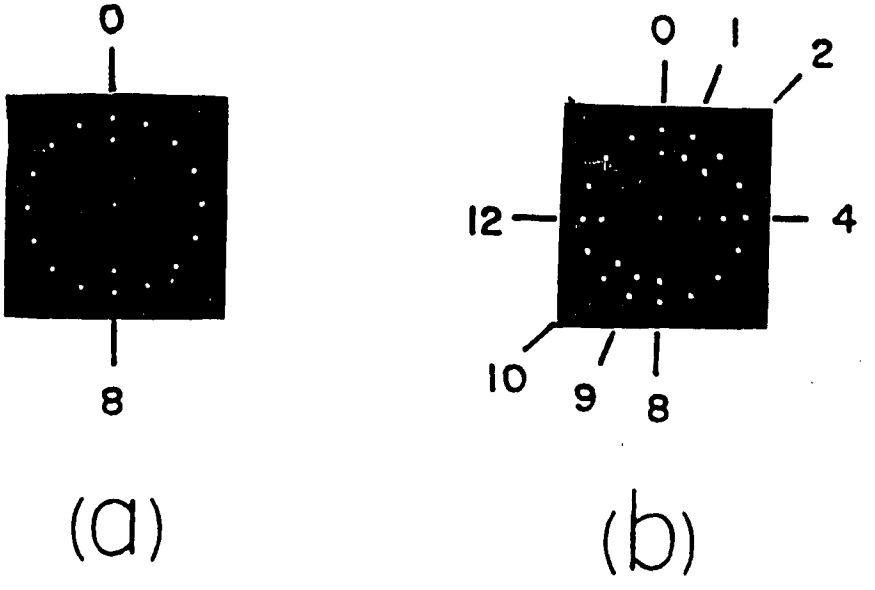

Fig.5.8 Experimental results of a 16-PE optical PM2I
(a) The input ring with two reference points
(b) The output result of four PM2I

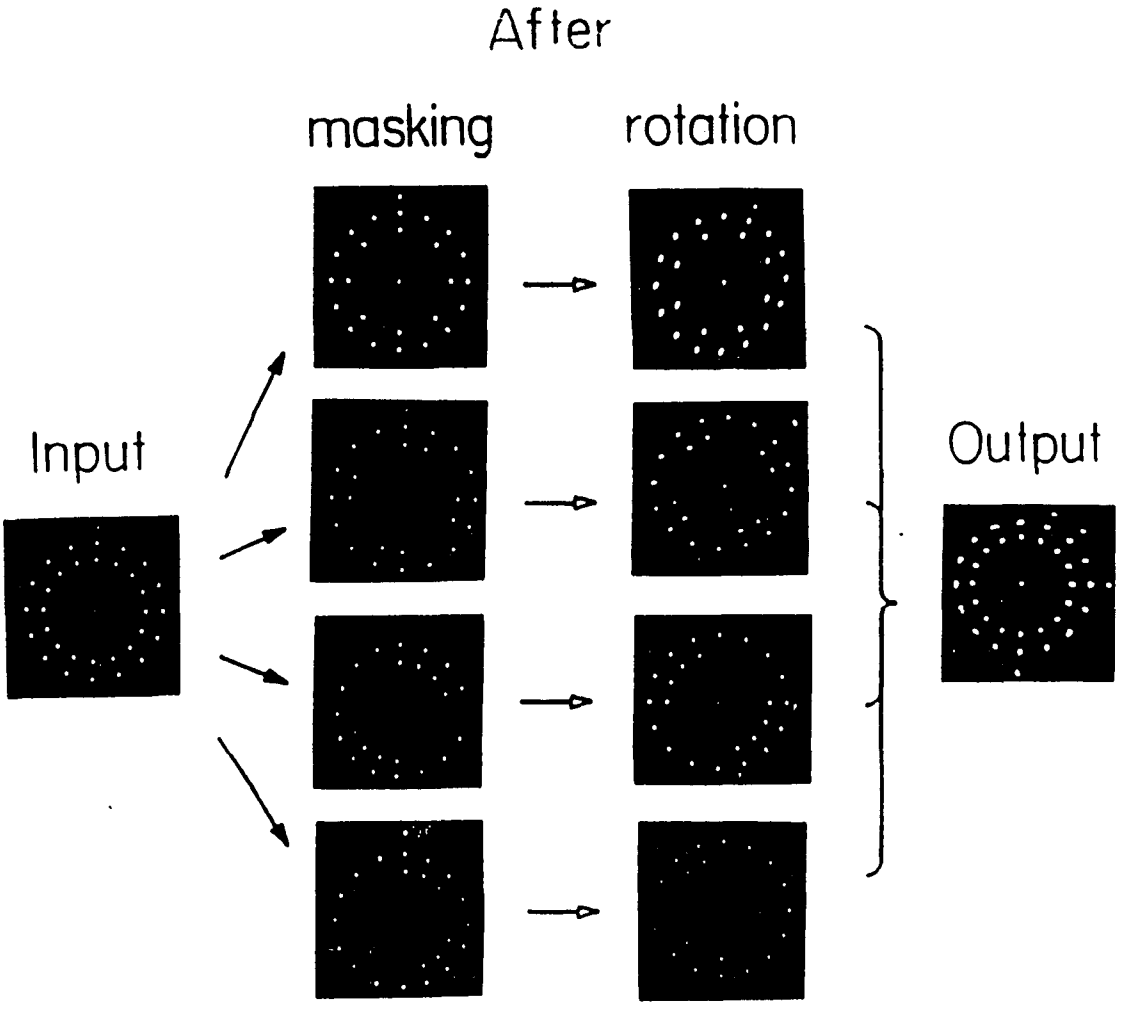

Fig.5.9 Experimental result of a 16-PE optical 4-cube
(a) input ring with a reference ring
(b) The masked results of (a) at four channels
(c) The channelized results of (b)
(d) A combination of outputs of (c)

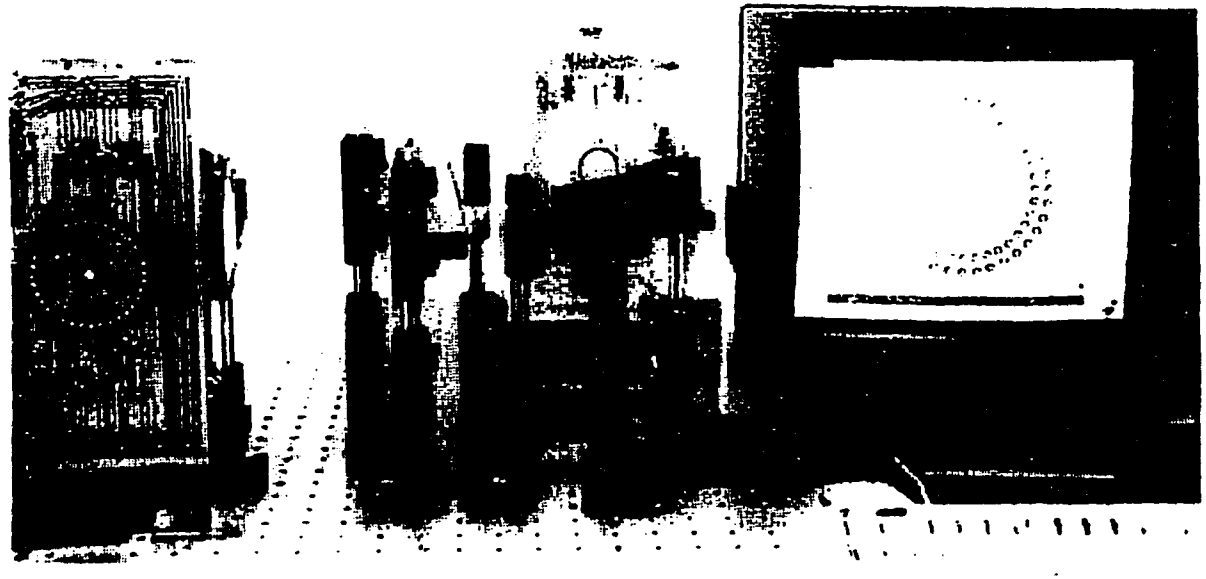

Fig.5.10 Photograph of the computer simulation setup

VI OPTICAL REFLECTIVE RING ARRAY INTERCONNECTS: AN OPTICAL SYSTEM DESIGN STUDY

6.1 Preliminary

In the bi-directional scheme of a ring array optical interconnect presented in last chapter (see Fig.5.6), the light sources and detectors must be placed on the two opposite faces of the processing array, and the entire light path cavity occupies a large space. In order to install the transmitters/receiver array directly to one plate, where the electronic PE array is located, a reflective geometry must be applied. In addition, in a reflective scheme, a single optical element may perform two symmetric interconnect routings simultaneously. In this chapter, a reflective imaging system for the ring array interconnects is presented. Based on the geometrical optics, a reflective prism is specially designed to perform any interconnect task for ring array of PEs. Based on an analysis of the system aberration and diffraction, the design of the optical system, specially the lens design is studied. The presented reflective system can provide a much more compact optical interconnect for the densely integrated computer processors [1].

6.2 A Reflective Prism for the Ring Array Interconnect

A ring array interconnect can be considered as an optical device performing a set of invariant image rotations along the ring. Suppose that a number of N PEs is uniformly distributed along a ring, and each PE has an individual light source and a detector for the signal transmission and detection. The separation angle between two adjacent PEs is $360^\circ/N$. To send signal to a PE located m PEs away form the source, the light beam should be rotated by an angle of

$$\beta = 360^\circ \frac{m}{N} \tag{6.1}$$

A simple way to rotate an image by an angle β is to flip it twice along two axes, between which the angle is $\frac{1}{2}\beta$ (see Fig.5.4). The image reversions can be achieved by reflective prisms using a reflective plane as the inversion plane. While

reversing the image, different reflective prisms change the light propagating direction in different ways. For example, while reversing the image, a right angle prism deviates the image propagation direction by 180° angle, and a Dove prism keeps the image propagating along the same direction.

Using a reflective optical system to realize a ring array interconnect, three requirements must be met: (1) the light beam should be deviated by 180° to return back to the object plane; (2) the reflected image must be rotated by an angle of β for a specific shift, implying that the reflected the image has to be left-handed to match the object being in a right-handed system; (3) the image center must overlap on the object ring center. To satisfy these requirements, a special reflective prism based system is designed using the following theory [2].

If the normal to a mirror is

$$M = li + mj + nk \tag{6.2}$$

then the image-coordinate matrix of this mirror can be expressed as

$$(r) = \begin{pmatrix} 1-2l^2 & -2lm & -2ln \\ -2lm & 1-2m^2 & -2mn \\ -2ln & -2mn & 1-2n^2 \end{pmatrix} \tag{6.3}$$

After reflected by a set of mirrors $M_1, M_2, \ldots, M_n$, a point (x_o, y_o, z_o) in the object space is imaged to point (x_n, y_n, z_n) on the image plane, based on the matrix equation

$$\begin{pmatrix} x_n \\ y_n \\ z_n \end{pmatrix} = (r_n)(r_{n-1})\ldots(r_2)(r_1)\begin{pmatrix} x_o \\ y_o \\ z_o \end{pmatrix} \tag{6.4}$$

or

$$X_n = (r_{n,1})X_o$$

A right-angle prism shown in Fig.6.1(a) reflects the image back to the incident direction, and flips the image along the Y axis. When a coordinate system is chosen inside the prism in such away, that the incident ray S_1 and the final reflected ray $-S_3$ are along the Z and -Z axes, respectively. The normals to the mirrors M_1 and M_2 are:

$$M_1 = \frac{\sqrt{2}}{2}j - \frac{\sqrt{2}}{2}k \qquad (6.5(a))$$

$$M_2 = -\frac{\sqrt{2}}{2}j - \frac{\sqrt{2}}{2}k \qquad (6.5(b))$$

The image-coordinate matrix of the reflecting surfaces M_1 and M_2 are

$$(r_1) = \begin{pmatrix} 1 & 0 & 0 \\ 0 & 0 & 1 \\ 0 & 1 & 0 \end{pmatrix} \qquad (6.6(a))$$

$$(r_2) = \begin{pmatrix} 1 & 0 & 0 \\ 0 & 0 & -1 \\ 0 & -1 & 0 \end{pmatrix} \qquad (6.6(b))$$

The combined image-coordinate matrix for these two surfaces is

$$(r_{1,2}) = (r_1)(r_2) = \begin{pmatrix} 1 & 0 & 0 \\ 0 & -1 & 0 \\ 0 & 0 & -1 \end{pmatrix} \qquad (6.6(c))$$

On the output image plane, for a particular image orientation, the image coordinate system may be represented by the transformation equation

$$X_n = AX_o \qquad (6.7)$$

If the image is designed to be rotated around the z axis with an angle β, the image rotation matrix should be set as:

$$A = \begin{pmatrix} \cos\beta & \sin\beta & 0 \\ -\sin\beta & \cos\beta & 0 \\ 0 & 0 & -1 \end{pmatrix} \qquad (6.8)$$

To achieve this design goal, an additional reflecting plane acting as an invention plane M_p should be added after M_2. Its orientation matrix should satisfy the following condition:

$$A = (r_p)(r_{2,1}) \tag{6.9}$$

The orientation matrix r_p then can be expressed as

$$(r_p) = A(r_{2,1})^{-1} = \begin{pmatrix} \cos\beta & \sin\beta & 0 \\ -\sin\beta & \cos\beta & 0 \\ 0 & 0 & 1 \end{pmatrix} \tag{6.10}$$

Denoting the elements of the (r_p)matrix as α_{ij}, the direction of the normal to the inversion plane can be solved using Eq.6.3:

$$l = \pm\sqrt{\frac{1-\alpha_{11}}{2}} \qquad m = -\frac{\alpha_{12}}{2l} \qquad n = -\frac{\alpha_{13}}{2l} \tag{6.11}$$

The normal to this inversion plane is solved as:

$$M_p = \sin\frac{\beta}{2}i - \cos\frac{\beta}{2}j \tag{6.12}$$

In order to simplify the system, instead of using a rotating prism, it is preferred to combine the inversion plane with the adjacent mirror M_2 to generate a three mirror system. The intersection edge of the second and third surfaces can be expressed by the vector product of $M_p X M_2$

$$E = M_p X M_2$$

$$= -\frac{\sqrt{2}}{2}\cos\frac{\beta}{2}i - \frac{\sqrt{2}}{2}\sin\frac{\beta}{2}j - \frac{\sqrt{2}}{2}\sin\frac{\beta}{2}k \tag{6.13}$$

The scalar product of the mirror normals gives the consine of the angle between these mirrors:

$$\cos\theta = M_p . M_2 = \frac{\sqrt{2}}{2}\cos\frac{\beta}{2} \tag{6.14}$$

The angle between the mirror surfaces may be either Θ or $180^0-\theta$. However, M_p can not be simply added to the system, because it is parallel to the light incident direction of M_p. The pair of M_2 and M_p should be rotated until the axial ray has equal angles of incidence on the two mirrors as $\frac{\theta}{2}$. The mirror normals after rotation are then called as M'_2 and M_3:

$$M'_2 = \sin\frac{\theta}{2}M_2 - \cos\frac{\theta}{2}(E' X M_2) \qquad (6.15(a))$$

and

$$M'_2 = \sin\frac{\theta}{2}M_2 + \cos\frac{\theta}{2}(E' X M_2) \qquad (6.15(b))$$

where E' is the normalized vector of E.

In general, the origin of the image ring does not overlap with that of the object ring after beams are reflected out of the prism. In order to meet the third requirement mentioned above, a lens must be inserted between the transmitter/receiver ring array and the prism rotator to form a reflective 4f imaging geometry. The lens is placed at such a position that the point source ring is at its front focal plane, and the optical distance from the lens through the prism and back to the lens, is twice of the focal length. The image has an identical size of the object, and it is rotated by an additional 180^0 by the lens. Therefore, while designing the prism, an additional 180^0 image rotation should be considered. For example, when a 180^0 image rotation angle is required, the prism should generate an unrotated image, which could be achieved by a combination of a right angle prism and a penta prism. Considering the additional 180^0 rotation, the angle Θ (between M'_2 and M_3), α_1 (between M_1 and M'_2) and α_2 (between M_1 and M_3) can be calculated as :

$$\cos\theta = \frac{\sqrt{2}}{2}\sin\frac{\beta}{2} \qquad (16.6(a))$$

$$\cos\alpha_1 = \frac{1}{2}\sin\frac{\beta}{2}\sqrt{\frac{2+\sqrt{2}\sin\frac{\beta}{2}}{1+\cos^2\frac{\beta}{2}}} \qquad (16.6(b))$$

$$\cos\alpha_2 = \frac{1}{2}\sin\frac{\beta}{2}\sqrt{\frac{2+\sqrt{2}\sin\frac{\beta}{2}}{1+\cos^2\frac{\beta}{2}}} \qquad (16.6(c))$$

In tables I and II, calculated angles of α_1, α_2 and θ for the design of a NN and of a PM2I networks are tabulated. If the angles between the three prism surfaces M_1, M'_2, M_3 are smaller than the critical angle of the material, aluminum coatings on the surfaces M'_2 and M_3 are necessary to ensure an efficient reflection.

Since the designed prism is a triple-mirror system, it normally deviates the light ray to the different directions resulting in six possible images [3]. A prism can rotate an image by an identical angle regardless of the mirror sequences that beams travel through if and only if the three mirrors are orthogonal, which is the case of a corner-cube prism. The ray deviations for the mirror sequences ($M_1M_2M_3$) and ($M_3M_2M_1$) are the same, but differ for the sequences ($M_1M_3M_2$) and ($M_3M_1M_2$). The image rotates by a pair of angles ($\pm\beta$) only when the light ray traces two opposite sequences of mirrors, for instance, ($M_1M_2M_3$) and ($M_3M_2M_1$) . Based on this phenomenon, to obtain a couple of conjugated image rotations, it is important to keep the light passing through the triple-mirror system in a certain manner. Since the sequence ($M_1M'_2M_3$) was chosen while determining the mirror normal directions, the light should pass through the prism along the sequence ($M_1M'_2M_3$) or ($M_3M'_2M_1$) . This implies that the illumination should be kept only be on M_1 or M_3, but not on M'_2. However, the source illumination on the M'_2 can not be avoided, if the center of illumination coincides with the center of the prism. In order to ensure the light ray passing through the prism in the sequence ($M_1M'_2M_3$) or ($M_3M'_2M_1$), illumination should only be on part of the M_1 and M_3 (see Fig.6.2). After reflected by M_1, M'_2 and M_3, the beam is parallel to the input illumination but with a position shift. To overlap the axis of the

reflected beam with that of the input beam, a pair of parallel reflecting surfaces M_4 and M_5 should be used. Replacing M_5 by a beamsplitter, an integrated prism in which the light beam is allowed to travels only through the sequences M_1, M'_2, M_3, M_4, M_5 and M_5, M_4, M_3, M'_2, M_1 is formed. With the angles specified as in the Table I and II, the prisms can perform different interconnect tasks for the ring array processors.

A reflecting prism can be spread to its equivalent parallel plate by the so-called tunnel diagram. For example, the thickness of the equivalent parallel plate of a designed reflective prism is approximately $t = 5D$, where D is the prism aperture. To form an imaging system, the optical distance (nl) between the two lenses should be 2f, and both the transmitter and detector arrays are placed at the lens focal planes. Keeping the lens a 0.05D distance from the prism, the optical distance from the lens through the prism and back to the lens is

$$nl = nt + 2*0.05D = 7.68D \tag{6.17}$$

When this distance equals to 2f, the numerical aperture of the system is determined by

$$u = \frac{D}{2f} = \frac{1}{7.68} = 0.13 \tag{16.18}$$

Sometimes when a larger numerical aperture is required for a higher illumination efficiency, u can be increased by choosing the nl less than 2f without affecting the imaging. The object size y is also limited by the geometric structure of the reflecting prism, and the maximum field angle $u_f = y/f$ is

$$u_f = \tan^{-1}\frac{nD}{2t} = \tan^{-1}\frac{1.517D}{7.68D} = 11.2^0 \tag{16.19}$$

for a refractive index n=1.517.

The reflecting prisms may also be used to build a multiple channel ring array interconnect, when beam-splitters and control switches are used to select the signal's routing channel. In order to reduce diffraction without further decrease of the numerical aperture, additional relay lenses should be inserted into the system. An

eight channel ring array PM2I network which interconnects 256 processing elements is shown in Fig.6.3. It contains 8 interconnect cells, each of them consisting of a prism and a lens, can perform a couple of interconnect tasks. In each channel, the light beam travels through three beamsplitters. In general, to perform M pairs of interconnect tasks ($M = \log_2 N$ for PM2I), $\log_2 M$ beamsplitters are needed.

6.3 An Aberration Correction Based Optical System Design for the Ring Array Interconnects

The cross-talk due to diffraction and aberrations of the employed optical elements is part of the main restrictions limiting the signal to noise ratio in a free-space optical interconnect. To reduce the cross-talk, a good imaging system must be employed [4]. Besides, the optical element design should be based on both the reduction of aberrations of each individual element, and on a compensation of one element's aberration to the other's [5]. In this section, some important design principles leading to a low-aberration imaging system for the ring array interconnect are described.

Since a self-illuminated object (a ring of point sources) provides an incoherent and oblique illumination, the main aberrations to be considered here are oblique aberrations, such as astigmatism, coma, distortion, field curvature, and oblique spherical aberrations. Because a ring is a central symmetric object, the distortion does not occur if the ring is centered on the optical axis. The field curvature can be removed by adjusting the image plane position, since all light rays to be considered are at an identical oblique angle. Therefore, unlike the use of either a linear or a rectangular array, here the aberrations to be considered are only the astigmatism, coma, and oblique spherical aberration. The free of field-curvature and distortion exclusively due to the ring distribution offers another opportunity to design a better yet simpler interconnect system than that of using a linear or rectangular array.

The ring array optical interconnect consists of two types of optical elements: prisms and lenses. The basic technique to design an optical system is to minimize aberrations of each individual element and to compensate the aberrations among the involved elements. The aberrations of an equivalent parallel plate of a prism are determined by the plate thickness t, the numerical aperture u, the field angle u_f, and the refractive index n of the prism material. In our application, the light sources are placed on the focal plane of the lens, and the prisms are working under a plane wave illumination (u=0). Thus, the prism itself does not cause any aberrations, and the lens design task is simply to correct the lens aberrations themselves. This is an advantage of the 4f ring array offers over other imaging counterparts.

With the u and u_f being fixed, the design parameters here are the shape of the lens and the position of the stop. The third-order aberration coefficients may be computed based on the paraxial approximation (see Fig.6.4 for defined rays and parameters). Applied to a thin lens with an aperture stop in contact with it (the chief ray passing through its center), the coefficients of the third-order spherical aberration and coma are a quadratic and a linear functions of the first surface curvatures $\rho_1(1/r_1)$, respectively:

$$\delta_s = h^4(a\rho_1^2 + b\rho_1 + c) \qquad (6.20(a))$$

$$\delta_c = h^2 yu(d\rho_1 + e) \qquad (6.20(b))$$

where h is the lens radius; u is the numerical aperture; y is the object height; f is the lens focal length; and a, b, c, d, and e are the parameters determined by the focal length, object distance and the material reflective index n. However, the astigmatism of a lens, with a stop contacted with it, is independent of the lens shape:

$$\delta_a = \frac{(yu)^2}{f} \qquad (6.20(c))$$

It is clear from Eq.6.20 that by shaping the lens (changing ρ_1) the spherical aberration and the coma can be changed. However, the astigmatism can not be

reduced as long as the system stop is contacted with the lens. In order to reduce the spherical aberration, astigmatism and coma simultaneously, the stop must be removed from the lens. When the stop is moved away from the lens, the chief ray passes through the lens at a position away from the center of the lens, and the aberration coefficients can then be computed from the stop-shift equations [6]:

$$\delta_s^* = \delta_s \qquad (6.21(a))$$

$$\delta_c^* = Q\delta_s + \delta_c \qquad (6.21(b))$$

$$\delta_a^* = Q^2\delta_s + 2Q\delta_c + \delta_a \qquad (6.21(c))$$

where Q is a stop-shifting parameter which is determined by the ratio:

$$Q = \frac{\bar{h}_1^* - \bar{h}_1}{h_1} \qquad (6.22)$$

where h_1 and $\bar{h}_1$ are the margin and chief ray heights on the lens before the stop-shift, and $\bar{h}_1^*$ is the chief ray height after the stop-shift. The following facts are observed from the Eq.6.21: (1) spherical aberration δ_s has nothing to do with the stop position; (2) when $\delta_s = 0$, stop shift does not affect the δ_c, and (3) when $\delta_s = \delta_c = 0$, the astigmatism can not be changed by shifting the stop position. This implies that it is impossible to correct coma, astigmatism and spherical aberration simultaneously simply by shifting the stop position. Fortunately, the entire reflective ring interconnect setup can be viewed as a symmetric system with a unit magnification. In such a symmetric system, often known as an aplanatic system, coma from the two half-systems can cancel out each other. Therefore, the two lenses can be designed to correct only the spherical and astigmatic aberrations, while the remaining coma can be self-compensated. This purpose can be achieved by a cemented lens to correct spherical aberration δ_s, while leaving some coma δ_c and astigmatism δ_a. In this case, a new stop position can be found out to satisfy Eq.6.21(c) by setting $\delta_a^* = 0$:

$$Q = \frac{\delta_a}{2\delta_c} \qquad (6.23)$$

The design procedure now is to correct the spherical aberration of a stop-contacted lens then to remove the stop to cancel the astigmatism. A lens cemented by a positive lens (f_1) and a negative lens (f_2) can be designed to correct the spherical aberration has three refractive surfaces with their corresponding curvatures ρ_1, ρ_2, ρ_3, where ρ_2 corresponds the curvature of the common surface of both lenses, i.e. the rear surface of the first lens ρ'_1 and the front surface of the second lens ρ_2. The aberrations of the cemented lens $\delta_{s,cem}$ and $\delta_{c,cem}$ can then be expressed as functions of ρ_2:

$$\delta_{s,cem} = h^4[(a'_1 + a_2)\rho_2^2 + (b'_1 + b_2)\rho_2 + (c'_1 + c_2)] \qquad (6.24(a))$$

$$\delta_{c,cem} = h_2 yu[(d'_1 + d_2)\rho_2 + (e'_1 + e_2)] \qquad (6.24(b))$$

where the parameters a, b, c, d, and e (a', b', c', d' and e') are determined by the refractive indices of the first (second) lens, and their focal lengths f_1 and f_2

In order to correct the spherical aberration, the f_1 and ρ_2 should satisfy the equation

$$\delta_{s,cem} = (a'_1 + a_2)\rho_2^2 + (b'_1 + b_2)\rho_2 + (c'_1 + c_2) = 0 \qquad (6.25)$$

While to eliminate the astigmatism, the stop-shifting coefficient Q should obey Eq.6.23, and thus can be evaluated according to Eq.6.20(b) and (c):

$$Q = -\frac{\delta_a}{2\delta c} = -\frac{(yu)^2/f}{2h^2 yu[(d_1 + d_2)\rho_2 + e'_1 + e_2]} = -\frac{u_f}{2uf^2[(d_1 + d_2)\rho_2 + e'_1 + e_2]} \qquad (6.26)$$

Geometrically, to form a 4-f system with the chief ray passing through the focal point, this Q should also be evaluated as

$$Q = \frac{\bar{h}^*}{h_1} = \frac{fu_f}{fu} = \frac{u_f}{u} \qquad (6.27)$$

which implies that

$$(d'_1 + d_2)\rho_2 + e'_1 + e_2 = -0.5/f^2 \qquad (6.28)$$

Solving this equation with Eq.6.25 simultaneously, the value of f_1 and ρ_2 for the initial design can be found. For example, while choosing $n_1 = 1.51680$ (crown glass, BK7) for the positive lens and $n_2 = 1.71736$(flint glass, SF1) for the negative lens, a pair of results are obtained:

$$f_1 = 0.49778f \qquad (6.29(a))$$

$$\rho_2 = -2.611/f \qquad (6.29(b))$$

Correspondingly, the lens's surface radii are

$$r_1 = 0.781f \qquad (6.29(c))$$

$$r_2 = -0.383f \qquad (6.29(d))$$

$$r_3 = -0.828f \qquad (6.29(e))$$

with the first surface r_1 facing the plane wave illumination.

The above aberration correction discussion is only based on the third-order aberration study. For a further improvement, a computer software should be used to optimize the design. As an example, a computer aide lens design software ZEMAX was employed to optimize the above initial design featuring a focal length of 100mm.

The computer simulation consists of three optimization steps. First, with the stop in contact with the lens, the merit function was chosen to minimize the spherical aberration and to set $\delta_a = -2\delta_c$. Then the stop was removed from the lens to the front focal plane, and this removal is practiced through adjusting the exit pupil distance to infinity in the merit function. As it was anticipated, the astigmatism was reduced to as small as 10^{-5} waves after the stop shifting. The third step is to build up a 4-f symmetrical system based on the designed lens. The stop must be placed at the system center which is a focal plane of both lenses, and this setting can be confirmed by modifying the merit function so that both the entrance pupil and the exit pupil are located in the infinity. After a few cycles of running the optimization function, the aberrations were minimized to a satisfactory level.

The computer simulation results demonstrated that the final optimization result turns out to be very close to the initial design:

$$r_1 = 73.873358mm \qquad d_1 = 9.277721mm \qquad (6.30(a))$$

$$r_2 = -38.999902mm \qquad d_2 = 1.762041mm \qquad (6.30(b))$$

$$r_3 = -88.826387mm \qquad (6.30(c))$$

As a way of judging the designed system, the modulation transfer function (MTF) of the optimization result is shown in Fig.6.5. These curves confirm that the design under the present condition meets the imaging requirement of the proposed interconnect specification.

6.4 Summary

A sketch of an optical reflective network for a ring array of single-instruction-multiple-data multiprocessor was presented. The specially designed reflective prism provides a pair of symmetric interconnect routings by rotating the image with two conjugated angles. Compared to other rectangular array optical interconnects, the proposed architecture is compact and easy to align. In addition, since all LEDs are located along a circle, the illumination oblique angle is unique for the ring array interconnects, and therefore, the aberration correction task only has to consider on this particular field angle. This feature gives a good opportunity to design a high quality optical interconnect economically.

To improve the performance quality, an imaging rather than a projecting system is employed to realize the interconnect, and the imaging lens is designed according the aberration correction. Basically, a lens can be designed to correct any aberrations using complex structure [2][4]. The more elements a lens consists of, the higher image quality it can offer. However, the cost is higher for more complex lenses. The design usually depends on the combined consideration of quality, cost and compatibility.

6.5 References

[1] B. Ha and Y. Li, "reflective optical ring array interconnects: an optical system design study," accepted by Appl. Opt.

[2] R. Kingslake, *Applied Optics and Optical Engineering* (Academic Press, New York and London, 1965) Vol. 3, ch.3.

[3] P. R. Yoder, "Study of light deviation error in triple mirror and tetrahedral prisms," J. OSA. 48, 496-499 (1958).

[4] M. Born and E. Wolf, *Principles of Optics* (Pergamon Press, Oxford, 1975) ch.8.

[5] A. E. Conrady, *Applied Optics and Optical Design* (Dover Publications, Inc., New York, 1957, Ch.10.

[6] T. T. Saha, " Transverse ray aberrations of Wolter type I telescopes," Proc. Soc. Photo-Opt. Instrum. Eng. 444, 112-117 (1984).

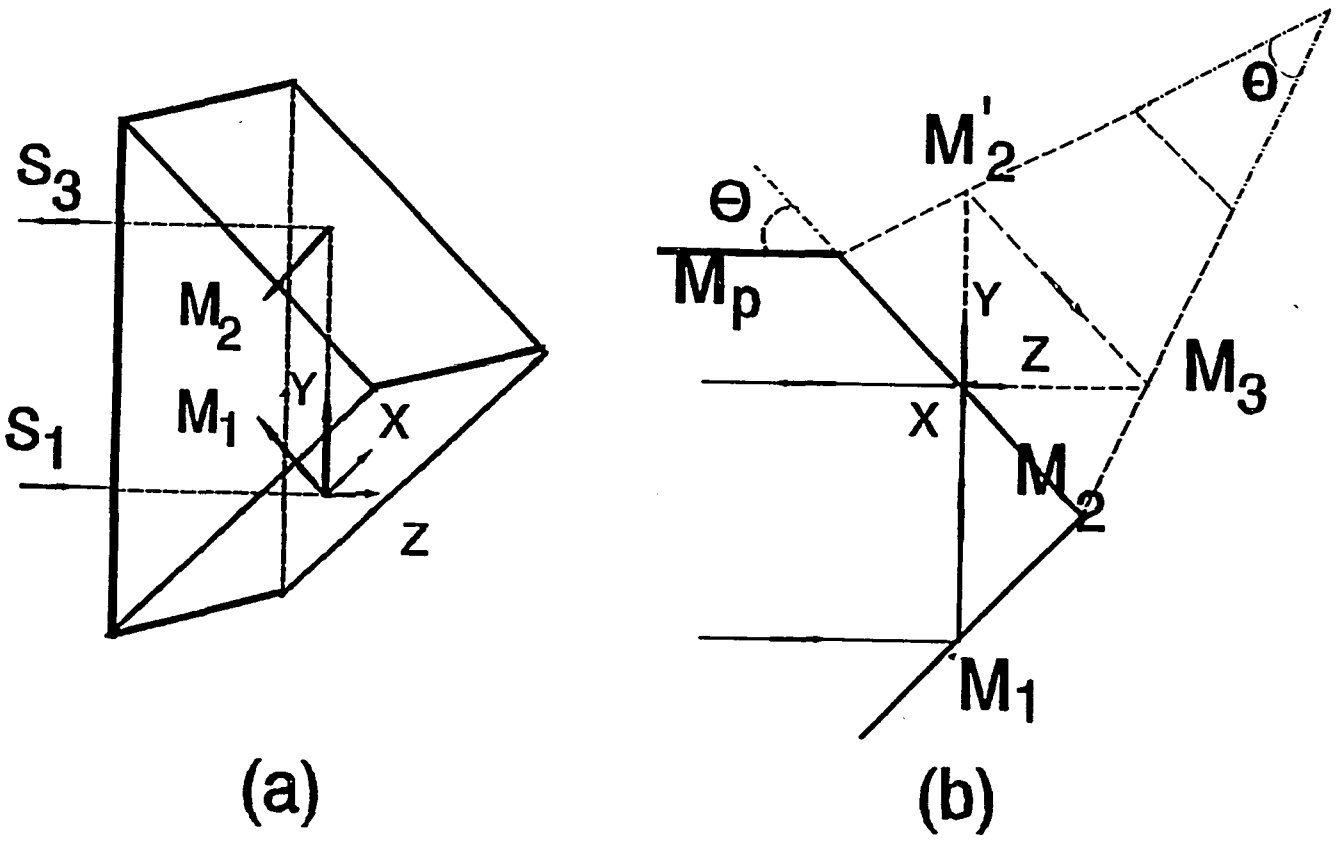

Fig.6.1 (a) The coordinate system for a reflective prism
(b) A reflective prism for ring interconnect

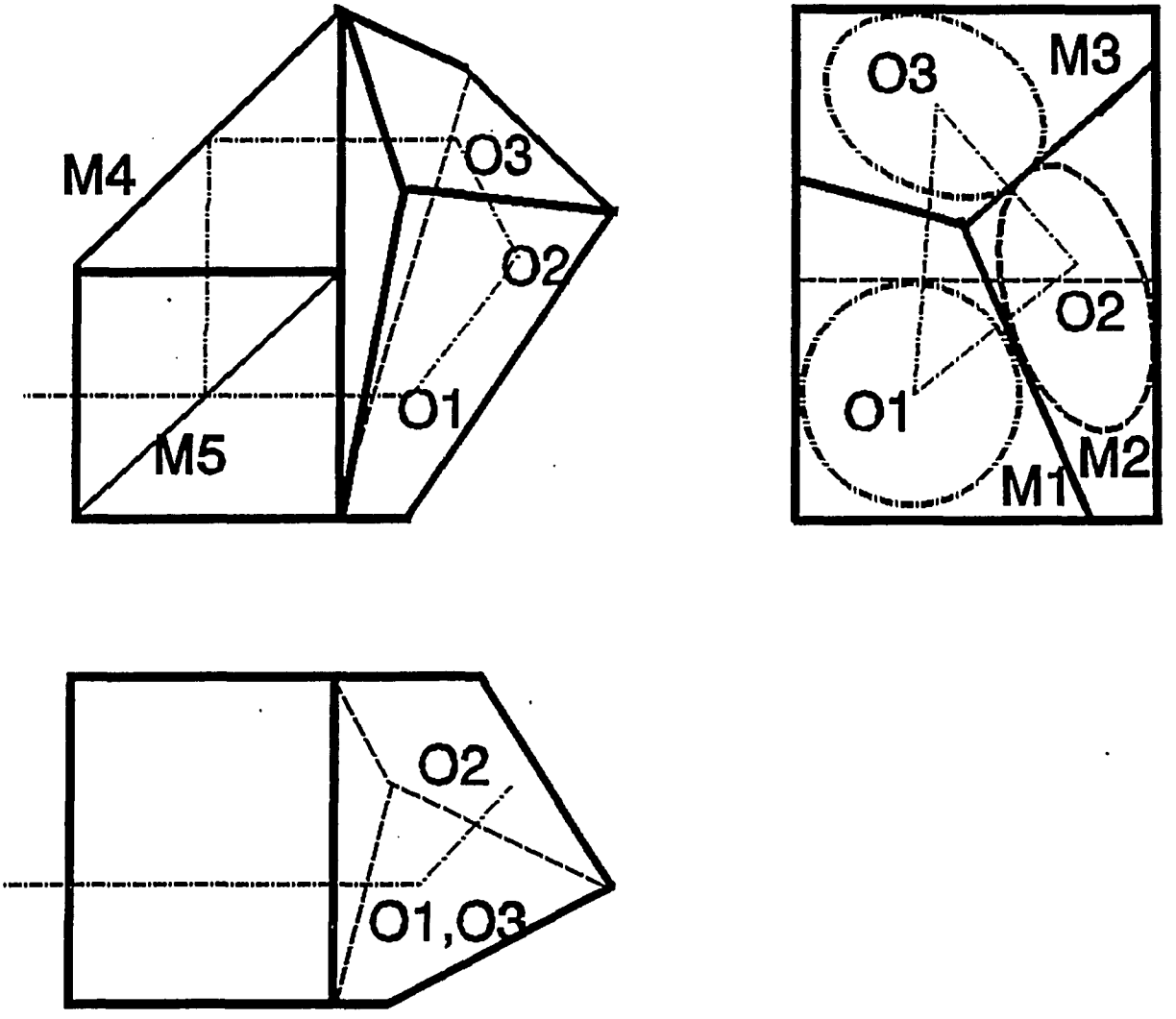

Fig.6.2 An integrated prism-based image rotator

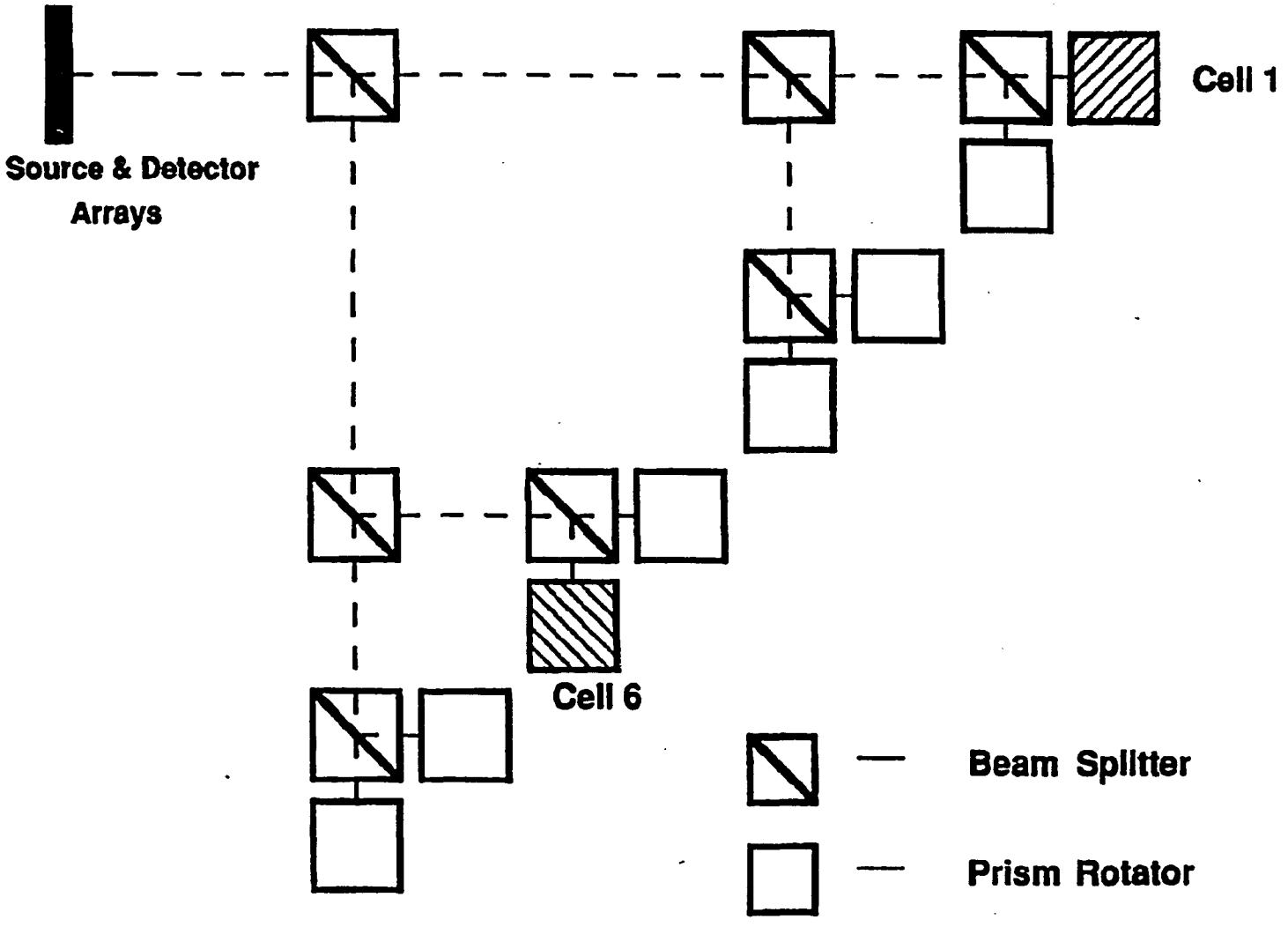

Fig.6.3 An eight channel ring array interconnect

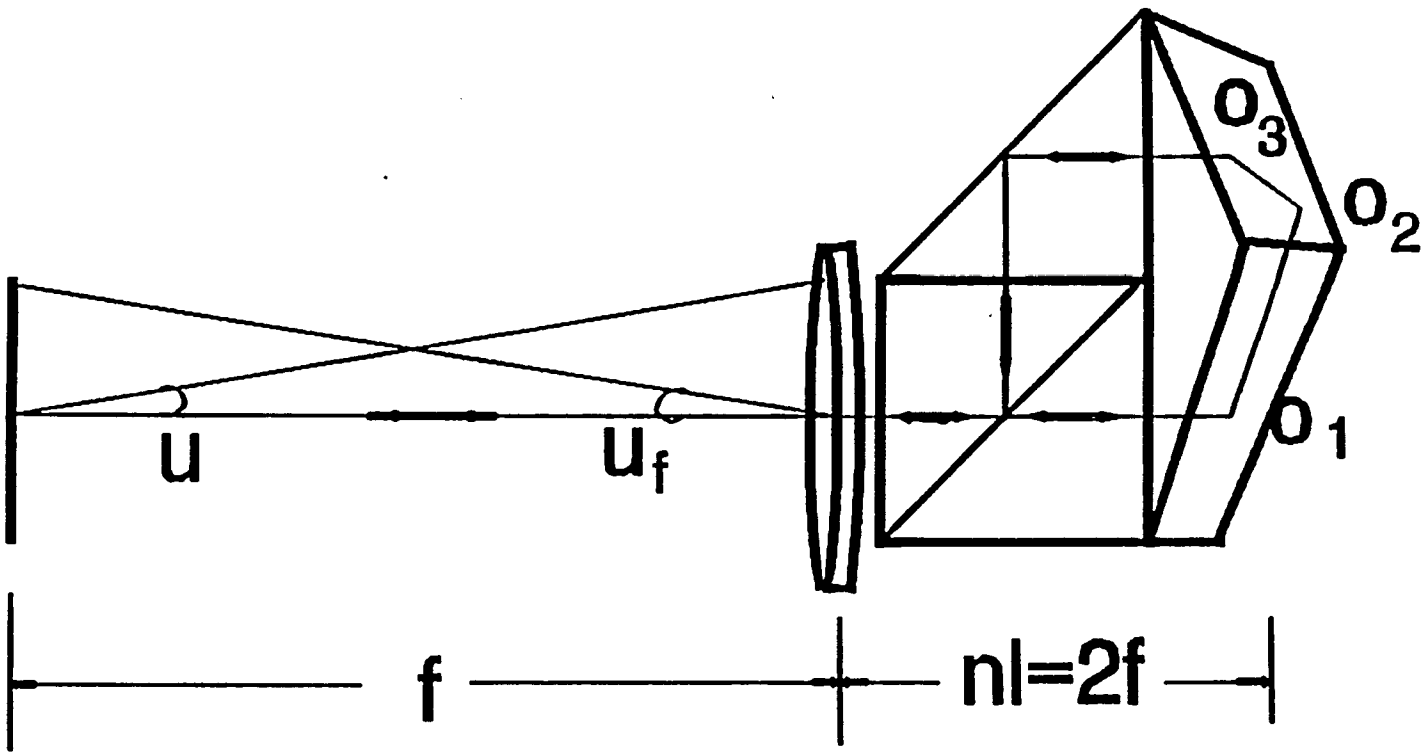

Fig.6.4 Margin and chief ray parameters for the lens design

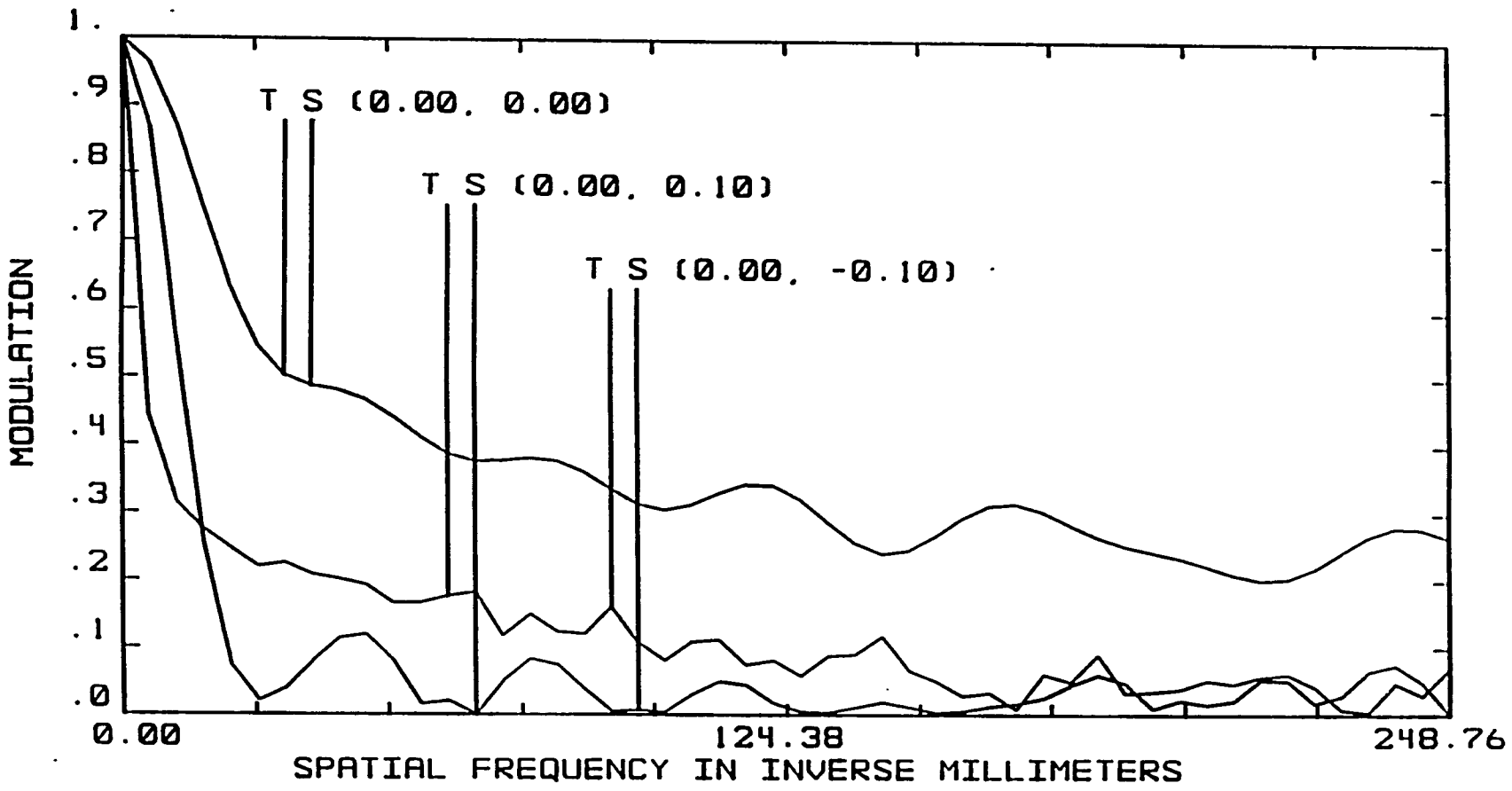

Fig.6.5 A modulation transfer function of the optical system

TABLE I PRISM ANGLES FOR A NN NETWORK

# PEs	for $i = \pm 1$ neighbors			for $i = \pm\sqrt{N}$ neighbors		
N	θ	α_1	α_2	θ	α_1	α_2
16	82.070	83.969	96.031	60	60	120
64	88.012	88.569	91.431	74.300	77.054	102.946
256	89.503	89.647	90.353	82.071	83.969	96.031
1024	89.876	89.812	90.088	86.026	87.088	92.912
4096	89.969	89.978	90.022	88.011	88.569	91.431

The definition of the angles in the Table I and Table II:

θ: angles between M'_2 and M_3,

α_1: angles between M_1 and M'_2,

α_2: angles between M_1 and M_3.

TABLE II PRISM ANGLES FOR A PM2I NETWORK

=PEs	prism angles	16	64	256	1024
$=1^{th}$	Θ	82.071	88.012	89.503	89.876
	α_1	83.969	88.569	89.647	89.912
	α_2	96.030	91.431	90.353	90.087
$=2^{th}$	Θ	74.300	86.026	89.006	89.951
	α_1	77.053	87.088	89.291	89.824
	α_2	102.92	92.912	90.709	90.176
$=4^{th}$	Θ	60	82.071	88.012	89.503
	α_1	60	83.969	88.569	89.647
	α_2	120	96.031	91.430	90.353
$=8^{th}$	Θ	45	74.300	86.026	89.006
	α_1	22.5	77.054	87.088	89.291
	α_2	157.5	102.946	92.912	90.709
$=16^{th}$	Θ	____	60	82.071	88.012
	α_1	____	60	83.969	88.569
	α_2	____	120	96.031	91.431
$=32^{th}$	Θ	____	45	74.300	86.026
	α_1	____	22.5	77.054	87.088
	α_2	____	157.5	102.946	92.912
$=64^{th}$	Θ	____	____	60	82.071
	α_1	____	____	60	83.969
	α_2	____	____	120	96.031
$=128^{th}$	Θ	____	____	45	74.300
	α_1	____	____	22.5	77.054
	α_2	____	____	157.5	102.946
$=256^{th}$	Θ, α_1	____	____	____	60
	α_2	____	____	____	120
$=512^{th}$	Θ	____	____	____	45
	α_1	____	____	____	22.5
	α_2	____	____	____	157.5

VII ANALYSIS OF THE INTERCONNECT CAPACITY OF FREE-SPACE OPTICAL INTERCONNECTS

7.1 Preliminary

various physical limitations exist on how many processing elements (PEs) can be linked in an optical free-space interconnect. Working in different circumstances, the processing capacity of a free-space optical interconnect is constrained by different limitations. For an imaging based interconnect like the proposed ring array interconnect, the system aberrations may be one of the main noise sources. The system diffraction, on the other hand, may become significant to cause a cross-talk in a projecting based interconnect, like the optical cross-over network introduced in this thesis. While for a holography based interconnect, the restricted aperture could be one of the major limits of the PE number to be interconnected. Above all, for all kinds of interconnect styles, power consumption is always an important issue to be considered. In this chapter, the interconnect capacity is analyzed in terms of the optical component aberration, and of the system diffraction and power utilization efficiency [1].

7.2 Aberration Restriction

The ambiguity and cross-talk due to aberrations of optical components are one of the main restrictions to the processing capacity of an imaging based optical interconnect. The aberration influence on the imaging quality mainly comes from all of the optical elements, such as lenses and prisms. The design of an imaging system based optical interconnect should be based on the aberration correction, including the design of each optical component with minimized aberrations and the compensation of one component's aberrations to the other's.

7.2.1 Aberrations of Prisms

Any reflecting prism can be spread to an equivalent parallel plate using a so-called channel diagram [1]. The thickness of the equivalent parallel plate is

$$t_D = JD \tag{7.1}$$

where D is the aperture, and J is the prism parameter, e.g.j = 3.3787 for a Dove prism and j = 3.4142 for a Penta prism.

The aberrations of a parallel plate is determined by the thickness of the plate t, the numerical aperture u, the oblique angle u_z and the index of the refraction n. The spherical aberration, coma, astigmatism and distortion of a prism are respectively given by

$$\delta_s = tu^3\frac{(n^2-1)}{n^3} \tag{7.2(a)}$$

$$\delta_c = \frac{tu^2u_z(n^2-1)}{n^3} \tag{7.2(b)}$$

$$\delta_t = \frac{tuu_z^2(n^2-1)}{n^3} \tag{7.2(c)}$$

$$\delta_d = \frac{tu_z^3(n^2-1)}{n^3} \tag{7.2(d)}$$

The field curvature is zero for a plate, and for a reflective prism as well [2][3].

When a prism is illuminated by a plane wave light beam, all the aberrations are vanished because of the zero value of u. When a LD with a diverging illumination angle u is used as the light source, it is suggested a lens being employed to collimate the beam to a plane wave. Another way to achieve the condition of u=0 is to ensure of the first surface of the prism is perpendicular to the incident light beam. If both these methods are not available, the prism's aberrations must be compensated by other optical components, such as a lens.

7.2.2 The Aberration of Lenses

With a fixed aperture and object size, the aberrations of a lens depend on the employed number of surfaces, the surface's curvature, the material's refractive index, and the stop position. In a specific system, some conditions

may be useful to simplify the aberration correction task. As an example given in chapter 6 section 3, the lens design was much easier by taking the advantage of the aberration feature of the ring object. First, a ring object does not cause any distortions, and the field coverture can also be eliminated by adjusting the image position. Sccondly, the symmetry of the entire system also provides an opportunity to correct the coma and distortion automatically.

Basically, a lens can be designed to correct any aberrations or to compensate the other component's aberrations. The more complicated the lens structure is, the less the aberration is left. However, the cost is bigger for the more complex lenses. The cost-quality trade-off is determined by how many PEs needed to be interconnected [4].

7.2.3 The Interconnect Capacity Limited by the System Aberration

No matter how well the aberrations are corrected, there always exist some remaining aberrations. Considering the aberration limit only, the processed PE number N is determined by the fact that the separation of the adjacent detectors should be greater than the remaining aberration δ_{remain} :

$$\frac{d}{N} \geq \delta_{remain} \tag{7.3}$$

where d is the total length occupied by all the PEs.

Normally, after a computer aided high-order aberration correction, the remaining aberration can be controlled with the order of

$$\delta_{remain} \leq \frac{\lambda}{u} \tag{7.4}$$

where u is the system numerical aperture and λ is light source wavelength. The interconnected PE number then is limited by

$$N \leq \frac{du}{\lambda} \tag{7.5}$$

7.3 Diffraction Limit Restriction

While analyzing the interconnect cross-talk, the influence of light beam diffraction must also be taken into account. In an imaging system based interconnect, the diffraction is caused by the system aperture, which is either the lens aperture or the aperture of a specially set stop. However, in a projecting system, such as the collinear optical cross-over interconnect proposed in chapter 2, the diffraction is caused by the aperture of the switching devices which is much smaller than the entire system aperture, and therefore the diffraction is much more serious, especially for a multiple-stage interconnect.

In an imaging system based interconnect, the diffraction of the system aperture may be one of the restrictions to the interconnect capability. Assuming that the Fraunhofer approximation can be adopted, the intensity distribution is generally referred to as the Airy pattern, with its first zero located on the radius of

$$\Delta = 1.22\frac{\lambda z}{R} = \frac{1.22\lambda}{u} \tag{7.6}$$

where λ is light wavelength, z is the object distance, R is input pupil radius, and $u = \frac{R}{z}$ is the system numerical aperture [5-6]. To avoid the diffraction caused crosstalk, the space between the adjacent PEs must be at least as large as 2Δ

$$\frac{d}{N} \geq 2\Delta = \frac{2.44\lambda}{u} \tag{7.7}$$

The number of PEs N then is limited by the diffraction

$$N < \frac{du}{2.44\lambda} \tag{7.8}$$

It can be seen that the limit by system diffraction is similar to the aberration limit defined by Eq.7.5. The interconnect capacity N limited by the aberration and diffraction of an imaging based optical interconnect is shown in Fig.7.1.

The diffraction of a projecting interconnect is much more serious. For example, in the proposed optical cross-over, the diffraction is caused by the aperture of the switching devices on the previous stage. Suppose that the aperture of the switching devices is Δ_d, then the half-width of the main lobe of the diffraction pattern on the next stage is $\lambda L_z/\Delta_d$, where L_i is the distance between the ith and (i+1)th stages. In order to avoid cross-talk caused by diffraction, the switching device's aperture must be at least large enough to cover the main lobe of the diffraction pattern

$$\Delta_d > \frac{\lambda L_i}{\Delta_d} \tag{7.9}$$

. This implying that the distance L_i is limited by diffraction

$$L_i < \frac{\Delta_d^2}{\lambda}. \tag{7.10}$$

According to Eq.2.3, the stage space L_i is determined by the total PE number N, the space of consecutive PEs Δl, and the illumination angle Θ:

$$L_i = \frac{N \Delta l c \tan\theta}{2^i} \tag{7.11}$$

Assuming that $\Delta l = 1.1\Delta_d$, considering the largest L_i between the first and second stages $l_1 = N\Delta l c \tan\theta/2$, the interconnect capacity N then is limited by

$$N < \frac{1.8\Delta}{\lambda c \tan\theta} \tag{7.12}$$

For a multiple stage interconnect, the cross-talk is the overlap of the cross-talks of the all previous stages, and therefore the total number of stages an interconnect can handle is also restricted by the system diffraction.

7.4 Power Consumption Restriction

In many optical free-space interconnects, the optical signals emitted from one source need to be distributed through several channels to various detectors.

In addition to this necessary power fan-out, the power losses are also due to the illumination vignetting, the reflection on the transmission surfaces and the light absorptions in the optical material. To meet the requirement of the detector's sensitivity, the interconnected PE number N is limited the by this power consumption efficiency. The signal repetition rate, measured by the element bit rate (EBR), is affected by the power received by detectors. In this section, the relations between the interconnected PE's number N, the system power loss and the EBR is investigated [7].

As an example, let us discuss the power utilization efficiency of the reflective ring array interconnects. A diagram of a multiple channel reflective ring interconnect is illustrates in Fig.6.3. The channel number M for a nearest neighbor (NN) is 2, while for a plus-minus 2 (PM2I) M is $M = \log_2 N$. Each light beam passes through a number of $\log_2 M$ of beamsplitters. To ensure the received power at each cell is identical, the beamsplitter's reflectance should be 0.5. Since the light beam passes twice each beamsplitter, the power transmit rate on each beamsplitter is $((0.5(1-L_{bs}))^2$, where L_{bs} is the power transmission loss in the beamsplitter. To save the light power loss on the beamsplitters, the first beamsplitter is chosen as a polarizing beamsplitter with a transmission loss $(1-L_{p.bs})^2$, and without the 0.5 distribution loss. After passing one polarizing beamsplitter and (M-1) common beamsplitter, the transmit rate becomes $((0.5(1-L_{bs}))^{2(\log_2 M-1)}(1-L_{p.bs})^2$. The received power at each interconnect cell can be expressed as

$$P_{rec} = P_{tran}((0.5(1-L_{bs}))^{2(\log_2 M-1)}(1\_L_{p.bs})^2(1-L_{cell}) \qquad (7.13)$$

where P_{rec} and P_{tran} denote the received and the transmitted power, respectively, and L_{cell} is the power loss in a single interconnect cell, including the illumination vignetting, the material absorptions, the reflections on the refraction surfaces.

In each cell, suppose that the typical illumination efficiency is $\eta = 0.7$ due to the vignette. The beamsplitter inside every cell also causes a power loss, including a 5% power loss on the surface and the distribution efficiency of the beamsplitter

as 0.5^2, and therefore makes the total efficiency of the beamsplitter t_{bs} to be around 0.24. Except for the two total-internal-reflecting surface M_4 and M_1, the other two prism reflective surfaces M_2 and M_3 can not perform a total-reflect, and therefore need to be coated to reduce the transmission loss to its minimum, say 1%. Since the light beam travels through the prism twice, the total transmission ratio of the prism reflective surfaces T_r is $(1-1\%)^2 = 0.99^2$. The transmissivity through the six coated refractive surfaces of the lens T_l could be 0.99^6. The transmissivity due to the absorption in a prism T_a is 0.985^t, where t is the light path length in the prism. Assuming that t=5D, and D=1cm, $T_a = 0.985^5$, the single-path power transmission rate in a single cell rotator is

$$1 - L_{cell} = \eta T = \eta T_{bs} T_r T_l T_a$$
$$= (0.7)(0.24)(0.99^2)(0.99^6)(0.985^5) = 0.(7414)$$

A distribution loss (DL) is defined to evaluate an optical system power consumption efficiency [8]. A typical total distribution loss in dB in the channel linked to cell 1 in Fig.6.3 may be evaluated as:

$$DL = 10\log_{10}\frac{P_{rec}}{P_{tran}}$$
$$= 20(\log_2(M-1)\log_{10}(0.5(1-L_{bs})) + 20\log(1-L_{p.bs}) + 10\log_{10}(1-L_{cell}) \quad (7.15)$$

Assuming that the $(1-L_{cell})$ is 0.14, and that the loss of both the normal and polarizing beamsplitter is 0.2, the distribution loss can be expressed as:

$$DL = 20(\log_2 M - 1)\log_{10}((0.5)(1-0.2))^2 + 20\log_{10}(1-0.2) + 10\log_{10}(0.14)$$
$$= 7.85\log_2 M + 2.52 \quad (7.16)$$

For the NN network, M=2 and the DL is as low as 11dB, while the DL of a PM2I is the function of the M, which equals to $\log_2 N$. For example, the DL is about 28 dB for a PM2I with N=1024, and is 31 dB for N=4096.

An element-bit-rate (EBR) is a system parameter that represents the number of bits which can be processed per second per element pair. We can estimate the EBR by assuming that a receiver sensitivity of 1000 photons per bit can be achieved,

which is 100 times more than the quantum limit for a bit rate of 10^{-9} [8]. This implies that for $\lambda = 0.9\mu m$, the power delivers to a single receiver has to be at least

$$P_{bit} = 1000h\nu = 1000(6.63)(10^{-34})\frac{3(10^{8})}{0.9(10^{-6})} \tag{7.17}$$

According to the above power loss calculation, the received power from a LD power of $2\mu W$ is

$$\begin{aligned} P_{rec} &= P_{tran}((0.5)(0.8))^{2(\log_2 M-1)}(0.8)^2(0.14) \\ &= (1.1)(10^{-6})(0.164)^{\log_2 M} \end{aligned} \tag{7.18}$$

Then the EBR can be evaluated as:

$$EBR = \frac{P_{rec}}{P_{bit}} = 50(0.164)^{\log_2 M} Gbit/s \tag{7.19}$$

The curves of the DL and the EBR vs. N are shown in Fig.7.2. As shown in this figure, the DL and EBR of a NN network are independent of element number N, being 11dB and 8.7 G Bit/s, respectively. However, both the DL and EBR of a PM2I interconnect are determined by the number of channels M, which is a function of N. For example, the EBR of a PM2I is 125 M Bit/s and 75 M Bit/s for N = 1024 and N=4096, respectively.

7.5 Summary

In this chapter, a systematic analysis of interconnect capability due to optical aberration, diffraction and detector power restriction are performed. The aberration limit can be minimized by the use of an optimized design. First, a suitable system structure should be chosen based on the aberration analysis. Then each optical element should be designed to eliminate the aberrations, and a compensation of aberrations among different elements is also helpful. The processing capacity limited by the system diffraction is basically proportional to the aperture size, which is the lens aperture or the aperture of the switching devices. The diffraction

influence to an imaging system is less serious than to a projecting system. In any case, the power consumption is an important issue to consider, especially for multiple channel interconnects. The relation among the interconnected numbers N, the system power loss, and the transmitting speed, is studied.

7.6 References

[1] B. Ha and Y. Li, "Reflective ring array interconnects: An optical system design study," accepted by Appl. Opt.

[2] W. J. Smith, *"Modern Optical Engineering"*, (McCraw-Hill, 1990) ch.3.

[3] R. Kingslike, *"Optical System Design ",(Academic Press, 1983) ch.5.*

[4] R. Kingslake, *Applied Optics and Optical Engineering* (Academic Press, New York and London, 1965) Vol.3, Ch.7.

[5] M. Born and E. Wolf, *Principles of Optics* (Pergamon Press, Oxford, 1975) ch.8.

[6] J. W. Goodman, *Introduction to Fourier Optics* (McGraw-Hill, New York, 1976) ch.4.

[7] T. Sakano, K. Noguchi, and T. Matsumoto, "Optical limits for spatial interconnection networks using 2-D optical array devices," Appl. Opt. 29, 1094-1100 (1990).

[8] R. Linke, "Power distribution in a planar-waveguide-based broadcast STAR network," IEEE Photo. Tech. Lett. 3, 1991.

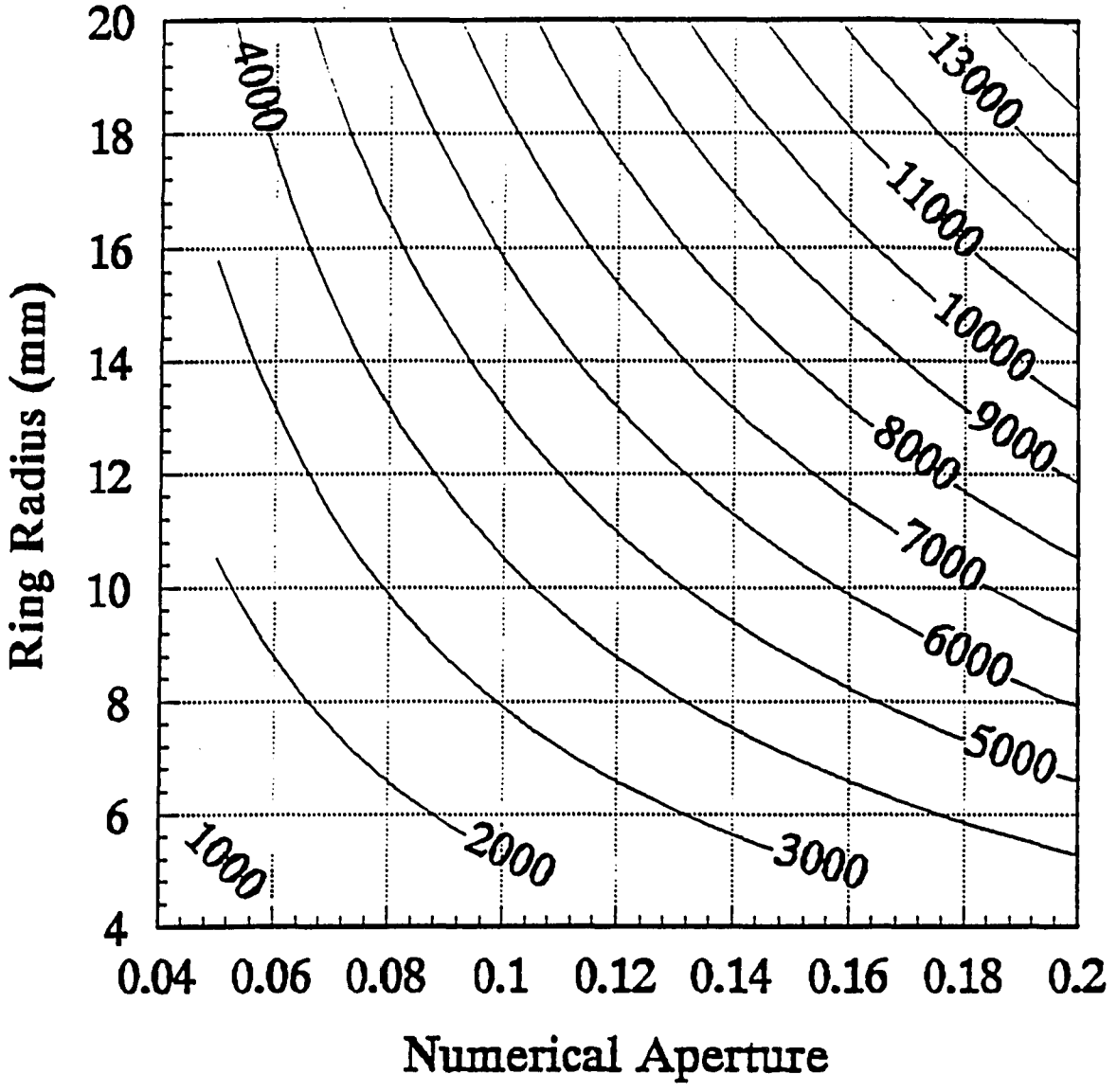

Fig.7.1 The PE numbers limited by aberration & diffraction

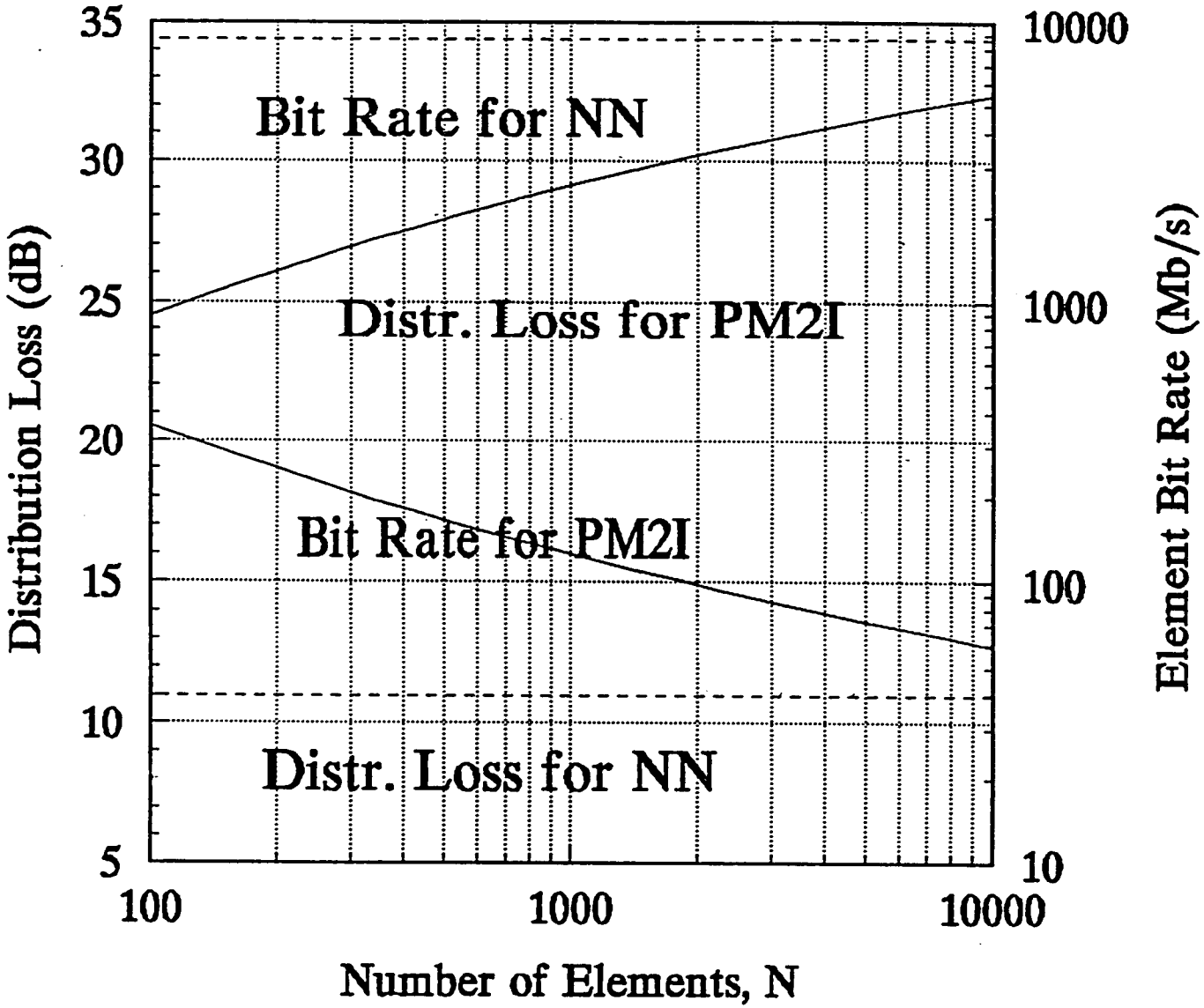

Fig.7.2 Distribution loss & element bit rate for NN & PM2I

VIII SUMMARY

In this thesis, optical implementations of various interconnects for multiprocessing computers were studied. A novel topology to arrange all elements in a ring array instead a rectangular array was introduced. Different approaches to implement ring array interconnects were studied. The interconnect capacity limited by system aberration, diffractions and power loss was also discussed. For most of the proposed free-space optical interconnects, the priciple-proof experimental results were inluded.

New approaches to implement crossover and perfect shuffle interconnects were presented. The main advantage of these novel approaches is their capability of forming a cascade of multiple stage interconnects, which is what has been demanded by most of their applications.

In this thesis, a concept of using interconnected contact switch array to perform binary symmetric logic computation was introduced. These contact-switch-based interconnects can yield a much faster binary symmetric logic computing than those gate-based computing devices do, which has shown that the interconnect networks not only can achieve a data communication among processors, but also can be a computing tool itself.

The topology of precessing element distribution was studied in this thesis. A new concept to arrange all PEs along a circular rather than a linear or a rectangular array was presented. The choice of using different interconnect topologies basically depends on the different interconnect purposes. The rectangular array can be chosen for the crossbar, gamma, delta and perfect shuffle networks. On the other hand, the ring topology demonstrates its challenge on other optical interconnects, such as the nearest neighbor and plus-minus 2^i which are not suitable to be realized with a rectangular array distribution by using only space-invariant optical elements.

Depending on various applications, interconnect architecture may be either unidirectional, bi-directional or reflective one. To meet these various interconnect requirements, different approaches to implement ring array interconnects were studied. Employing a couple of Dove prisms, a ring array interconnect shows its competitively

of performing both uni- and bi-directional interconnects. A specially designed reflective prism was also presented to implement a couple of conjugated ring array interconnect patterns. All these new approaches can provide a fast and synchronized data communication for SIMD computers.

The range of optical interconnects can be from gate-to-gate, chip-to-chip, to board-to-board, and even to computer-to-computer. The optical perfect shuffle is an example of chip-to-chip interconnect, while the optical binary symmetric logic network is basically a gate-to-gate interconnect. According to its massive parallel processing feature, optical interconnects may find more applications in the chip-to-chip and board-to-board interconnects than in the gate-to-gate interconnects. For the interconnect networks between computer-to-computer, optical fibers have a bright future.

The main feature to evaluate an optical interconnect is its performance reliability, processing speed, and power utilization efficiency. In this thesis, both classical and physical optics were used to analyze the performances of free-space optical interconnects. The relation among the interconnect capacity, measured by the linked number of PEs, the signal repetition rate, in terms of EBR, and the performance reliability was established. Based on an analysis of aberration and diffraction restriction, an optional design of the optical devices was also presented.

Optical interconnects have shown a powerful competence in the multiprocessing computers. The massive parallelism of processing and ultrafast switching speed of the optics provide an opportunity to increase the bandwidth and speed of the data communications. Based on various electro-optic (EO), acousto-optic (AO) and nonlinear optical effects, fast optical switching and modulation devices, together with various of optical space-invariant and space-variant interconnect schemes, form a major support for the optical interconnects. Compared with other optical operators, like an optical adder or a optical counter, optical interconnects demonstrate more powerful competence. With the rapid progress of the modern technology and new materials optical devices will replace the electrical wires to perform a high speed and reliable interconnect for the advanced computers in the near future.

IX BIBLIOGRAPHY

Arnold, A. F and M. A. Harrison, IEEE Trans. comput. EC-12, 244 (1963).

Born, M. and E. Wolf, *Principles of Optics* (Pergamon Press, Oxford, 1975) ch.8.

Clark, N. A. and S. T. Lagewall, App. Phys. Lett., 36, 899-901 (1980).

Cloonan, T. J. and M. J. Herron, Opt. Eng., 28, 305-314 (1989).

Conrady, A. E., *Applied Optics and Optical Design* (Dover Publications, Inc., New York, 1957, Ch.10.

Eichmann, G. and Y. Li, Appl. Opt., 26, 1167-1169 (1987).

Esener, S. L. Proc. OE/LASE 90 Conference on Digital Optical Computing (Critical Reviews), Los Angelas, CA. Jan., 15-19, 1990.

Friberg, S. R., A. M. Weiner, Y. Siberberg, B. G. Sfez, and P. S. Smith, Opt. Lett., 13, 904 (1988).

Gibbs, H. M., S. L. McCall and T. N. C. Venkatesan, Phys. Rev. Lett. 36, 1135 (1976).

Goodman, J. W., *Introduction to Fourier Optics* (McGraw-Hill, New York, 1976) ch.4.

Goodman, J. W., F. J. Leonberger, S. Y. Kung, and R. A. Athale, Proc. IEEE, 72, 850-860 (1984).

Goodwin, J. W., A. J. Moseley, D. J. Robbins, J. Thompson, and R. C. Goodfellow, Proc. SPIE, 1215, 55-62 (1990).

Guha, A., J. Bristow, C. Sullivan, and A.Husain, Appl. Opt., 29, 1077-1093 (1990).

Ha, B. and Y. Li, "Reflective ring array interconnects: An optical system design study," accepted by Appl. Opt.

Huang, A. Proc. IEEE, 72, 780-786 (1984).

Hunter, S. *et. al*, Appl. Opt., 29, 2058-2066 (1990).

Hwang, K. and F. A. Briggs, *Computer Architecture and Parallel processing.* (McGraw-Hill, New York, 1984), ch.5.

Jahns, J. and M. J. Murdocca, Appl. Opt. 27, 3155-3160 (1988).

Jewell, J. L., Y. H. Lee, H. M. Gibbs, N. Peyghambarian, A. C. Cossard, and W. Wiegmann, Appl. Phys. Lett., 46, 918 (1985).

Johson, K. M., M. R. Surette, and L. A. Pagano-Stauffer, Opt. Eng., 26(5), 385-391 (1987).

Johson, K. M., M. R. Surette and J. Shamir, Appl. Opt., 1727-1733 (1988).

Kiamilev, F., S. Esener, V. H. Ozguz, and S. H. Lee, Proc. SPIE CR-35, 197-220 (1990).

Kingslike, R. *Optical System Design*,(Academic Press, 1983) ch.5.

Kingslake, R. *Applied Optics and Optical Engineering* (Academic Press, New York and London, 1965) Vol.3, Ch.7.

Klir, G. J., *Introduction to the Methodology of Switching Circuits*, Chaps. 5 and 6, D. Van Nostrand Co., New York (1972).

Kohavi, Z., *Switching and Finite Automata theory*, Ch.6, McGraw-Hill, New York (1978).

Li, P., D. Y. Zang and C. S. Tsai, Appl. Opt. 27(9), 1780-1785 (1988).

Li, Y., B. Ha, T. Wang, S. Wang, A. Katz, X.J. Lu, and E. Kanterakis, Appl. Opt. 31, 5548-5558 (1992).

Li, Y., B. Ha and G. Eichmann, Opt. Eng. Vol.28, p.380-389 (1989).

Li, Y., B. Ha and G. Eichmann, Appl. Opt. 30, 3288-3293 (1991).

Li, Y., B. Ha, and G. Eichmann, Appl. Opt. 30, 531-539 (1991).

Li, Y., T. Wang, and B. Ha, Opt. Lett. 279-281 (1991).

Lin, S-H, T. F. Krile and J. F. Walkup, Proc. SPIE, 752, 209-216 (1987).

Linke, R., IEEE Photo. Tech. Lett. 3, 1991.

Lohmann, A. W., Optica Acta, 32, 1465-1470 (1985).

Lohmann, A. W., Appl. Opt., 25, 1543-1549 (1986).

Lohmann, A. W., W. Storck and G. Stucke, Appl. Opt. 25, 1530-1531 (1986).

Marcus, M. P., IRE Trans. Electron. Comput. EC-5, 237 (1956).

Miller, D. A. B., D. S. Chemla, T. C. Damen, T. H. Wood, C. A. Burrurs, A. C. Gossard, and W. Wiegmann, IEEE, Quantum Electron, QE-21, 1462 (1985).

Saha, T. T., Proc. Soc. Photo-Opt. Instrum. Eng. 444, 112-117 (1984).

Sakano, T., K. Noguchi, and T. Matsumoto, Appl. Opt. 29, 1094-1100 (1990).

Sheng, Y., Appl. Opt. 28, 3290-3292 (1989).

Smith, W. J., *"Modern Optical Engineering"*, (McCraw-Hill, 1990) ch.3.

Song, Q. W. and F. T. S. Yu, App. Opt. 27, 1222-1223 (1988).

Spanke, R. A. and V. E. Benes, Appl. Opt. 26, 1226-1229 (1987).

Stirk, C. R. Athale and M. Haney, Appl. Opt. 27, 202-203 (1988).

Surmatsu, Y. and S. Arai, Proc. IEEE 75, 1472 (1987).

Wada, O. and S. Yamakoshi, Proc. SPIE, 1215, 28-37 (1990).

Wang, C. Y., S. H. Lin, and Y. M. Houng, Appl. Phys. Lett. 51, 83 (1987).

Wherrett, B. S., Appl. Opt. 24, 2876-2883 (1985).

Yoder, P. R., J. OSA. 48, 496-499 (1958).